DEVELOPMENT OF ADVANCED THIN LITHIUM METAL ANODES FOR HIGH-PERFORMANCE LITHIUM METAL BATTERIES

CAI JIEHUA

PhD

The Hong Kong Polytechnic University

2025

The Hong Kong Polytechnic University

School of Fashion and Textiles

Development of Advanced Thin Lithium Metal Anodes for High-Performance Lithium Metal Batteries

CAI Jiehua

A thesis submitted in partial fulfilment of the requirements for the degree of Doctor of Philosophy

March 2025

CERTIFICATE OF ORIGINALITY

I hereby declare that this thesis is my own work and that, to the best of my knowledge and belief, it reproduces no material previously published or written, nor material that has been accepted for the award of any other degree or diploma, except where due acknowledgement has been made in the text.

_____(Signed)

CAI Jiehua (Name of student)

Abstract

Nowadays, the ever-increasing demand for next-generation portable and flexible electronics has stimulated great efforts to explore high-energy storage devices. Considering that the energy densities of lithium-ion batteries (LIBs) have almost reached their theoretical limit, it urges the development of advanced battery technologies that go beyond LIBs. Since lithium (Li) metal has the highest theoretical capacity and the lowest electrochemical potential, Li metal batteries (LMBs) have emerged as the most promising candidate. However, the commercialization of LMBs is hindered by the uncontrollable Li dendritic growth on the anode. Despite the significant strategies proposed, the practicality of LMBs is still far from satisfactory because the Li metal involved is excessively thick. To enhance energy density, it is essential to employ a thin (thickness, ≤ 50 μm) Li metal anode (LMA) in battery configurations, which can reduce the excess weight and volume within the battery. However, challenges remain in balancing the electrochemical stability, mechanical flexibility, and energy density of thin LMA-based batteries. To address these challenges, we try to develop advanced thin LMAs through material selection, lithiophilic modification, and structural design. Three types of thin LMAs, which were developed based on different substrates, aiming to achieve high-performance LMBs, are demonstrated.

Firstly, a conductive textile framework with Janus wettability to Li was developed by depositing lithiophilic antimony (Sb) material on the Ni coated carbon cloth. As such, a thin yet ultrastable Janus Li-textile anode was rapidly fabricated through selective wetting, which yielded a thin Li (~50 μm) coating only on the lithiophilic side of the textile framework. This Janus Li-textile anode demonstrated well-strengthened stability and record-lengthened lifespan by suppressing the formation of dendrite through the guided-deposition behavior and top-buffering space. Even at a high depth of discharge (DOD) of 75%, the Janus Li-textile anode presented an ultralong lifespan of over 3000 hr. The LMBs using the Janus Li-textile anode exhibited an improved energy density by 30%, and achieved an outstanding working life of 2000 cycles with capacity retention of 99.94% per cycle. The as-assembled pouch cell showed excellent cycling stability and impressive flexibility with high bending tolerance.

Furthermore, to achieve high flexibility without sacrificing the energy density of the

battery, a thin, ultralight, and flexible composite LMA was developed by sandwiching a thin Li foil in between two ultralight fabric layers through mechanical rolling. The sandwiched Li (SW Li) anode showed a lightweight nature, which was only 37.4% of the weight of foil-based thin LMAs. The SW Li anode was compatible with different high-loading commercial cathodes, showing improved electrochemical stability due to the fabric framework and interfacial alloy layer. Meanwhile, the mechanical support provided by the fabric layers endowed the SW Li with exceptional flexibility, allowing it to be folded into an origami shape and bent 10000 times at a radius of 1.5 mm. LMBs adopting SW Li not only delivered high energy of 309 Wh kg^{-1}, but also presented outstanding flexibility with a remarkably high figure of merit for flexible battery (163.8), outperforming the state-of-the-art flexible batteries.

Finally, a facile approach was developed to achieve high-performance anode-free LMBs through thermally evaporating an ultrathin (50 nm) layer of Sb on the surface of Cu foil (CuSb). The simple surface modification effectively improved Li deposition behavior, thus enhancing cyclic stability and prolonging the lifespan of the anode-free batteries. Specifically, the modified Cu foil showed a prolonged cycling life of 400 cycles with an impressive average Coulombic efficiency (CE) of ~99.3%. The anode-free NCM811||CuSb batteries also demonstrated a remarkable energy density of 425 Wh kg^{-1}, and improved cycling stability at a practical high areal capacity of over 4 mAh cm^{-2}.

In conclusion, we proposed feasible strategies to develop electrochemically stable, mechanically flexible, and high-energy thin LMAs through facile processing techniques. Such thin LMAs have demonstrated their potential in advancing the performance of batteries, contributing to achieving long-term stability, long-life cycle, high energy density as well as outstanding flexibility. Therefore, this study provided promising and effective avenues for the development of advanced thin LMAs, paving the way for the realization of next-generation LMBs.

List of Publications

Related Journal Publication

1. **Jiehua Cai**†, Lei Wang†, Qiyao Huang, Wancheng Yu, Chuan Xie, and Zijian Zheng. A Thin, Stable, and Flexible Janus Lithium-Textile Anode for Long-Life and High-Energy Lithium Metal Battery. *Advanced Energy Materials* **2024**, 14, 2303088. († Equal contribution)

Paper in Preparation

1. **Jiehua Cai**, Yanpeng Guo, Yufeng Luo, Shujing Wen, Junhua Zhou, Fan Chen, Qiyao Huang, Zijian Zheng. Sandwiched Lithium Metal Anodes for High-Energy and Highly-Flexible Lithium Metal Batteries.

Other Journal Publications

1. Yufeng Luo, Chi Zhang, **Jiehua Cai**, Zhenyao Wei, Qiyao Huang, and Zijian Zheng. Understanding and Passivation of Surface Corrosion of Cufor Stable Low-N/P-Ratio Lithium-Sulfur Battery. *Advanced Functional Materials* **2024**, 2418043.

2. Zhenyao Wei, Yufeng Luo, Wancheng Yu, Yufei Zhang, **Jiehua Cai**, Chuan Xie, Jian Chang, Qiyao Huang, Xiaoxiong Xu, Yonghong Deng, and Zijian Zheng. Bipolar Textile Composite Electrodes Enabling Flexible Tandem Solid-State Lithium Metal Batteries. *Advanced Functional Materials* **2024,** 36, 2406386.

3. Junhua Zhou, Chi Zhang, Huimin Wang, Yanpeng Guo, Chuan Xie, Yufeng Luo, Chao Wang, Shujing Wen, **Jiehua Cai**, Wancheng Yu, Fan Chen, Yufei Zhang, Qiyao Huang, and Zijian Zheng. Dual-Interphase-Stabilizing Sulfolane-Based Electrolytes for High-Voltage and High-Safety Lithium Metal Batteries. *Advanced Science* **2024**, 11, 2410129.

4. Fan Chen, Xian Song, Jingjing Fu, Jiaheng Liang, Junhua Zhou, **Jiehua Cai**, Yufei Zhang, Mengjia Zhu, Yichun Ding, Jinxing Jiang, Zijian Chen, Youchao Qi, Zhihao Zhou, Qiyao Huang, Yingying Zhang and Zijian Zheng. An all-fibrous, permeable, adhesive, and stretchable self-powered electronic skin for sign language recognition. *Journal of Materials Chemistry A* **2024**, 12, 30298-30308.

Conference Presentations

1. **Jiehua Cai**, Zijian Zheng. Thin, Stable, and Flexible Lithium Metal Anodes for High-Performance Lithium Metal Batteries. **EcoMat Conference 2024**, July 8-10, 2024, Newcastle upon Tyne, UK.

2. **Jiehua Cai**, Lei Wang, Zijian Zheng. Janus Lithium-Textile Anode for Long Life, High-Energy, and Flexible Lithium Metal Battery. **The 22nd International Meeting on Lithium Batteries (IMLB 2024)**, June 16-21, 2024, AsiaWorld-Expo, Hong Kong SAR, China.

3. **Jiehua Cai**, Lei Wang, Zijian Zheng. Janus lithium-textile electrode for high-performance lithium metal battery. **EcoMat Conference 2023**, June 20-24, 2023, The Hong Kong Polytechnic University, Hong Kong SAR, China.

Award

Best Poster Presentation Award, **Jiehua Cai**, Zijian Zheng. Thin, Stable, and Flexible Lithium Metal Anodes for High-Performance Lithium Metal Batteries. EcoMat Conference 2024, July 8-10, 2024, Newcastle upon Tyne, UK.

Acknowledgements

First of all, I would like to express my sincere gratitude to my supervisor Prof. Zijian Zheng for providing me with the invaluable opportunity to join this excellent group of Advanced Interfacial Materials and Devices (AIMD). His extensive knowledge and enthusiastic attitude towards scientific research profoundly inspired and shaped me, especially in the way of thinking logically and critically. Great thanks to his patient guidance and insightful enlightenment, I have acquired a broader scientific understanding and research experience with enhanced critical thinking and problem-solving abilities, which will be of great benefit to my future study and life.

I am also grateful for all the members in the AIMD group, from whom I have gained kind help and support during these years. I would like to thank Dr. Huang Qiyao, Dr. Sze Wing Ng, Dr. Wang Lei, Dr. Luo Yufeng, Dr. Xie Chuan, Dr. Guo Yanpeng, Dr. Guo Qianyi, Dr. Yu Wancheng, Dr. Wei Zhenyao, Dr. Zhou Junhua, Dr. Xu Hailong, Dr. Wang Huimin, Dr. Wang Chao, Dr. Yang Yongqiang, Dr. Li Xinyan, Dr. Guo Can, Dr. Han Bing, Dr. Yi Pei, Dr. Gao Yuan, Dr. Xu Junling, Dr. Rong Mingming, Dr. Chen Fan, Dr. Zhuang Qiuna, Dr. Zhong Leni, Dr. Zhang Yaokang, Dr. Zhang Yufei, Dr. Fu Jingjing, Dr. Ding Yichun, Dr. Zhang Chi, Dr. Song Xian, Dr. Qi Youchao. Dr. Zhou Zhihao, Dr. Zhang Yueying, Dr. Jiao Wenli, Dr. Wang Ziran, Dr. Wang Pengwei, Dr. Fan Haining, Dr. Wu Yingsi, Dr. Hu Hong, Dr. Ge Wenjiao, Dr. Wang Wenshuo, Dr. Ng Puifai, Dr. Zhang Pengxiang, Dr. Kong Xiangtong, Dr. Nan Hanyi, Dr. Ting Tian, Mr. Chen Zijian, Ms. Shi Yuqing, Mr. Ma Xiaohao, Mr. Fang Lingtao, Ms. Wen Shujing, Mr. Jiang Jinxing, Mr. Chen Lixi, Mr. Li Zhibo, Ms. Wu Zhizhi, Ms. Wang Huiming, Mr. Liang Jiaheng, Ms. Zhu Mengjia, Mr. Yang Ruofan, Mr. Wang Zhaokun, Ms. Su Ruiqi, Ms. Zhou Yunlu, Mr. Gu Qiuyu, Mr. Yang Sheng for their kind assistance, insightful discussion, and valuable suggestions, both in the experiments and daily life.

Besides, I would like to express my gratitude to all the staff in the department of SFT and AP, as well as the Materials Research Centre, for their kind support in equipment

training and assistance with the material characterizations. I would like to gratefully acknowledge the financial support from the Hong Kong Government and the Hong Kong Polytechnic University.

Most importantly, I would like to express my deepest gratitude to my family members for their love, care and unconditional support. I am especially thankful to my boyfriend, Chen Xiao, who accompanied me through every challenge and hardship during the postgraduate study. His understanding, support, and encouragement gave me warmth and made me more independent and confident. Lastly, I would like to express sincere gratitude to my dear friends for their support and companionship in these years.

Table of Contents

List of Figures

List of Tables

List of Abbreviations

3D	Three-dimensional
CC	Carbon cloth
CE	Coulombic efficiency
CuSb	Antimony modified copper foil
DOD	Depth of discharge
DEC	Diethyl carbonate
DOL	1,3-Dioxolane
DME	Dimethoxyethane
EC	Ethylene carbonate
EIS	Electrochemical impedance spectroscopy
FEC	Fluorinated ethylene carbonates
GCD	Galvanostatic charge/discharge
HFE	1,1,2,2-tetrafluoro-3-(1,1,2,2-tetrafluoroethoxy)propane
Li	Lithium
LMAs	Lithium metal anodes
LIBs	Lithium ion batteries
LMBs	Lithium metal batteries
LCO	Lithium cobalt oxides
LFP	Lithium iron phosphate
$LiPF_6$	Lithium hexafluorophosphate
$LiNO_3$	Lithium nitrate
LiFSI	Lithium bis(fluorosulfonyl)amide
LiTFSI	Lithium bis(trifluoromethylsulphonyl)imide
Ni-CC	Nickel coated carbon cloth
NiSb	Nickel antimony alloy
NiSb-CC	Nickel antimony alloy coated carbon cloth
NCM	Lithium nickel manganese cobalt oxide
PI	Polyimide
PI-Sb	Polyimide with antimony modification
Cu-PI-Sb	Polyimide with copper and antimony modification
PAMD	Polymer assisted metal deposition
SEI	Solid electrolyte interface
SEM	Scanning electron microscopy
XRD	X-Ray Diffraction
XPS	X-ray photoelectron spectroscopy

Chapter 1 Introduction

1.1 Background and Challenges

The rapid development of flexible and wearable electronic devices [1-4], such as smart textiles, implantable monitors, and foldable displays, has put a heavy demand on energy storage systems that are lightweight, possess high energy density, and exhibit exceptional flexibility and stability. Traditional batteries, however, remain rigid and bulky, making it difficult to integrate into next-generation technologies [5]. In this regard, the development of advanced energy storage solutions that combine outstanding stability with superior flexibility and high energy density is of critical significance.

In the past three decades, lithium-ion batteries (LIBs) have been commercialized in our daily life, serving as the dominant energy supply [6-9]. Currently, LIBs based on graphite anode typically achieve energy densities of 250~300 Wh kg^{-1}. The inherent limited theoretical energy density of graphite makes it challenging to satisfy the growing demands of energy density [10-13]. As a result, there is an increasing amount of research devoted to exploring other types of alternative batteries, especially lithium metal batteries (LMBs) due to the ultrahigh theoretical capacity and the lowest electrochemical potential of the lithium (Li) metal [14].

In terms of practical application, LMBs are still hindered by their cyclability performance and safety issues due to the uncontrollable Li dendritic growth on the anode [15, 16]. Over the past decade, research attention has mainly focused on the stabilization of Li metal anode (LMA) through developing various strategies to mitigate the growth of dendrites during repeated cycling. [17-27]. Despite these advancements, many approaches heavily relied on using excessive amounts of Li, which diminished the practicability of LMBs with significantly reduced energy density.

In recent years, the great importance of equipping battery configurations with thin

LMAs (thickness, ≤ 50 μm) has been proposed [28-31]. To date, there are mainly four types of approaches to achieving thin LMAs, namely mechanical rolling, thermal infusion, physical vapor deposition, and electrochemical deposition [24, 28, 30, 32, 33]. Normally, as the thickness of Li metal decreases, the energy density of the battery increases. When the thickness of Li metal drops to zero, then the energy density of the battery could be maximized, which is the so-called anode-free LMB [34-36]. Meanwhile, researchers have tended to adopt thinner and lighter current collectors to host Li metal [37-39], thus further increasing the energy density of the practical batteries.

However, it should be noted that it becomes more susceptible to mechanical degradation and dendrite formation in thinner LMAs [40]. Typically, the Li reserves in thin LMAs are very limited. During the cycle, the irreversible loss of Li, such as the formation of the SEI layer and dead Li, will have a significant impact on the capacity-limited thin LMAs, resulting in faster capacity decay and battery failure. As such, there is a tradeoff between energy density and electrochemical stability in the field of thin LMAs. Meanwhile, it still remains a critical challenge to achieve long-term cycling stability of thin LMA-based batteries, especially at a high depth of discharge.

Furthermore, despite the thin LMAs providing a viable solution for practical batteries with high energy density, the mechanical flexibility and bending tolerance of thin LMAs are extremely poor [41, 42]. They can hardly meet the requirements of the flexibility of the next-generation portable electronics and wearable devices, such as wearable belts, foldable phones, and roll-up displays [43, 44]. Both intrinsic rigid Li foil and metal-foil-based current collectors are vulnerable to suffering from cracks or even failure when subjected to external deformation [41, 45], such as bending and folding. In this regard, innovative thin LMAs with promising substrate selection and novel structural design towards high flexibility are also in urgent demand.

Typically, there is an intensive amount of research dedicated to the exploration of

textile-based Li anode [24, 46-50]. Textiles serve as the mechanical support, which can dissipate the stress concentration during bending, imparting the anode system with good flexibility [48]. Besides, the source of them is abundant with economic affordability, and the textile/fabric processing is highly scalable, making it feasible to be industrialized. It means that adopting textiles as current collectors is indeed a convincing option in constructing advanced thin LMAs. Nevertheless, the introduction of the textile host inevitably increases the unnecessary weight without contributing to additional capacity of the battery system. Acquiring outstanding flexibility while maintaining high energy density in the thin LMA-based cells is still a bottleneck to be solved.

Therefore, great efforts are still needed to solve the above-mentioned challenges in thin LMAs based on multidisciplinary knowledge from materials sciences, configuration design, and feasible processing techniques. Specifically, the development of advanced thin LMAs with balancing electrochemical stability, high energy density, and superior flexibility of batteries, is highly demanded. As such, the great potential of thin LMAs could be fully unlocked, paving the way for the realization of high-performance LMBs for next-generation applications.

1.2 Research Objectives

To address the challenges stated above, this research aims to develop advanced thin LMAs for accomplishing LMBs with good stability, high energy density, and superior flexibility, by proposing facile and feasible strategies. The detailed objectives are listed below:

1. To develop and characterize the surface-modified conductive substrates including metallic textiles, fabrics, and foils as current collectors of thin LMAs.
2. To enhance the long-term cycling stability and mechanical flexibility of LMBs by designing a thin Li anode with a textile host and Janus structure via selective wetting.

3. To realize exceptionally flexible and high-energy LMBs by adopting an ultralight thin LMA with superlight fabric and sandwiched configuration through mechanical rolling.
4. To achieve life-prolonged anode-free LMBs by modifying Cu foil with an ultrathin interphase layer through thermal evaporation.

1.3 Research Originality

In this research, the feasibility of developing advanced thin LMAs with structural design and modification through facile processing techniques for high-performance LMBs is demonstrated. This study provides useful feasible strategies for designing thin LMAs with balanced electrochemical stability, high energy density, and superior flexibility, which thus paves the way for the realization of next-generation LMBs. The reported strategies are also believed to be applicable to other battery technologies in achieving high energy density as well as high flexibility.

Firstly, a conductive textile with Janus wettability to Li is developed. As such, we propose a novel strategy of selective wetting to rapidly achieve a thin Janus Li-textile anode. Specifically, the lithiophilic side of the textile is coated with a thin Li layer (~50 μm) while the other lithiophobic side remains a porous textile structure. Such a thin LMA with Janus structure demonstrates well-strengthened stability and record-lengthened lifespan by suppressing the formation of dendrites through the guided-deposition behavior and top-buffering space. In the full-cell study, the LMBs achieve an ultralong lifespan of 2000 cycles with capacity retention of 99.94% per cycle. The as-assembled pouch cell also shows impressive flexibility.

Secondly, to solve the trade-off between high flexibility and high energy density in LMBs, two superlight fabrics with surface functionalization are utilized to sandwich a thin Li strip through one-step mechanical rolling. On the one hand, the adopted superlight fabrics could minimize the whole-cell weight without sacrificing the energy

density of the battery. On the other hand, the sandwiched structure with soft fabrics on two sides provides robust mechanical support to the middle Li layer, thus allowing this thin LMA to be folded into an origami shape and bent 10000 times at a radius of 1.5 mm. The practicability of the sandwiched thin LMA is further demonstrated in LMBs, which is compatible with various kinds of high-loading commercial cathodes. Especially, a remarkably high figure of merit for flexible battery (163.8) is achieved in our thin LMA-based battery, which outperforms the state-of-the-art flexible batteries.

Furthermore, a simple strategy of surface modification enabled by thermal evaporation is proposed to achieve anode-free batteries with both high energy density and improved cycling stability. The ultrathin interphase layer (50 nm) modified on the Cu substrate can facilitate a rapid Li ion diffusion and reduce the nucleation barrier. As such, the modified Cu foil demonstrates a significantly improved deposition behavior in both morphological and electrochemical investigations. The anode-free batteries with a high areal capacity of over 4 mAh cm^{-2} are fabricated, which shows prolonged cycling life and a practical energy density of 425 Wh kg^{-1}.

The electrochemically stable, mechanically flexible, and high-energy thin LMAs are demonstrated in this project. It reveals a great promise in advancing the performance of LMBs by developing novel thin LMAs with rational design strategies. Hopefully, the feasible and effective avenues for the development of advanced thin LMAs in this study can be further extended to other kinds of energy storage systems.

1.4 Outline of the Thesis

The thesis is organized as follows:

Chapter 1 briefly introduces the background of LMBs and the critical challenges of balancing stability, energy density, and flexibility in thin LMAs-based batteries. The objectives and originality of this research are demonstrated as well.

Chapter 2 presents a brief introduction of the LMBs, including the development history, dendrite-induced challenges, and related plating/stripping process for nucleation and dendrite formation. The strategies for stabilizing Li metal anodes are summarized and discussed.

Chapter 3 describes the importance and approaches of developing thin LMAs. The pathways to develop LMBs with high energy density and high flexibility are also reviewed.

Chapter 4 illustrates the experimental methodology in detail, including materials, fabrication methods, instruments, and characterization techniques.

Chapter 5 proposes a novel strategy of selective wetting to achieve a Janus structured thin LMA for stable and flexible LMBs. The morphological evolution of the thin LMAs under different cycles is carefully investigated to reveal the reliability for long-term cycling. The electrochemical stability and mechanical flexibility of full cells are further demonstrated.

Chapter 6 reports a lightweight and flexible thin LMA through mechanical rolling to simultaneously achieve high-energy and highly-flexible LMBs. Comprehensive electrochemical performances and dynamic bending tolerance in thin LMAs-based batteries are investigated in depth.

Chapter 7 introduces an ultrathin layer modified Cu as an electrode for high-performance anode-free LMBs. The deposition behavior and cycling stability are studied. The electrochemical properties and stability of LMBs when paired with high-loading commercial cathodes are also investigated.

Chapter 8 concludes the results of the thesis and proposes an outlook for the further development of stable, flexible and high-energy LMBs.

Chapter 2 Overview of Lithium Metal Batteries (LMBs)

2.1 General Background of Lithium Metal Batteries (LMBs)

2.1.1 Introduction of LMBs

Energy storage systems are essential for the development of renewable energy, laying a solid foundation for the transition towards a more sustainable and environmentally friendly energy landscape. As an important form of energy storage [51], batteries are almost everywhere, penetrating into every field of social operation, from consumer electronics to large-scale industrial applications. Due to the merits of long cycle life, relatively low self-discharge rate and no memory effect, nowadays, lithium-ion batteries (LIBs) have become the dominant technology in the field of energy storage [9, 52]. It is no exaggeration to say that LIBs have revolutionized and reshaped modern society, particularly in the fields of communication and transportation. With the rapid development of smart terminals, portable electronic devices, and electric vehicles (EVs), higher requirements have been imposed on battery energy density. However, the graphite-based LIBs have almost approached their theoretical limit in energy density [10, 53]. In this regard, the LIBs with limited energy fail to meet the ever-growing demand for high energy density, which is crucial to extend the driving range of EVs and improve the comprehensive performance of portable electronic devices. Hence, there is an urgent need to develop advanced battery technologies that go beyond LIBs.

Lithium (Li) metal batteries (LMBs), which employ Li metal as the anode, have emerged as the most promising candidate for next-generation energy storage devices [8, 13, 54, 55]. Firstly, Li metal is the lightest metal with a density of only 0.534 g cm^{-3} and has good metal ductility [56], which can be beneficial to increase the gravimetric energy density and volumetric energy density of the assembled battery. Meanwhile, the Li metal anode (LMA) possesses the highest theoretical capacity of 3860 mAh g^{-1} [14], which is ten times that of the graphite. Compared with traditional graphite or silicon-

carbon anodes at the same capacity, the thickness of Li anode can be significantly reduced. Additionally, the LMA exhibits the lowest electrochemical potential of -3.04 V versus the standard hydrogen electrode. Consequently, in contrast to other anodes, such as graphite and silicon carbon, pairing the anode of Li metal with the same cathodes to assemble full cells can achieve higher operating voltages [11], thereby enhancing the energy density of batteries [10] (Figure 2.1). These charming features of LMA make LMBs highly attractive for next-generation applications, which can offer a high energy output while minimizing the lightweight and thickness of the power system. In general, LMBs come as advanced battery technology, holding broad research prospects and great development potential.

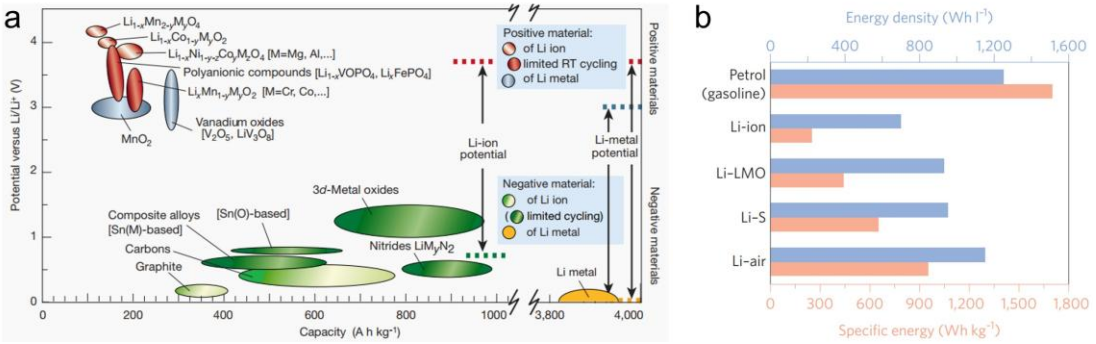

Figure 2.1 (a) The output voltage of LIBs and LMBs [11]. (b) Comparison of energy density of different batteries [10].

2.1.2 Development History of LMBs

The discovery of Li can be traced back to 1817, when Swedish scientist Arfwedson identified Li as a distinct element while analyzing the mineral petalite [56]. Later, the Li was named after the Greek word "lithos" meaning stone, which indicated its mineral origins. In the 1970s, Panasonic Corporation made progress by inventing a commercial Li primary battery. In 1972, Nobel Prize winner M. Stanley Whittingham developed the first Li secondary battery with titanium sulfide (TiS_2) as the cathode and Li metal as the anode [57], which was a significant breakthrough and a milestone in battery technology, showing the potential and feasibility of Li metal for energy storage.

This progress continued in 1977 with the design of a 45 Wh Li||TiS_2 battery for electric vehicles [58]. In the 1980s, Molly Energy Corporation commenced the commercialization of LMBs, which adopted the molybdenum disulfide (MoS_2) as cathode and the excess metallic Li as anode. The Li|| MoS_2 cylindrical batteries were mass-produced and flowed into the consumer market. Unfortunately, frequent battery fires accidents exposed the severe safety risks of LMBs, eventually leading to the recall of all batteries [59]. In the following years, great efforts were made in reliability testing of LMBs, but the battery safety issue resulted from Li dendrites has not been resolved [11]. At the same time, Sony Corporation began to use carbon-based anodes to replace Li metal, and successfully manufactured safe and reliable LIBs, starting the glorious era of LIBs. Therefore, although the LMBs system has shown great application advantages, its research and development have encountered a long period of stagnation. However, since the current performance of LIBs is approaching their limit, the revival of LMBs has become an urgent need [15, 60].

2.1.3 Configurations and Components of LMBs

Configurations: As shown in Figure 2.2, battery configurations for LMBs include coin cells, pouch cells, cylindrical cells, and prismatic cells [31, 61]. Coin cells are often used in laboratory research due to their simple assembly and ease of use [62]. Meanwhile, coin cells can be rapidly prototyped without sacrificing a large number of active materials, which is beneficial for initial testing and data collection. In terms of pouch cells, they adopt the aluminum (Al)-plastic composite film as packaging material, featuring with flexible and lightweight design [63], which can accommodate a variety of shapes and sizes. Currently, in laboratories, ampere-hour-level pouch cells are also adopted to characterize the reliability and feasibility of batteries. Cylindrical cells are batteries that use high-strength stainless steel as their outer shell. They have a good thermal management system with explosion-proof safety valves [64]. After a long-term development and technological maturity, the commercial products of cylindrical cells are widely available. As for prismatic cells, they are packaged in a square Al alloy shell,

which provides a compromise between the flexibility of pouch cells and the robustness of cylindrical cells. Compared with cylindrical batteries, the prismatic batteries have high space utilization and lighter shells, so they are usually adopted in the automotive industry where high capacity and compact design are critical [65].

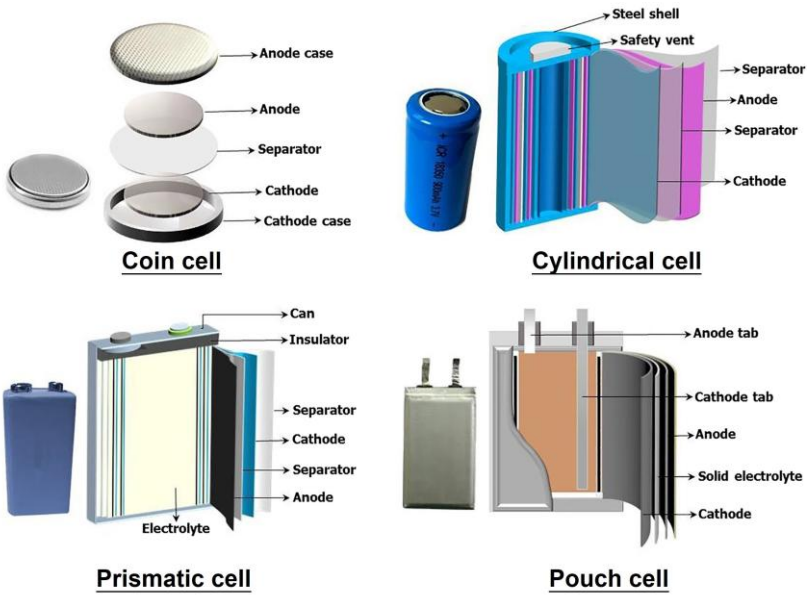

Figure 2.2 Schematic illustration of configurations and components of batteries [61].

Components: Regardless of the specific configuration of an LMB, it consists of several basic components, including an anode, cathode, separator, electrolyte, and current collector. The Li metal serves as the anode, while the cathode material varies depending on the specific chemistry employed. The cathodes, such as phosphates [66], transition metal oxides [67], and sulfides [68], are capable of reversibly intercalating Li ions. It is worth noting that the choice of cathode plays a key role in determining the electrochemical properties since it will affect the voltage output, delivery capacity, and even cycling performance. When it comes to the separator, it is a porous membrane that physically separates the anode and cathode to prevent electrical short circuits between the electrodes [69, 70]. Meanwhile, it allows Li ions to pass freely, thus promoting the normal operation of the battery. As for the electrolyte, it acts as the medium for Li ion transport between electrodes during cycling [71]. Notably, the electrolyte is crucial to

the efficiency of the battery, which is usually composed of Li salts dissolved in a solvent or a solid-state matrix [72, 73]. Finally, the current collector is responsible for collecting and conducting electrons between the external circuit and the electrodes during the charge and discharge process [74, 75]. Typically, conductive copper (Cu) foil is adopted as the current collector for the anode while conductive Al foil is employed as the current collector for the cathode. Overall, the five components of the LMB, namely, anode, cathode, separator, electrolyte, and current collector, are indispensable, each of which plays an important role in supporting the battery operation and affecting the battery performance.

2.1.4 Working Principle of LMBs

The working principle of LMBs involves the reversible electrochemical reactions between the anode of Li metal and the selected cathode during the charge and discharge cycles [76], thus facilitating energy conversion and storage.

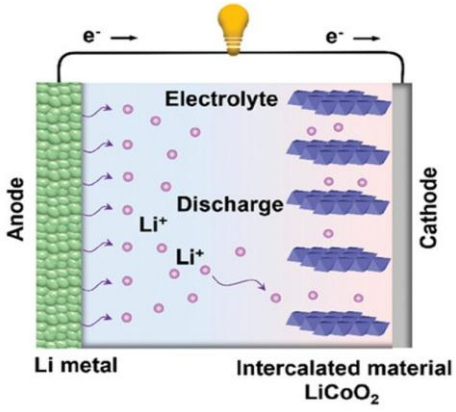

Figure 2.3 Working principle of LMB using intercalated $LiCoO_2$ cathode during the process of discharging [77].

For example, in LMBs that employ intercalated material of lithium cobalt oxide ($LiCoO_2$) as cathode, the charging process begins with an oxidation reaction at the cathode. This oxidation reaction is accompanied by the extraction of Li ions from the layered $LiCoO_2$ cathode. These Li ions migrate through the electrolyte and reach the

anode. Simultaneously, electrons flow through the external circuit to the anode, where they reduce the Li ions, resulting in electrochemical plating to form elemental Li metal. Conversely, during the discharging process, the Li metal at the anode undergoes electrochemical stripping, releasing Li ions back into the electrolyte and electrons into the external circuit. These Li ions and electrons move to the cathode, where they participate in the reduction of the $LiCoO_2$ structure (Figure 2.3) [77]. Specifically, this reduction process involves the intercalation of Li ions into the layered structure of $LiCoO_2$. Such a cycle of Li ion migration and electron flow enables the storage and release of electrical energy. And the electrochemical reactions of LMBs using $LiCoO_2$ cathode can be summarized as the following equations [78].

During charging:

$$\text{Anode: } xLi^+ + xe^- \rightarrow xLi$$

$$\text{Cathode: } LiCoO_2 \rightarrow Li_{1-x}CoO_2 + xLi^+ + xe^-$$

$$\text{In total: } LiCoO_2 \rightarrow Li_{1-x}CoO_2 + xLi$$

During discharging:

$$\text{Anode: } xLi \rightarrow xLi^+ + xe^-$$

$$\text{Cathode: } Li_{1-x}CoO_2 + xLi^+ + xe^- \rightarrow LiCoO_2$$

$$\text{In total: } xLi + Li_{1-x}CoO_2 \rightarrow LiCoO_2$$

2.1.5 Failure Mechanism of Lithium Metal Anode (LMA)

Equipping with Li metal anodes (LMAs) and commercial cathodes, the LMBs serve as a promising battery technology to enhance energy density. However, the formation of Li dendrites on the anode surface often leads to the failure of LMA and battery, exhibiting an inferior cyclic performance and even a short circuit. Fundamentally, Li

dendrites refer to the localized uneven nucleation and deposition of Li on the LMA surface during the plating process. There are various factors that affect the growth of dendrites, such as the substrate, the solid electrolyte interphase (SEI), the distribution of electric field and Li ions near the electrode surface [79-82]. Under the unfavorable factors, the uneven Li deposits gradually accumulate to form curved-, loose-, needle-, or mossy-like dendritic morphologies [83], which brings challenges in safety and cyclability of the battery. At present, the practical application of LMBs is still hindered by the Li dendrites [84-86], posing a significant obstacle to the industrialization of LMBs.

In Figure 2.4, the fatal challenges induced by Li dendrite in the LMBs are summarized [15]. Firstly, the dendrites increase the specific surface area of the electrode, further inducing the aggregation of Li ions at the dendrite tips. In this case, it exacerbates side reactions and irreversibly consumes active Li metal and electrolyte, which has a negative impact on battery performances. Additionally, during discharge, the high current density at the dendrite roots leads to rapid electron loss and potential fracture. As a result, the uneven detachment of dendrite is converted into the electrochemically inactive dead Li. The produced dead Li severely impedes the diffusion pathways of Li ions and electrons, leading to significant polarization and interface degradation, which eventually results in rapid capacity decay and poor cycling performance. Moreover, the continuous formation of dead Li causes severe structural damage to the LMA surface, resulting in numerous pores and Li metal pulverization, which leads to inevitable volume expansion [87, 88]. Commonly, volume expansion is an issue encountered by almost all electrodes during battery operation. For instance, a commercial intercalation-type anode like graphite exhibits a volume expansion of approximately 10% [89], while an alloy-type anode such as silicon shows a large volume change up to 400% [90]. Unfortunately, without the framework constraints, the volumetric expansion of Li metal can be nearly infinite during the deposition and extraction of Li ions, seriously affecting safety. Finally, dendrite formation on the anode surface may pierce the separator, reaching the cathode and causing internal short circuit within the working battery [91].

Meanwhile, the short circuit usually makes the battery extremely prone to safety issues such as thermal runaway and battery explosion, since the liquid electrolytes used in LMBs are mostly organic solvents with low ignition points. Overall, the practical application of LMBs remains severely constrained due to the instability of LMAs caused by Li dendrites. Therefore, achieving dendrite-free behavior and stable cyclic performance in LMBs is of great significance, facilitating progress towards their commercial viability.

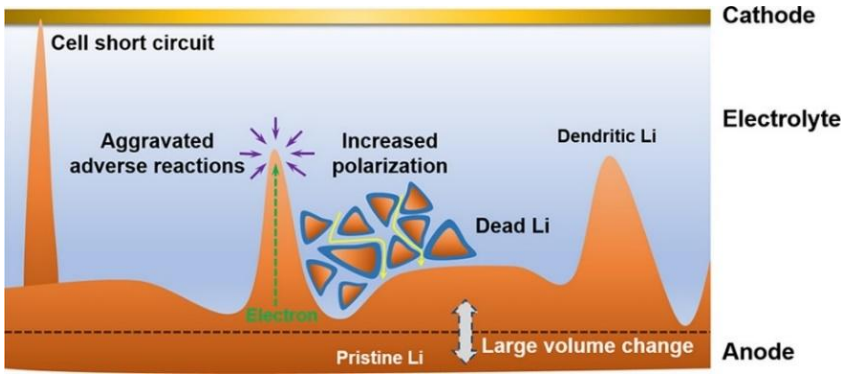

Figure 2.4 Scheme of fatal challenges caused by Li dendrite in LMBs [15].

In the subsequent sessions, we will offer a detailed introduction of the plating and stripping behaviors of LMAs. This introduction aims to enhance the understanding of the nucleation, growth, and dissolution processes of Li dendrites. By exploring the mechanisms, the key factors influencing dendrite formation can be clearly identified. In this regard, strategies to mitigate the dendrite growth for anode stabilization can also be developed.

2.2 Plating Behavior on LMA

Dendrite growth on the anode surface during the Li plating process is widely recognized as a key obstacle impeding the commercialization of LMBs. The existence of Li dendrites not only compromises the safety and efficiency of the batteries, but also limits cycling lifespan. To address this issue, it is essential to gain a thorough understanding of the plating behavior of Li, especially focusing on principles of the Li nucleation and

subsequent Li dendrite growth. Initially, we will introduce the various nucleation models to gain insights into the conditions and factors that influence the dendrite formation. Later, we will discuss the subsequent growth of Li dendrites after nucleation. Understanding the process of dendrite growth is beneficial for developing strategies to surpass the formation of dendrites.

2.2.1 Initial Nucleation Models

In LMBs, the anode of Li metal undergoes repeated plating and stripping on the substrate. Importantly, during the plating process of Li, the initial nucleation is crucial to determine the subsequent deposition behavior. Typically, the Li nucleation process is governed by both kinetic and thermodynamic factors. Over the past 40 years, several meaningful and foundational models have been developed to explain the initial stage of nucleation during the Li plating process [92, 93]. These models include the heterogeneous nucleation model [94, 95], the space-charge model [96], and the solid-electrolyte interphase (SEI)-induced nucleation model [97, 98], etc., both of which provide important insights into the mechanisms influencing Li nucleation.

Heterogeneous nucleation model: In Figure 2.5, the mechanism of Li nucleation on the framework is illustrated, involving the adsorption of Li ions, bond formation, and charge transfer of electrons [99]. Specifically, Li ions in the solvated structure gradually detach from the solvent molecules, then gain electrons for reducing Li ions to establish a new chemical bond on the framework surface [100]. This process, where Li ions receive electrons and subsequently deposit onto the framework/current collector, is characterized as heterogeneous nucleation. In other words, the heterogeneous nucleation process refers to the formation of a new phase at preferential sites on the surface or interface. According to the previous research by Ely's team [101], this process involves several stages, mainly including the initial nucleation suppression stage, then the incubation stage, and the subsequent growth stage. In addition, through theoretical simulation, they clarified the key factors affecting heterogeneous nucleation

from the perspectives of thermodynamics and kinetics, such as overpotential, surface tension, electric fields distribution, etc. As such, the heterogeneous nucleation can be stabilized by controlling the applied potential of the battery system and the roughness of the plating surface.

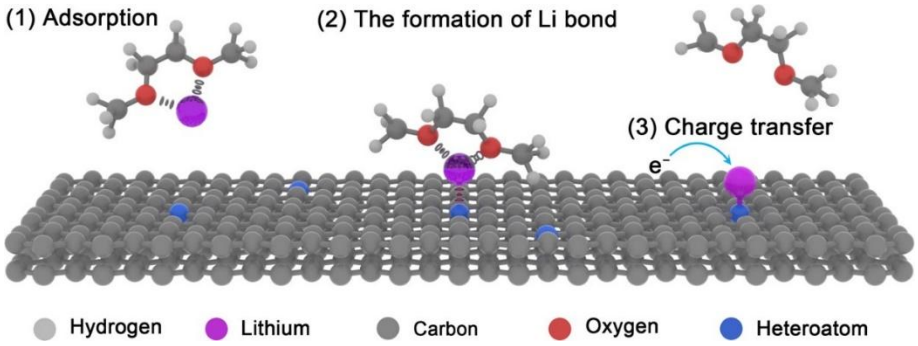

Figure 2.5 Scheme illustration of Li nucleation on the framework [99].

Additionally, the initial heterogeneous nucleation was also explored by Cui's group [94, 102]. They discovered that the nucleation of Li metal is influenced by the type of substrate, revealing a substrate-dependent pattern. For the substrate of Cu (Figure 2.6a), a certain amount of overpotential (~40 mV) was necessary to overcome the barrier for heterogeneous nucleation caused by the significant thermodynamic mismatch between the Cu and Li. In contrast, the gold (Au) could alloy with Li, resulting in a heterogeneous nucleation overpotential of zero (Figure 2.6b). Importantly, Li preferentially deposited on the Au strip rather than on the Cu foil (Figure 2.6c-2.6e), demonstrating that the heterogeneous nucleation model was selective and could be intentionally induced Li deposition. Moreover, the crucial influence of current density on the initial nucleation process was also investigated in depth [94]. It was found that the nuclei size decreased with increasing overpotential, while the nuclei number was proportional to the cube of the overpotential. These studies advance our understanding of heterogeneous nucleation and facilitate the development of effective strategies to better regulate the initial nucleation process.

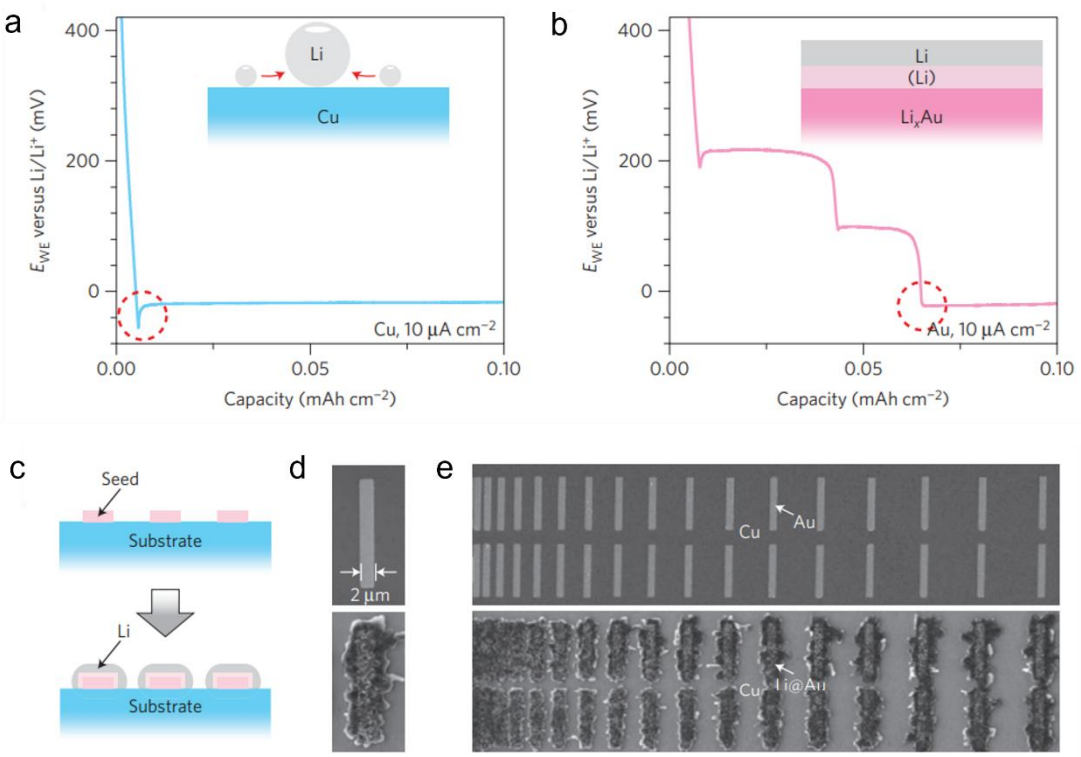

Figure 2.6 Capacity-potential curves of Li deposition on the substrate of (a) Cu and (b) Au. (c) Schematic illustration of Li deposition on the patterned seeds. (d, e) Morphologies of selective Li deposition on Au strips rather than Cu foil [102].

Space-charge model: In 1990, Chazalviel developed the space-charge model to clarify the distribution of LI ions in liquid electrolytes for understanding the nucleation of Li dendrites [96]. This proposed model suggested that uneven distribution of ion concentration near the anode surface would cause a substantial space charge and non-uniform electric field, thus resulting in the ramified Li deposition. Accordingly, when the current density (J) in the battery system is sufficiently lower than the critical current density (J^*), the ion concentration and Li deposition on the anode side remain uniform and stable. Conversely, excessive current density ($J > J^*$) would lead to ion depletion followed by unstable Li deposition, and dendrite growth.

$$J^* = \left(\frac{2eC_0D}{L}\right)\left(\frac{\mu_a + \mu_c}{\mu_a}\right)$$

where the e is cation charge number, C_0 is the original cation concentration, D

represents the diffusion coefficient, L means the distance between electrodes, μ_a and μ_c denote the mobility of anion and cation, respectively.

Based on the space-charge model, the time when dendrite formation starts is defined as the Sand's time (τ) [103]. Typically, when the τ is reached, the Li ion concentration at the anode surface drops to zero, and the resulting uneven electric field distribution initiates dendrite growth. According to the following equation, the time for Li dendrite growth is inversely related to the effective current density (J) at the electrode surface [104]. Typically, as shown in Figure 2.7, strategies involving lower current densities are effective in suppressing dendrite formation [105].

$$\tau = \pi D \left(\frac{C_0 e}{2J}\right)^2 \left(\frac{\mu_a + \mu_c}{\mu_a}\right)^2$$

where the e is cation charge number, C_0 is the original cation concentration, D represents the diffusion coefficient, J means effective current density, μ_a and μ_c denote the mobility of anion and cation, respectively.

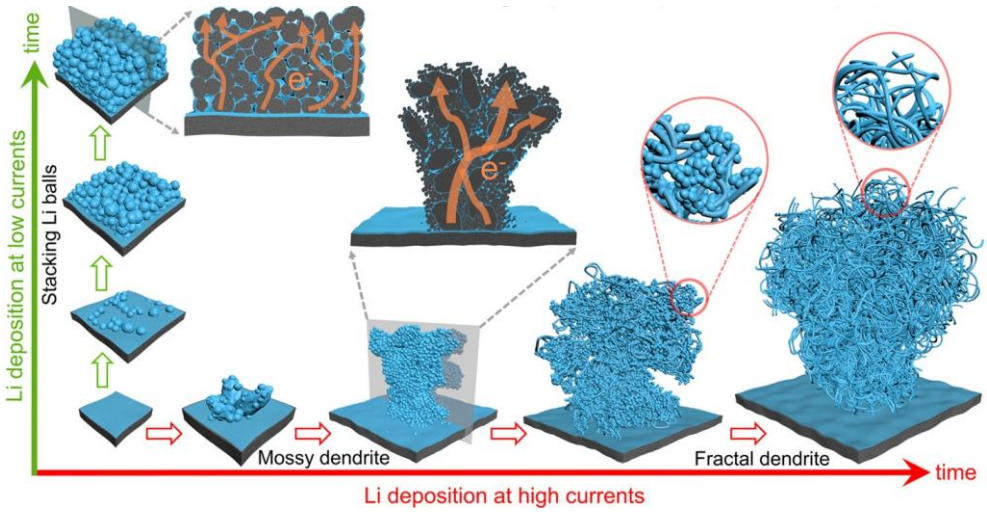

Figure 2.7 Scheme illustration of Li deposition under low and high current density [105].

SEI model: In contrast to conventional metals like Cu and Al, which possess high redox

potentials, Li metal exhibits an extremely high chemical reactivity. Consequently, when contacting electrolyte, a passivation layer of solid electrolyte interphase (SEI) is spontaneously formed on the surface of Li metal [106]. However, the SEI layer is prone to instability and easily cracks or ruptures due to significant volume expansion and mechanical stress during repeated process of plating and stripping. Such cracking of the SEI layer exposes fresh metallic Li, creating electrochemical hotspots that promote the uneven nucleation and subsequent dendritic growth [107, 108], which is regarded as the SEI model.

Specifically, Li ions can be transported to the reaction interface and tend to deposit more rapidly at the weaker points in the SEI film (Figure 2.8) [97]. This uneven deposition leads to stress concentration within the SEI. When localized stress exceeds the critical threshold, the SEI layer fractures to relieve the stress, typically near the junction of the root. The newly formed SEI film is relatively fragile, facilitating easier Li ion transport. Consequently, Li preferentially deposits and nucleates at the root, forming a new stress concentration, which causes the SEI film to rupture again. This process is repeated continuously, resulting in the formation of Li whiskers that extend in a single direction. As the deposition progresses, these Li whiskers grow and interweave, eventually forming a mossy or tree-like dendritic Li.

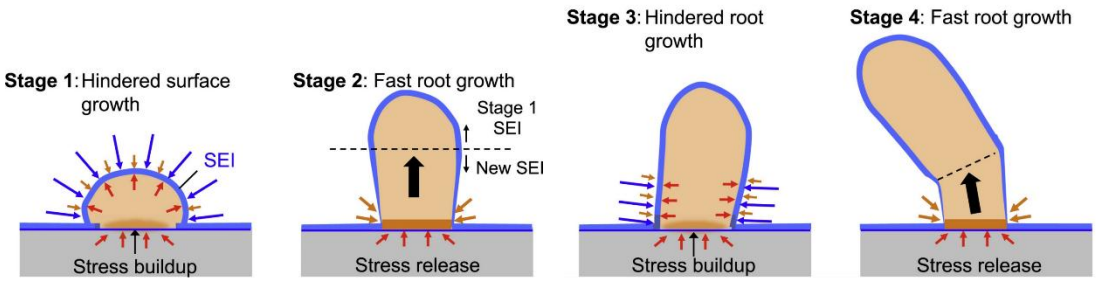

Figure 2.8 Schematic illustration of SEI-induced root nucleation and growth of Li whiskers [97].

In general, the fragile property, uncontrollable Li diffusion rate together with the

localized stress concentration in the SEI layer are the main causes for uneven Li deposition and dendrite formation. In this case, the corresponding guiding principles such as adopting a high-strength artificial SEI layer and designing a SEI film with high ionic conductivity would be beneficial for regulating the deposition behavior.

2.2.2 Dendritic Growth After Nucleation

Once nucleation occurs on the substrate or the current collector, uneven Li deposits would grow continually, resulting in dendritic formation with increased diameter and length. The growth of Li dendrite is a highly complicated process influenced by various factors.

Firstly, the direction and rate at which Li ions migrate, governed by the concentration gradient of Li ions and the distribution of electric field, significantly affect the growth rate of Li deposits. Additionally, external factors including the applied current density, the testing temperature, and the applied pressure also influence the internal electrochemical environment within the battery, thus affecting the process of Li growth. Moreover, the characteristics of the SEI film, including its mechanical strength and ionic conductivity, and the properties of the electrolyte, such as salt concentration and ionic mobility, also matter. Both of them play crucial roles in the subsequent growth of Li by determining the Li ion migration in the cell.

In the early stage of Li growth, the electric field serves as the primary driving force. As growth progresses, the process becomes a diffusion-dominated process. The diffusion-reaction model proposed by Akolkar specifically considered the transient diffusion transport of Li ions in the diffusion boundary layer [109]. Normally, the growth of Li dendrites is highly related to the current density. At a lower current density, the growth rate of Li dendrites decreases. According to the estimation of Akolkar's model, when applying a high current density of 10 mA cm^{-2}, the growth rate of Li dendrites was approximately 0.02 mm s^{-1}, which aligned with the results reported by Nishikawa [110].

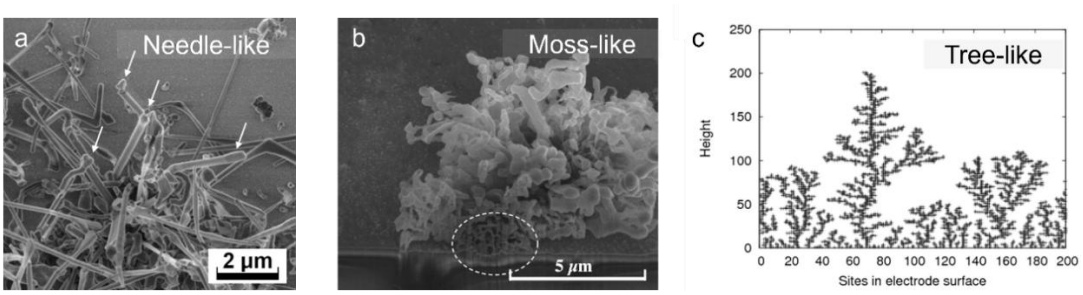

Figure 2.9 The dendrite morphologies with (a) needle-like, (b) moss-like, (c) and tree-like structure[111-113].

It is difficult for Li to grow with a stable and regular structure. Generally, Li metal tends to grow in dendrite morphology rather than depositing smoothly. The dendritic morphology can be categorized into three patterns based on their growth structure: needle-like [111], moss-like [112], and tree-like morphologies [113], as illustrated in Figure 2.9. Unfortunately, these morphologies promote the production of inactive Li and result in electrolyte depletion due to their large specific surface area. This leads to an irreversible loss of active components and a sharp increase in interfacial impedance, significantly hindering battery performance. Moreover, the Li dendrites may penetrate the soft separator, which causes the failure of the battery with an internal short, posing a severe safety risk.

Understanding dendrite growth and its morphologies are necessary, which is beneficial for us to design effective solutions to inhibit dendrites and regulate uniform Li growth. Overall, in order to enable the LMBs with improved cyclic stability and extended lifespan, it is crucial to avoid the uneven Li nucleation and irregular Li deposition through various advanced techniques or strategies.

2.3 Stripping Behavior on LMA

The plating behavior with a particular emphasis on the nucleation model and subsequent growth of dendrites has been mentioned above, which reveals the formation of metallic dendrites and related factors. As for a practical anode of Li metal, the

stripping process is as essential as the plating process. This section will focus on the stripping behavior of Li.

2.3.1 Stripping Process

The stripping process inevitably affects the subsequent plating process and cycling performance [114-116]. In contrast to traditional intercalated-based anodes, such as graphite, the anode of Li operates through a conversion mechanism involving Li ions, Li atoms, and electrons in electrochemical reactions.

During stripping, Li metal undergoes an electrochemical reaction where it loses electrons, as depicted in the following equation. Once oxidized, Li ions detach from the anode and move into the electrolyte environment through the SEI layer. Typically, during this dissolution process, uneven stripping of Li dendrites would cause the formation of inactive/dead Li, which leads to the irreversibility of deposited Li, inducing significant loss of active materials and poor electrochemical performance. In this regard, it is crucial to carefully consider factors such as the interfacial reaction rate and the diffusion rates of Li ions when regulating the stripping behavior.

$$Li - e^{-} \leftrightarrow Li^{+}$$

2.3.2 Stripping Models

Huang's research team proposed models for stripping to fully discover the connection between the dissolution sites and inactive/dead Li formation. In total, three models were given according to the locations of dissolution (Figure 2.10), including top, bottom, and a combination of top and bottom [117].

Top-stripping model: In the scenario where stripping occurs from the dendrite tip, no dead Li is generated because the Li dendrites maintain firm contact with the substrate/current collector. With repeated stripping, most of the metallic dendrites can dissolve without forming dead Li, demonstrating the most favorable stripping

performance.

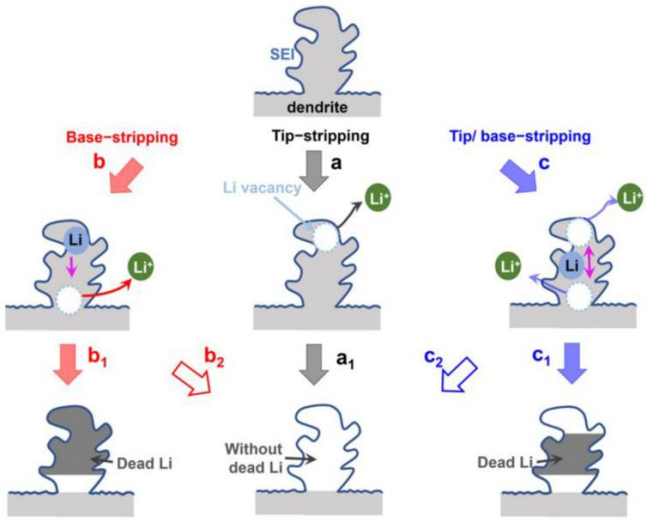

Figure 2.10 Schematic of three stripping models [117].

Bottom-stripping model: Since the dendrite root is revealed with a much higher current density in contrast to the top sites, the stripping process is more likely to occur at the root, inducing a bottom-stripping model. As a consequence, more active Li will be directly removed from the bottom side and finally result in inactive Li or dead Li. In this case, to mitigate the production of inactive Li or dead Li, it is essential to decrease the diffusion rate of Li ions around the dendrite root. Additionally, the self-diffusion rate of Li atoms within the anode should be increased and regulated. This can be achieved by enhancing the number of vacancies and improving the vibrational energy of Li atoms.

Top/bottom-stripping model: In terms of the combined top/bottom-based stripping model, both the top site and the bottom site of a Li deposit are considered active spots for the electrochemical stripping process. In this context, it is advantageous to develop an appropriate structure, such as a heterostructure or a gradient design of electronic conductivity, to promote a faster stripping rate at the top site. Consequently, the dead Li formation could be effectively suppressed.

2.4 Strategies for Stabilizing LMA

As previously discussed, Li dendrites cause the poor cycling performance (e.g., rapid capacity decay and limited lifespan) and even pose a severe safety hazard to LMBs. In this case, providing practical guidance on Li deposition behavior and developing effective strategies to suppress dendrite formation are critical missions for realizing the practical LMBs with high performance. In recent years, substantial efforts have been made by researchers to stabilize the LMA, contributing to the remarkable advancements in this field.

2.4.1 Applying Artificial SEI Layer

The mismatch between the rapid charge transfer kinetics on the surface of the anode and the slow mass transport process at the interface is a key electrochemical factor contributing to dendritic deposition. Note that the charge and discharge kinetics of the Li anode are highly related to the SEI layer, researchers can regulate a desirable SEI layer to facilitate the kinetics process of charge transfer and mass transport during cycling. It was reported that the electrochemical kinetics, specifically ionic conductivity, and the mechanical properties, such as strength, of the SEI layer were crucial factors in determining the deposition behavior of Li [118]. Consequently, in recent years, research on artificial SEI layers has gained significant attention [119-124], so as to prevent the growth of metallic dendrites and ensure even plating behavior.

The artificial SEI layer is an especially engineered thin layer located on the anode surface, serving as an interface to separate the Li and bulk electrolyte. A favorable SEI layer should equip itself with good ionic conductivity while providing electronic insulation (Figure 2.11a) [125]. Importantly, a robust mechanical stability of the SEI layer is also essential, which can endure significant volumetric changes and inhibit the formation of dendrites. As such, current studies mainly concentrate on two directions: one aims to enable the SEI layer with high ionic conductivity to facilitate the efficient

mass transfer of Li ions on the electrode surface; the other seeks to improve the target SEI layer with improved mechanical strength to suppress dendrite formation.

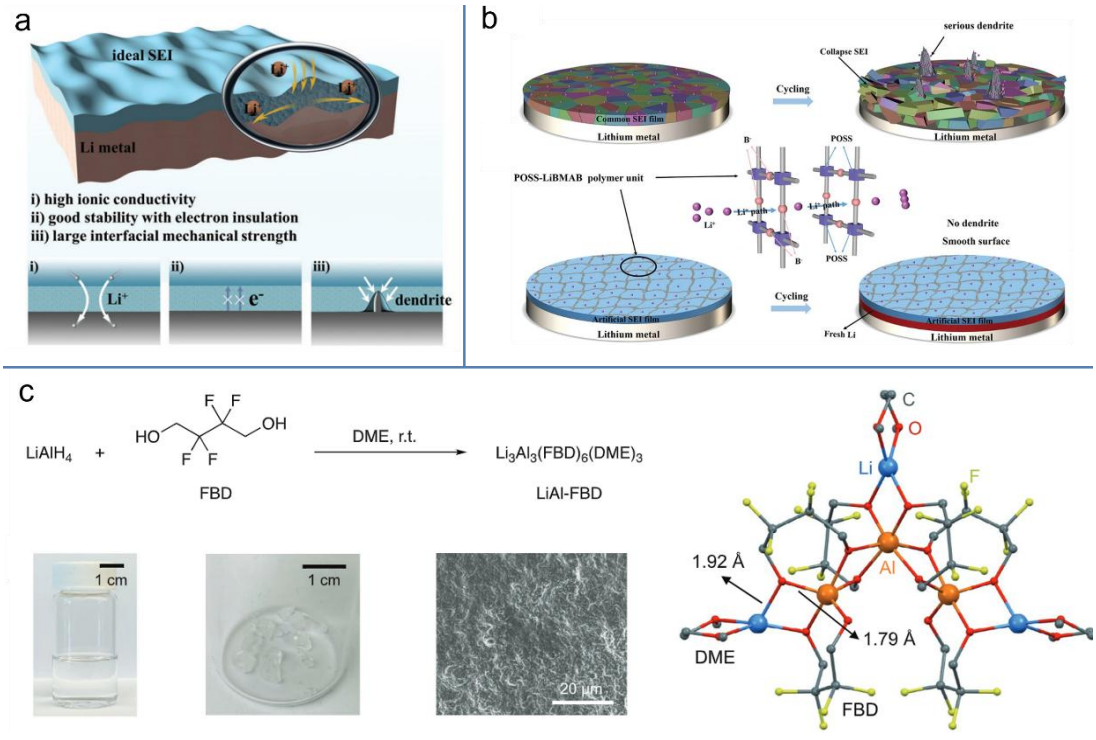

Figure 2.11. (a) Scheme illustration of a favorable SEI layer [125]. (b) Dendrite-free behavior achieved by applying an artificial SEI strategy [126]. (c) The fabrication process of a target SEI layer [127].

A novel polymer-based SEI layer with better ionic conductivity and higher transfer number of Li was designed on the anode surface [126]. Such a layer was beneficial for promoting a faster Li ion transportation, which could regulate the Li deposit beneath this artificial layer (Figure 2.11b), thus contributing to a dendrite-free behavior for longer cycling life. Results demonstrated that the LMA could maintain a stable electrochemical performance with a well-extended cycling lifespan for more than 1000 hr when adopting the artificial SEI layer.

In addition, in a joint effort between academic and industrial researchers, an SEI artificial layer with high mechanical strength was developed [97]. The morphology and molecular structure of the artificial layer achieved through a facile solution approach

were given in Figure 2.11c. This innovative layer with crystalline structure endowed itself with a high modulus while exhibiting a good ionic conductivity. Both of these characteristics benefited the stabilization of the Li anode, thus realizing a better cycling stability of LMBs.

However, in systems of LMBs where Li utilization is high, the electrochemical kinetics and mechanical stability of the artificial SEI layer still need to be further enhanced. Because there will be a huge structural change on the interface and electrode caused by large depths of discharge and charge. Meanwhile, researchers should also persistently develop effective protection strategies and investigate the underlying mechanisms to further stabilize LMAs for high-performance LMBs.

2.4.2 Engineering Electrolyte

Electrolytes are significantly crucial to the electrochemical performances of batteries [128]. They facilitate the movement or transfer of ions between the anode and cathode, effectively connecting the two electrodes to ensure the proper functioning of a working battery. In the field of LMBs, electrolytes are particularly important since they have the ability to stabilize the interfaces between the electrolyte and electrodes during cycling. In this regard, engineering the electrolyte comes as a facile strategy to achieve stable LMBs.

Typically, by engineering liquid electrolytes, it is possible to simultaneously adjust the structural characteristics of the SEI layer and the morphology of Li deposition. This strategy holds promise for improving the cycling stability of LMAs. Admittedly, compositions of the SEI layer, were directly influenced by the electrolyte used in the battery system [129]. Meanwhile, the interfacial properties, deposition behavior, and the electrochemical performances of the battery were then affected. As shown in Figure 2.12a, if a commercial electrolyte of EC/DEC with 1M $LiPF_6$ was employed, the Coulombic efficiency (CE) of the battery was no more than 80% with limited cycle life. When replacing it with a high concentration electrolyte (6M LiFSI EC/DEC), the CE

of the cell was effectively enhanced by ~ 98% while the cyclic life was also prolonged.

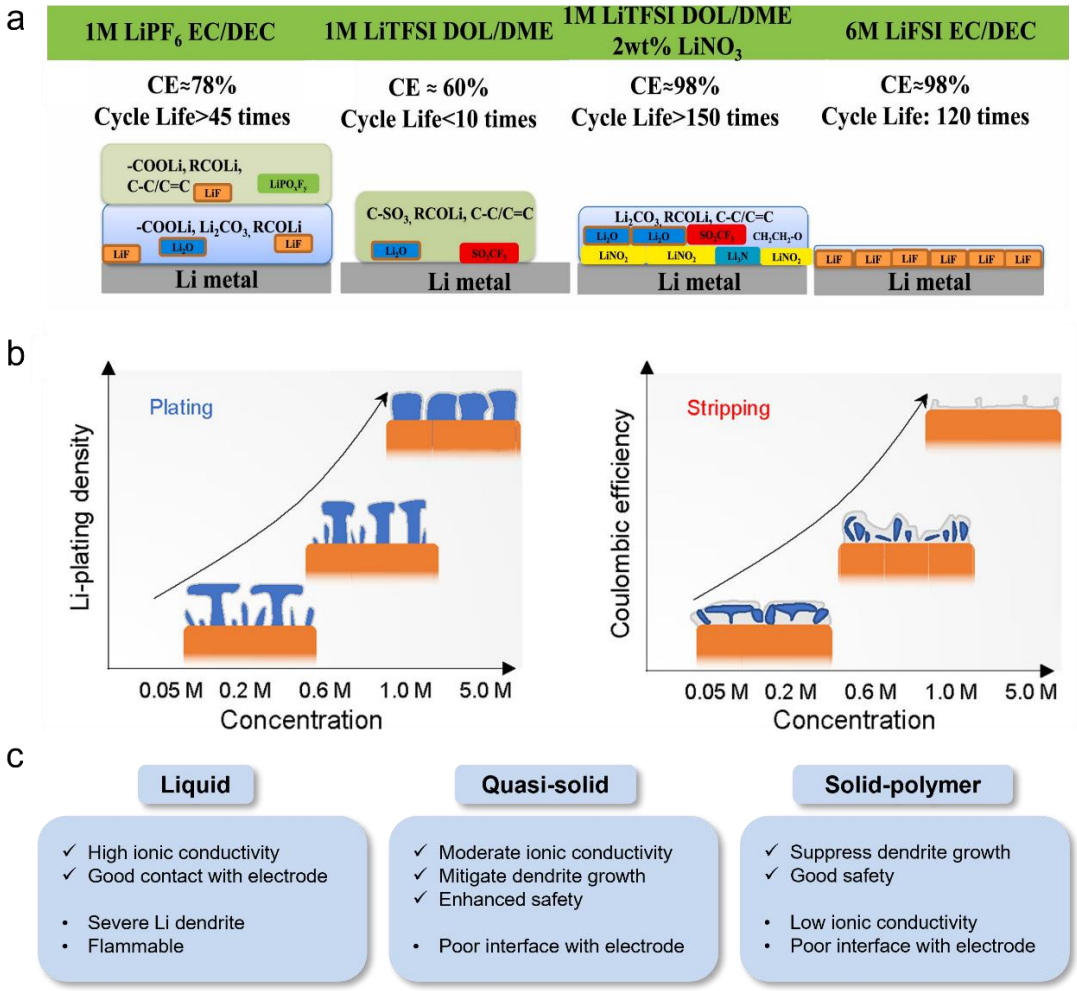

Figure 2.12 (a) The SEI properties and electrochemical performances of LMAs under various electrolyte system [129]. (b) The plating and stripping morphologies and corresponding performance under different salt concentrations in electrolyte [130]. (c) comparison of liquid-based, quasi-solid-based, and solid-polymer-based electrolytes.

Since the interfacial properties are determined by electrolyte, the selection of electrolyte also influences the relevant performance of LMBs, including the rate capability, fast-charging performance, and operational temperature window [131]. Recent advancements in liquid electrolyte engineering, including the optimization of additives [132], the adjustment of solvent formulations [133-135], and the employment of high-concentration electrolytes [136, 137], etc., have significantly improved the recyclability

and stability of LMBs.

For instance, a study of Li salts concentration ranging from 0.05 M to 5 M in common DME solvent revealed the critical role of salts in determining deposition morphology and cycling reversibility [130]. It was observed that a high concentration of Li salts promote the formation of dense yet large Li deposits during the plating process, while facilitating a better stripping process with much less amount of Li residual (Figure 2.12b). The as-improved plating and stripping behavior were beneficial for achieving better reversibility of the battery with a high CE and extended cycling life. Additionally, Bao's research group developed a novel solvent for enhancing the electrolyte stability through extending its -CF_2- main chain [138]. Specifically, a dual-solvent electrolyte was established after mixing it with DME solvent and Li salts. This advanced electrolyte system could not only achieve a high CE of >99%, but also achieve an ultrahigh oxidation stability up to 6 V.

Quasi-solid-state and solid-state electrolytes have also been utilized in LMBs due to their high mechanical modulus, which can effectively suppress the growth of Li dendrites. Recently, Chen's group reported long-life LMBs by adopting a quasi-solid electrolyte [139]. The quasi-solid electrolyte design involves novel materials and a charming skeleton with multi-level ion transport pathways. Consequently, this developed quasi-solid electrolyte accelerated ionic transportation and contributed to the long-life cycling of LMBs. An impressive lifespan of 3000 working cycles in the full cell was successfully achieved. Nevertheless, the quasi-solid and solid-state electrolytes inevitably have thicker electrolyte layers, leading to lower energy density, which requires further enhancement in the future. Their specific properties are also summarized in Figure 2.12c. In comparison to flammable liquid-based electrolytes, both quasi-solid and solid-state electrolytes are beneficial for battery safety. However, the interfacial issues in quasi-solid and solid-state electrolyte also need to be addressed.

2.4.3 Modifying Separator

The separator plays a crucial role in the battery by preventing direct contact between electrodes while facilitating ion transport. Typically, porous polyolefin films, such as polyethylene (PE) and polypropylene (PP), are commonly used as separators in LMBs [140, 141]. However, traditional separators of PE and PP face challenges due to their relatively poor thermal stability, which would lead to thermal runaway when battery shorts caused by dendrite issues [142, 143]. Moreover, the mechanical stability, ionic conductivity, and wettability of polyolefin-based separators are still far from satisfactory.

According to the investigation by Howlett [144], an advanced separator is highly crucial to the battery's cycling life since it could be beneficial in many aspects, including building a stable SEI layer, suppressing dendrite formation, reducing electrolyte depletion. Hence, modifying the separator to achieve high-performance LMBs, is a promising strategy [70]. The separator primarily acts as a physical barrier within the battery, preventing direct electrode contact and inhibiting Li dendrites from bridging two electrodes, which could result in a short circuit. Both novel coating and smart structural design can be adopted to alter the separator, thus optimizing the ionic transport channel within the battery, which is closely linked to the plating behavior. Importantly, constructing a functional separator will not significantly sacrifice the energy density of LMBs since it does not introduce great changes in mass weight and volume. Thus, developing functionalized separators offers an effective solution for realizing practical LMBs with well-regulated deposition behavior and stable electrochemical performance.

In recent years, researchers have been exploring innovative separators aimed at enhancing wettability, mechanical properties and ionic transportation [145, 146]. For example, two layers of PAN-based functional nanofiber were combined to serve as the separator (Figure 2.13a), which could not only facilitate a rapid yet high-amount uptake

of the electrolyte, but also strengthen the thermal and mechanical stability [142]. Meanwhile, it also promoted the Li ion transport with an improved transference number. Result found that the LMBs employing this advanced PAN-based separator could achieve a better electrochemical performance with a capacity of more than 1300 mAh g^{-1} even cycling at a high C-rate. Additionally, a separator modified with an anionic MOF materials was designed (Figure 2.13c), which also showed significant improvement in terms of Li ion transport, thereby enhancing the electrochemical stability of LMAs despite cycling under high current density [147].

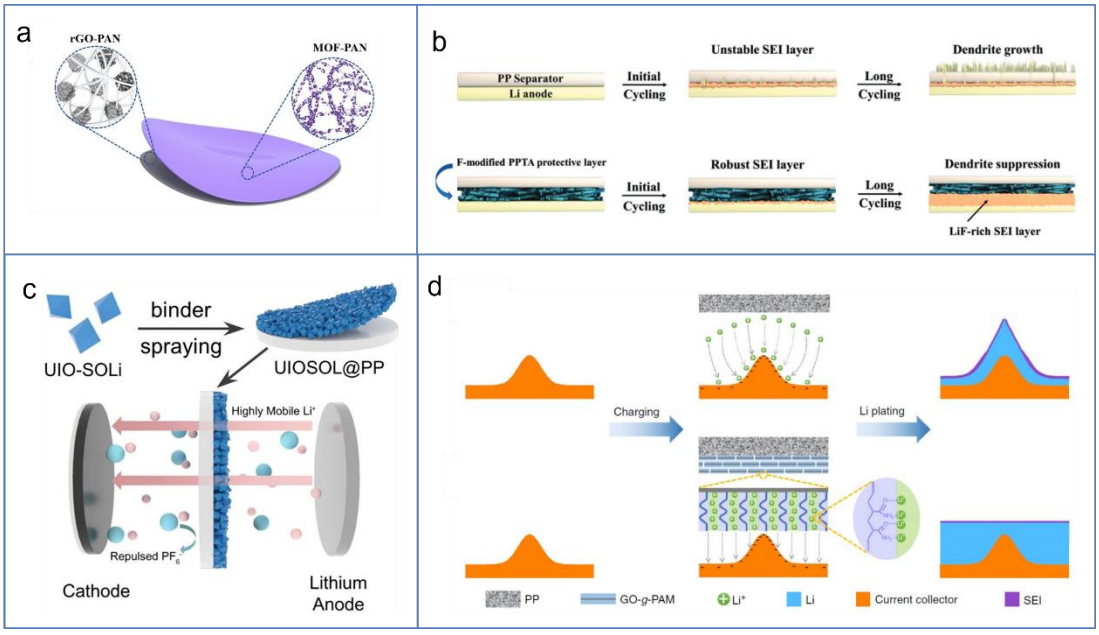

Figure 2.13 (a) Schematic illustration of functionalized PAN-based separator [142]. (b) Comparison of cycling behavior between commercial PP separator and modified separator [148], (c) The fabrication and design principle of a novel PP-based separator [147]. (d) The schematic diagram of improved plating behavior through modifying the PP separator [149].

Moreover, a modified PP-based separator with enhanced Li wettability and mechanical stability was achieved by adopting the fluorine-treated thermal-stable nanofibers as a protective layer for the PP separator [148]. Consequently, apart from the contribution to thermal safety, the stable cyclic performance of batteries was also gained with a

desirable SEI layer and satisfactory dendrite suppression (Figure 2.13b). Furthermore, a novel separator was designed by introducing functional GO-based materials and lithiophilic modification on the PP film (Figure 2.13d) [149]. Significantly, this design could facilitate a fast diffusion rate of Li ions while promoting homogeneous Li ion distribution on the surface of the anode. By using this modified separator, an even Li deposition behavior and a high electrochemical reversibility of batteries were achieved. The as-assembled full cells also demonstrated an outstanding long-term cycling stability with a lifespan of over 1900 hr.

Overall, the strategy of separator modification has demonstrated its effectiveness on the stabilization of anode and battery. Since there is still a risk of the coated active material falling off from the separator and the modification technology is not mature enough, great efforts are still needed for the development of the next-generation separator.

2.4.4 Adopting 3D Current Collector

The approach of utilizing a three-dimensional (3D) current collector that possesses both good electrical conductivity and mechanical flexibility is particularly appealing for stabilizing LMAs [150, 151]. Compared with the traditional current collector of Cu foil, this 3D framework not only imparts flexibility to the battery system but also provides better charge transfer due to its porous or hierarchical nature. Moreover, the 3D substrate, with its large specific surface area, significantly promotes a uniform plating behavior by offering a shorter diffusion path [48]. Typically, it is effective to suppress dendrite formation by lowering the localized current density and enhancing the stability of the SEI layer. Additionally, the 3D current collector with porous structure provides abundant space to accommodate Li during deposition and extraction in the charge and discharge cycles, thus beneficially mitigating volume expansion. Therefore, integrating Li metal with a 3D current collector has drawn increasing interest in recent years.

In general, a charming 3D current collector should possess the merits of excellent mechanical properties, a large surface area, and a high lithiophilicity. Based on Sand's

time model [92, 152], the adoption of 3D hosts with a specific large surface area would effectively lower the localized current density, which is beneficial for delaying the ion depletion at the anode surface, thereby inhibiting dendrite formation. Meanwhile, the 3D framework can offer additional pathways for ion diffusion along the boundaries of voids, which promotes the ionic transportation and effectively homogenizes the distribution of Li ions [153].

Usually, a strong binding energy between the substrate and Li results in a desirable lithiophilicity [154]. Apart from the binding energy, the investigation, such as the nucleation barrier and the molten Li wettability could also be adopted, to assess the lithiophilicity of substrates. Notably, the lithiophilic modification on the 3D framework contributes to regulating the uniform deposition behavior of Li. Because the lithiophilic materials have a higher affinity for Li, thus lowering the thermodynamic mismatch with reduced nucleation barrier. However, the inherent lithiophilicity of current collector materials is generally poor, which needs strategies to enhance their affinity for Li. One approach involves the modification of the 3D substrate with oxygen-containing functional groups [155], which is able to adjust the distribution of surface electrons and thus improve the lithiophilicity of the system. Additionally, the introduction of lithiophilic materials such as Au [156], Ag [157], and ZnO [158], on the 3D framework is a feasible choice. Because they could serve as nucleation seeds to promote uniform Li deposition on the substrate. Studies also found that heteroatom doping was effective in enhancing Li affinity [159, 160], by altering the electron structure or the interlayer spacing of substrate materials, thereby generating numerous active sites.

In this regard, mechanically robust and electrically conductive 3D frameworks with microstructures or lithiophilic integration are highly preferred. For example, a Cu foam with a hierarchical structure of nanowires was further treated with lithiophilic antimony (Sb) [161], which could not only provide massive rooms to alleviate the volume expansion, but also regulate a uniform distribution of Li ion flux (Figure 2.14a). As such, by using the modified 3D substrate to host Li, it exhibited a dendrite-free behavior

and achieved a stable cycling life of more than 900 hr with much-reduced overpotential. Apart from the above-mentioned metal-based porous framework, polymer-based 3D current collector also shows the feasibility in regulating Li deposition. In 2016, Cui's group reported a thermally stable polyimide (PI) fabric with lithiophilic ZnO modification to serve as a promising matrix to host Li through the thermal infusion method (Figure 2.14b) [162]. Uniform plating/stripping behavior was found on the as-fabricated Li composite anode while the volume expansion during cycling was minimized. Meanwhile, due to the introduction of lithiophilic ZnO, the overpotential of the battery system was also significantly reduced.

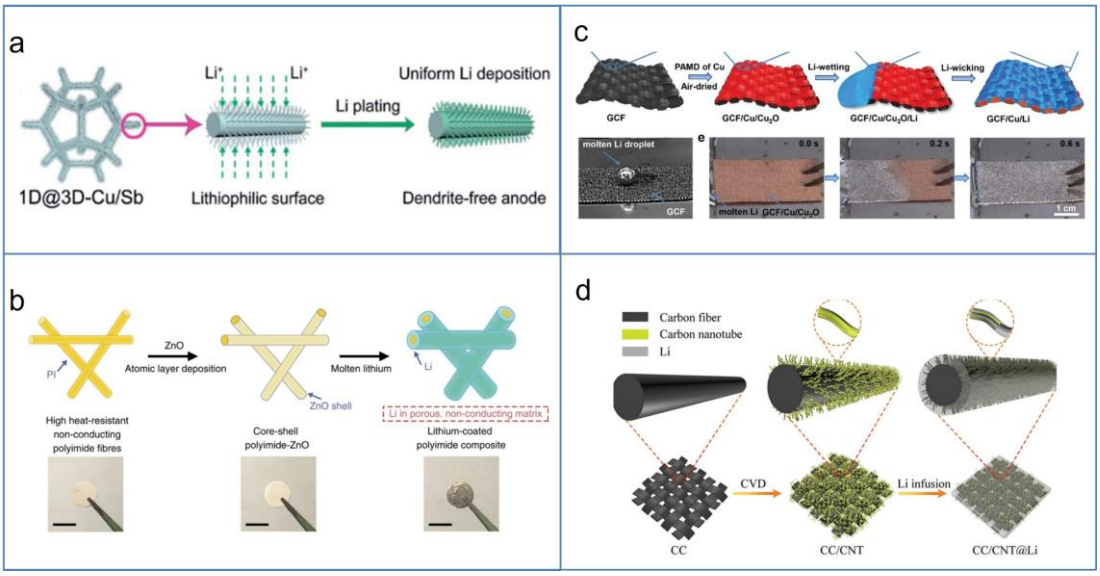

Figure 2.14 Various 3D substrates with lithiophilicity design to host Li metal, including (a) Cu foam [161], (b) PI fabric [162], and (c, d) carbon cloth [41, 163].

Since the polymer-based matrix is usually non-conductive, the use of carbon-based materials, such as carbon fiber or carbon cloth, as 3D hosts has received increasing attention [164-166]. For instance, the Cu/Cu2O modified carbon cloth was used as a viable 3D substrate for carrying molten Li to develop a mechanically flexible and electrochemically stable Li composite anode (Figure 2.14c) [41]. Remarkably, this method offered a highly scalable strategy that achieved an ultrafast fabrication speed, meeting the production requirements for industrial applications. Additionally, the

carbon nanotube (CNT) was employed to modify the lithiophobic carbon cloth as depicted in Figure 2.14d [163]. With the lithiophilic nucleation sites and abundant buffering space, the battery using this 3D current collector presented a desirable deposition morphology and achieved a better cycling stability of more than 500 hr.

In section 2.4, we mainly introduce four strategies to stabilize LMAs, including constructing artificial SEI, engineering electrolyte, modifying the separator and adopting a 3D current collector. These strategies have demonstrated their effectiveness in suppressing dendrite formation to some extent, promoting to realization of LMBs with stable cycling life. However, most of these strategies are carried out under a large excessive amount of Li metal, which significantly hinders the practical use of the LMBs due to the resulted low energy density. Meanwhile, the flexibility of the LMAs remains poor. In other words, despite the progress in anode stabilization, joint efforts are still needed to pave the way for next-generation high-performance LMBs.

Chapter 3 Development of High-Performance LMBs

3.1 Thin Lithium Metal Anodes (LMAs)

3.1.1 Significance of Adopting Thin LMAs in Batteries

In terms of practical application, the lithium (Li) metal batteries (LMBs) are hindered by their cyclability performance and safety issues due to the uncontrollable Li dendritic growth on the anode surface. As a consequence, great efforts have been made to suppress dendritic growth for anode stabilization, which has been discussed in the previous chapter. However, many approaches proposed are based on the employment of thick Li foil (400~750 μm in thickness). As such, the practicability of LMBs remains unsatisfactory since the stabilization of batteries is usually at the cost of energy density due to the large excessive amount of Li metal involved in the cell configuration.

Considering practical applications, equipping with thin LMAs in battery configuration is of great significance [28-31]. On the one hand, using the thin LMA can simultaneously promote the battery with remarkably enhanced gravimetric energy density and volumetric energy density by reducing the unnecessary weight and thickness of the anode. On the other hand, it facilitates the battery with a low yet appropriate capacity ratio of negative to positive electrode (N/P ratio), making the testing result more reliable instead of misleading. Meanwhile, adopting thin LMAs to replace thick ones can save both cost and resources. Furthermore, it also contributes to improving battery safety due to the less high-reactivity active material involved.

Typically, thin LMA is defined as possessing a thickness of the Li layer of no more than 50 μm. Theoretically, a 1 μm Li layer corresponds to a capacity of 0.2 mAh cm^{-2}. In this regard, a 50 μm Li metal equals 10 mAh cm^{-2}, which can promote an appropriate N/P ratio in the battery when using practical cathodes with an areal capacity of >3 mAh cm^{-2}. As shown in Figure 3.1a, by thinning the Li layer from 400 μm to 50 μm, the

oversized Li in the battery system can be significantly reduced from 1800% to 19%. Meanwhile, the gravimetric energy density of the battery can be meaningfully enhanced by ~35% with a value of over 300 Wh kg^{-1} when replacing the 400-μm thick Li with a thinner one (50 μm). It reveals that adopting thin LMAs can effectively improve the energy density and enhance Li utilization in the battery. In addition, it promotes the battery with remarkably enhanced volumetric energy density by reducing the unnecessary thickness of the anode. The stack volumetric energy density of Li-ion battery is around 700 Wh L^{-1} while the LMB using the 150 μm-thick Li metal anode fails to reach the value of 500 Wh L^{-1} (Figure 3.1b) [167]. In contrast, if using a 15 μm-thick Li layer as anode, the LMB can deliver a remarkably high value of 1090 Wh L^{-1}. Therefore, thinning LMAs is of great importance for the development of practical LMBs with enhanced energy density.

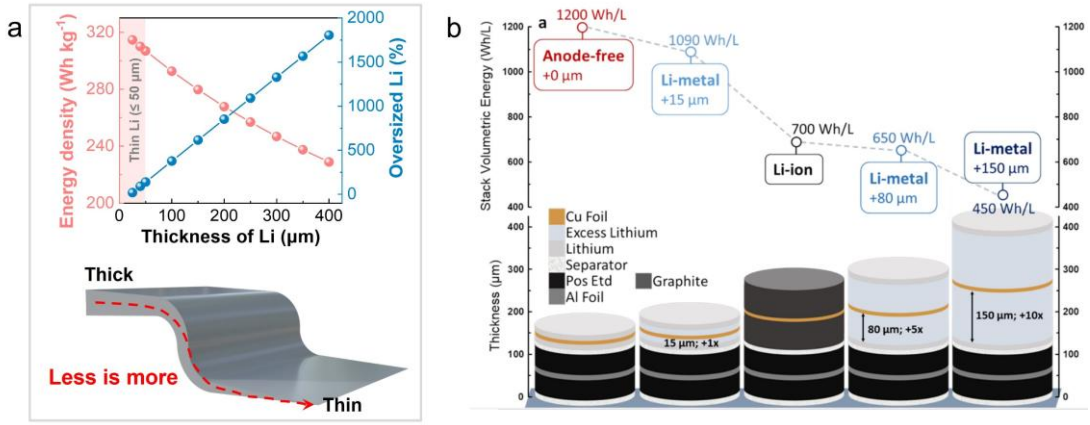

Figure 3.1 (a) The gravimetric energy density and oversized Li of LMBs as a functional of the thickness of LMA. (b) The comparison of the volumetric energy density of batteries as a function of the thickness of the LMA [167].

3.1.2 Approach to Achieve Thin LMAs

So far, there are four main kinds of approaches to achieve thin LMAs. Firstly, the physical vapor deposition method can produce a high-purity Li layer with precisely controlled thickness [168]. The process involves vaporizing Li and allowing it to

condense onto a substrate, finally forming a target thin LMA. For example, a 10 μm-thick Li layer was successfully developed on the surface of the solid electrolyte (Figure 3.2) [18], which showed a reduced interfacial resistance, thus improving the electrochemical stability. However, the PVD technique requires massive effort in vacuum maintenance to avoid the contamination of Li species. Besides, it shows low fabrication throughput and high manufacturing cost, which is unlikely to be adopted in large-scale industrial production.

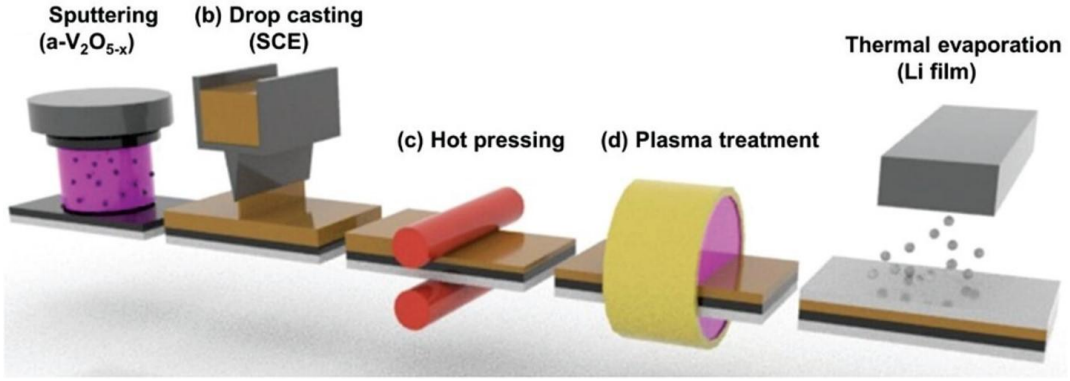

Figure 3.2 Thermal evaporation to develop the thin Li film on the surface of solid electrolyte [18].

Secondly, the technique of electrodeposition involves depositing Li ions onto a substrate through an electrochemical process [39, 46, 169]. It can also precisely control the Li amount deposited on the substrate, which is a commonly used approach in laboratory research. For instance, Zheng's group reported a metalized fabric, which was employed as a promising host for Li metal anode via the electrodeposition method, enabling the cell with controlled Li loading of only 100% oversized than sulfur cathode (Figure 3.3a) [24]. The as-developed Li/CuCF anode demonstrated a stable cycling life with the lowest overpotential (Figure 3.3b). The feasibility of this thin LMA in pairing with S cathode was also investigated, showing an excellent cycling stability of 260 cycles even at a high sulfur loading of 3.2 mg cm^{-2} (Figure 3.3c and 3.3d). However, the electrodeposition still involves a resource- and time-consuming assembly and disassembly process. Additionally, it is a low-efficiency way with a complicated

process and inevitable component introduction, which may also hinder large-scale production.

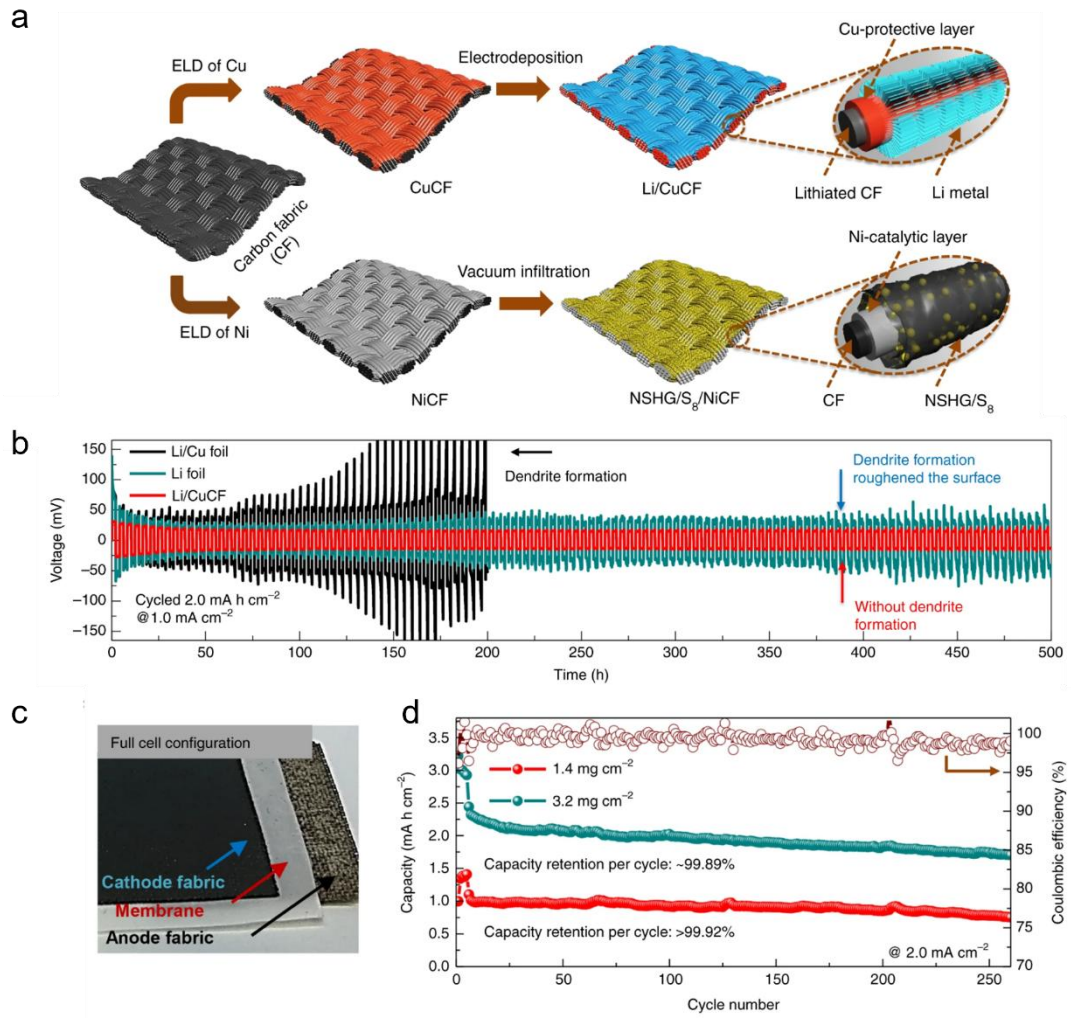

Figure 3.3 (a) The electrodeposition was adopted to developed only 1-fold excess thin Li composite anode, (b) the electrochemical stability of symmetric cells using different Li-based electrodes, (c) the full cell configuration of fabric-based Li-S battery, and (d) corresponding cycling performance [24].

Thirdly, in comparison, the thermal melting method is a facile and efficient way to rapidly develop the thin LMA. In this approach, Li is melted and then spread on/into the substrate. Normally, the substrate will be modified with microstructure or coated with lithiophilic layer, to promote the wetting process [33, 162, 170]. Figure 3.4 shows the thermal processing for thin LMAs preparation, including stamping [171], infusing

[30], and blading [172]. Specifically, Hu's group achieved a Li-Sn alloy anode with a thickness of 15 μm through directly stamping the molten Li-Sn alloy on the Cu substrate [171]. And the cycling life of the as-prepared pouch cell can sustain 25 cycles. Cui's team developed an ultrathin yet freestanding LMA by infusing the molten Li into the graphene oxide host [30]. Typically, by controlling the thickness of the host material, the targeted LMA thickness could be well-adjusted. It should be noted that the process for thermal melting involves high temperature, which poses a great limitation on the substrate selection.

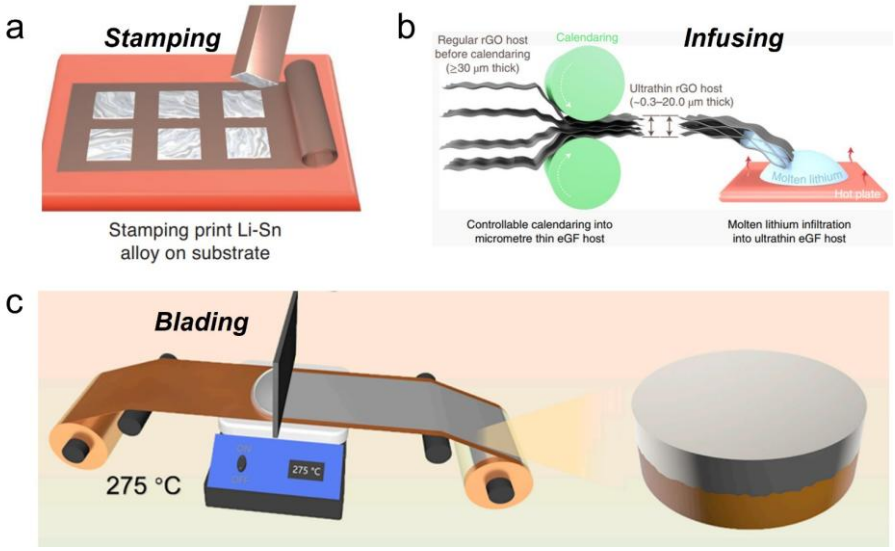

Figure 3.4 The molten-Li based thermal processing for thin LMAs preparation, such as (a) stamping [171], (b)infusing [30], and (c) blading [172].

Finally, the mechanical rolling is a facile and simple approach that involves physically compressing Li metal. Taking advantage of simplicity and scalability, mechanical rolling is the most commonly used method for developing thin LMA [173-176]. For example, a 30 μm-thick Li stacked with MXene was developed through mechanical rolling. When assembling with a high-loading NCA cathode (20.5 mg cm^{-2}), the LMBs showed an improved cycling stability with capacity retention of ~45% after 30 cycles.

Additionally, Huang et al. reported an ultrathin Li strip (less than 20 μm) through

mechanical rolling with an innovative design of applying ZDDP as an anti-wear additive. Nevertheless, the rolling process would introduce significant mechanical stress and defects on the Li, which may adversely affect the electrochemical performance.

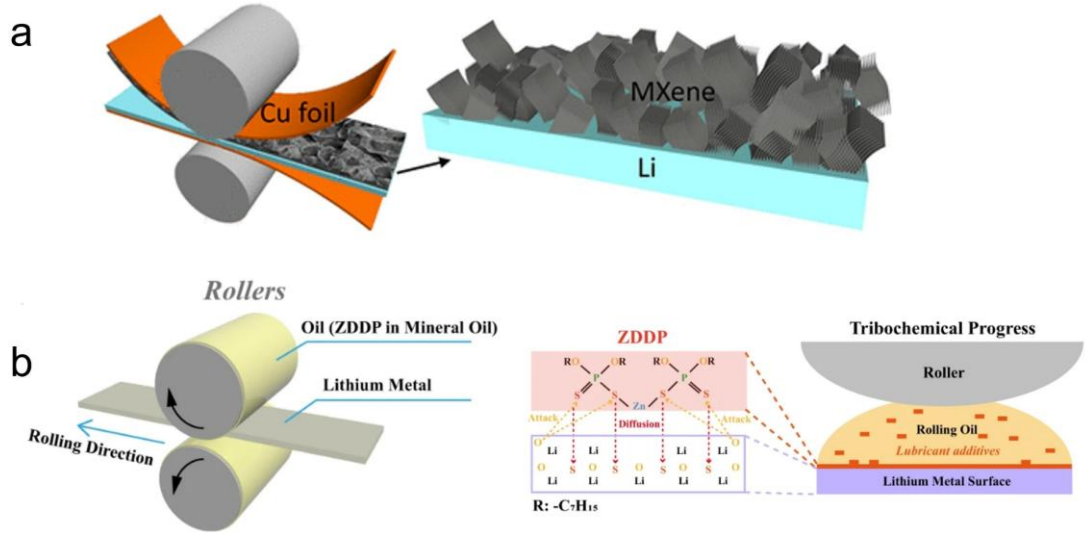

Figure 3.5 (a, b) Mechanical rolling for the fabrication of thin LMAs [176, 177].

The fabrication of thin LMAs through four types of approaches has been introduced. Importantly, achieving uniform deposition and preventing defects during the manufacturing process for thin LMA are critical to electrochemical performance. Thin anodes are more susceptible to mechanical degradation and dendrite formation, which would compromise the safety and longevity of the battery. How to maintain the mechanical integrity and electrochemical stability of thin LMA-based batteries during cycling is critical.

3.2 Pathway to Develop High-Energy LMBs

Energy density is a critical metric for evaluating the performance of LMBs. On the anode side, directly reducing the thickness of Li can effectively minimize excess lithium, thereby enhancing the energy density of the battery. This approach has been

carefully introduced and discussed in chapter 3.1.1. On the cathode side, increasing the proportion of active materials within the electrode can also boost energy density. However, due to limited charge transfer kinetics, thick cathode electrodes often suffer from poor rate capability and cycling stability.

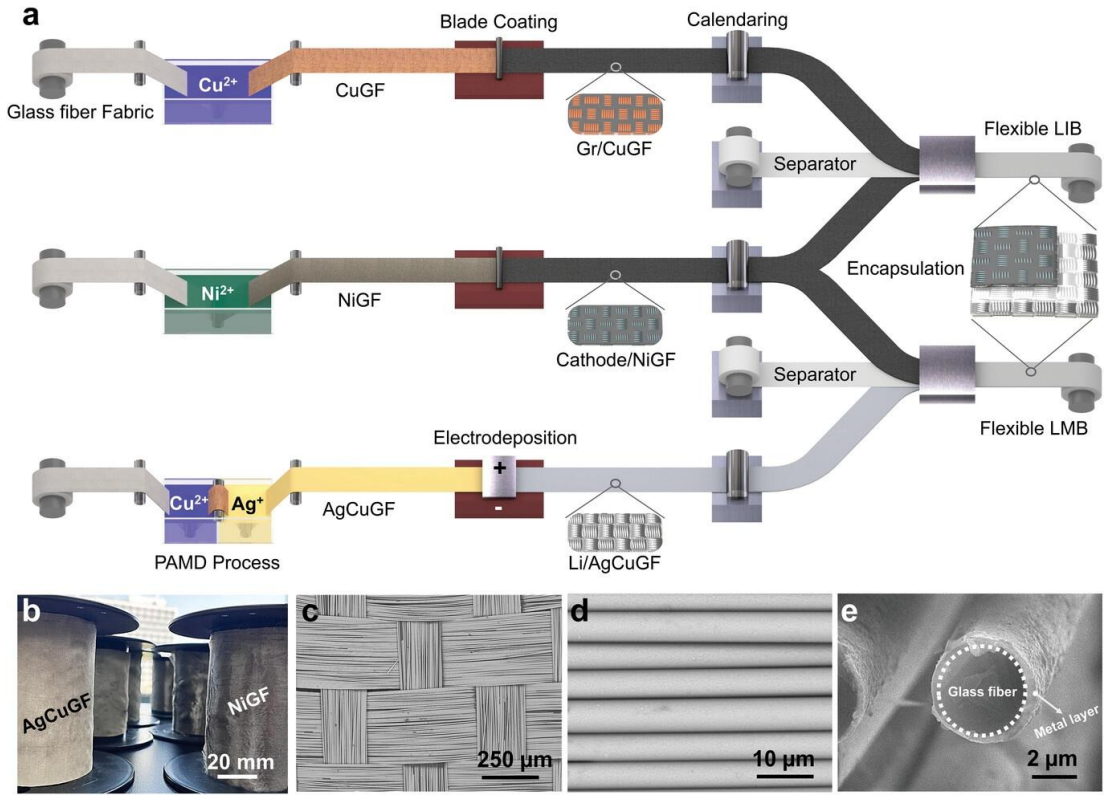

Figure 3.6 (a) The fabrication process to develop metallic glass fiber (GF) [178], the (b) optical image and (c) SEM images of the developed metallic GF.

Another feasible strategy is to adopt a thinner or lighter current collector [75, 179, 180], which can also significantly enhance the whole-cell energy density. Over the past two decades, the thickness of metal foils has been reduced meaningfully [179, 181, 182], with Cu as thin as 6 μm (~5.4 mg cm^{-2}), thereby improving the whole-cell energy density. However, further thinning the metal foils faces great technical challenges. Beyond simply thinning the foils, employing lighter substrates as current collectors comes as a promising approach. For instance, a lightweight metallized polyimide (PI) enabled by sputtering technology was reported by Cui's group [180]. Such a developed Cu coated PI as a current collector can contribute to a 75% weight reduction when

compared with a 9 μm-thick Cu foil. Additionally, our group has developed a lightweight metal-layer-coated glass fiber (GF) using a scalable solution-based method (Figure 3.6). With a weight of 2.9~3.2 mg cm^{-2}, the lightweight metal-coated GF as a current collector to replace the traditional metal foil can effectively increase the battery energy density by 9~18% without affecting the battery performance [178], showing great prospects in the development of high-energy batteries.

3.3 Pathway to Develop Highly-Flexible LMBs

To meet the ever-growing demand for emerging new technologies, such as portable electronics and wearable devices, the development of high-energy and flexible batteries has become increasingly crucial. Flexible batteries are required to supply power stably when subjected to external deformations, such as bending or folding. The maximum compressive/tensile strain (ε) applied on cell components of a flexible battery is related to both bending radius (r) and cell thickness (h), and it can be obtained by the equation of $\varepsilon=h/2r$. According to the Institute for Printed Circuits (IPC-2292 standard), the bending radius of the flexible electronic device should be ten times the thickness of the device. In this regard, the strain applied to the flexible battery would be no less than 5%.Here, thin LMAs-based batteries are particularly promising in meeting the energy density requirements. However, during the bending deformation, thin LMAs easily suffers from a large crack since the mechanical property of thin Li metal is poor, with a yield strain of merely 0.4% [42], which fails to meet the requirement for flexible electronics. Moreover, Cu foil, which is used as the current collector for the anode, also exhibits inherent rigidity and limited yield strain with low deformability [183]. In this regard, the development of flexible thin LMAs is crucial to developing batteries that not only meet the high energy demands of modern devices but also provide the mechanical flexibility required for their multiple applications.

In previous studies, the pathway to develop flexible batteries can be divided into two main strategies as shown in Figure 3.7 [45]. Firstly, the soft structure strategy involves

constructing a soft structure within the battery, such as spine-like and metal interlocked structures. These structures are designed to bear the mechanical deformation and dissipate stress concentration, thereby enhancing the flexibility of the battery. Given that the soft structure design introduces a large amount of non-active volume and weight, it inevitably leads to lower energy density. For example, Hikmet et al. proposed a segmented-based lithium ion battery (LIB), which showed a good bending tolerance at a small bending radius of >1mm, demonstrating an outstanding flexibility [184]. Nevertheless, the energy density was sharply reduced to 40 Wh L^{-1}. In 2013, Rogers et al. developed a stretchable LIB through designing a metal serpentine structure, and the energy density of the battery remained low with the value of 50 Wh L^{-1} [185]. Later, in 2018, a flexible LIB with an interconnected metal spine-like structure was put forward [186], where the hard section was used for energy storage while the soft components acted as a buffering section to provide flexibility. This as-developed LIB could maintain normal function when subjected to a bending radius of >10mm, but the energy density was still limited to 242 Wh/L. In addition, the structural design involved in the soft structure strategy is usually intricate with a complicated preparation process, which makes it difficult to achieve large-scale manufacturing.

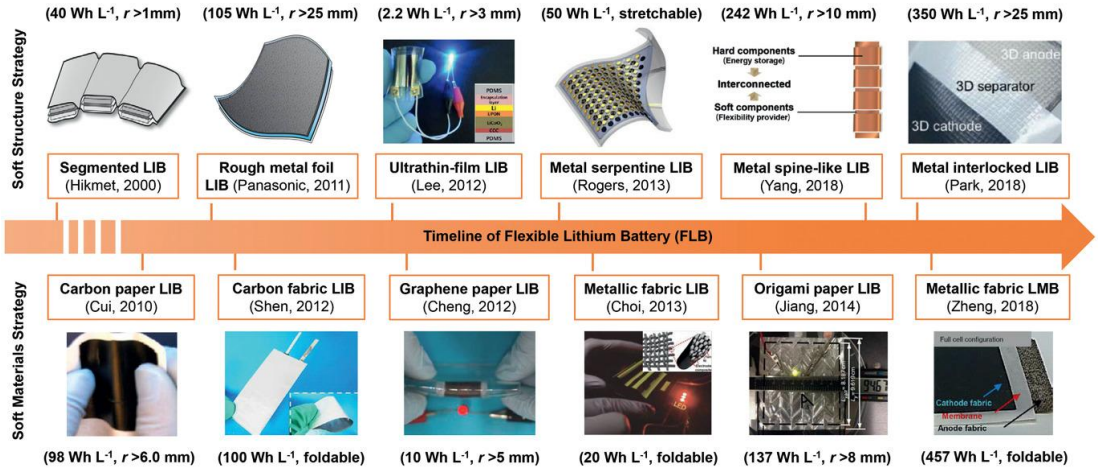

Figure 3.7 The development pathway for flexible lithium batteries [45].

Mechanically, there exists a neutral plane where strain vanishes during the bending

process. Here, the strain at the top surface (ϵ_t) of the bending film, such as Li foil, is proportional to the distance from the neutral surface, and it can be obtained by following equations [187, 188]:

$$\epsilon_t = \left(\frac{d_f + d_s}{2r}\right)\frac{(1 + 2\eta + \chi\eta^2)}{(1+\eta)(1+\chi\eta)}$$

$$\eta = \frac{d_f}{d_s}$$

$$\chi = \frac{Y_f}{Y_s}$$

where *r* is the bending radius, d_f and d_s denote the thickness of Li foil and substrate while Y_f and Y_s represents the corresponding elastic moduli. If a Li foil is applied on a softer or more compliant substrate ($Y_f > Y_s,\ \chi > 1$), then the neutral plane will shift toward the rigid Li foil side, thus receiving a reduced strain on the top surface. Moreover, if the Li foil is placed in the neutral plane, sandwiched in between two soft substrates with low modulus and small thickness, the whole system will achieve good flexibility, which can withstand extremely small bending radius or even be folded.

As such, the second one is a soft material strategy, which involves replacing the rigid metal foil with soft materials. This strategy provides robust mechanical support for the rigid Li foil or active materials during the bending process, thereby imparting flexibility to the battery. In 2010, Hu and colleagues utilized self-supporting CNT films as current collectors to fabricate a flexible LIB with an energy density of 98 Wh/L [189]. The as-developed LIB could maintain stable performance after 50 bending cycles at a radius of 6 mm. Interestingly, in recent years, soft textile materials have attracted much attention. In contrast to the metal-foil-based electrode (MFE) (Figure 3.8a) [48], combining textiles and active materials to obtain the textile-based composite electrodes (TCE) shows advantages in many aspects (Figure 3.8b). The TCE is more easily functionalized and modified through various preparation techniques, including but not

limited to rolling, coating and spinning (Figure 3.8d), whereas there are fewer methods available for the MFE (Figure 3.8c). Furthermore, the TCE with porous and hierarchical structure can dissipate the external stress, shorten the Li ion diffusion length, and reduce the localized current density, thus exhibiting superior flexibility and improved charge transfer kinetics (Figure 3.8e and 3.8f). In 2018, our group developed a flexible LMB based on a soft metallic textile substrate, achieving an energy density of up to 457 Wh/L [24]. This flexible LMB was capable of withstanding hundreds of bending cycles or even folding, demonstrating its superior electrochemical stability and outstanding mechanical flexibility. Such a strategy of adopting soft material provides a feasible way to develop highly-flexible LMB.

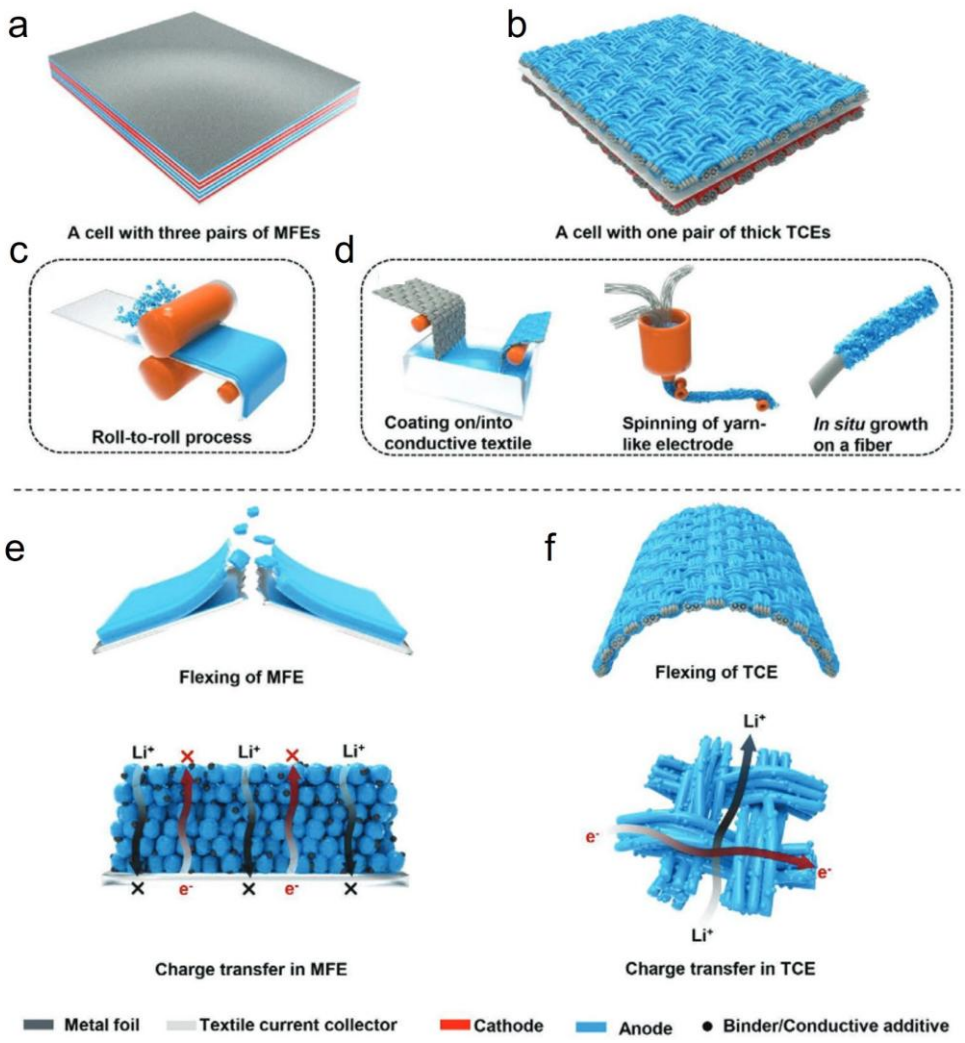

Figure 3.8 Stack cell configuration of (a) metal-foil-based electrodes (MFEs) and (b)

textile-based composite electrode (TCEs). The fabrication process for (c) MFEs and (d) TCEs. Schematic illustration of the bending tolerance of (e) TCEs and (f) TCEs [48].

3.4 Conclusion and Summary of Research Gaps

To meet the requirements of high energy density and flexibility for flexible and wearable electronics, great efforts have been made in advancing LMBs, from aspects of anode thickness, materials innovation, and structural design. Equipping with thin LMAs in batteries shows great promise in boosting energy density. However, thin LMAs usually exhibit very limited electrochemical stability and poor mechanical flexibility. In addition, the pursuit of flexibility in batteries severely sacrifices the energy density, These limitations hinder the practicability of LMBs for further applications. The development of advanced thin LMAs for high-performance LMBs with balanced stability, energy density, and flexibility remains a great challenge. Major research gaps are listed as follows:

1. It is difficult to achieve long-term cycling stability in thin LMA-based batteries, especially at a high depth of discharge. Thin LMAs are prone to electrochemically unstable. During cycling, the mechanical degradation and dendrite growth of thin LMA lead to poor electrochemical stability. Typically, due to the limited Li reservoir, the irreversible loss of Li, such as the formation of the SEI layer and dead Li, results in faster capacity decay and battery failure with compromised longevity. The development of high-performance thin LMAs with strengthened electrochemical stability for long-life LMBs is highly demanded.

2. Despite progress in developing flexible batteries, it remains challenging to achieve high flexibility while maintaining high energy density. Currently, the reported strategies of soft structure and soft material have demonstrated their effectiveness in improving the flexibility of the batteries. However, substantial amounts of non-active materials are involved in battery configuration, resulting in flexible batteries

with very limited energy density. As such, there is an urgent need for feasible and effective approaches to fabricate lightweight yet flexible thin LMAs. The development of flexible thin LMAs is essential to achieve high-performance LMBs that not only meet the high energy demands but also provide the mechanical flexibility required for future applications.

3. Considering a further improvement in energy density and battery safety, anode-free LMBs with Li thickness reduced to zero show great application potential. Commonly, Cu foil is directly used as an electrode to pair with the cathode materials. However, there is a large nucleation barrier between Cu and Li during deposition due to their thermodynamic mismatch. When replacing Cu foil with other 3D frameworks, the deposition behavior could be adjusted. However, the 3D substrate will inevitably absorb more electrolytes as well as consume more Li, leading to a compromised energy density, rapid capacity decay, and limited cycling lifespan. Currently, there is a lack of simple and effective methods to develop zero-excess-Li electrodes for high-performance anode-free LMBs without compromising energy density and electrochemical performances.

Chapter 4 Methodology

In this chapter, the general methodology of this thesis, including materials preparation, cell assembly, and characterization, is introduced. The polymer-assisted metal deposition (PAMD) and thermal evaporation are illustrated for the metallization and surface modification of electrode components. The methods for cell assembly and the equipment for different characterizations are also given in detail. Additionally, the metrics of the battery properties are elaborated.

4.1 Materials Preparation

4.1.1 Materials

The carbon cloth (CC) and polyimide (PI) fabric are purchased from CeTech Co. Ltd. and Jiangxi Xiancai Nanofiber Technology Co. Ltd, respectively. The lithium foils (50 μm and 400 μm) in the shape of sheet and strip are obtained from Guangdong Canrd New Energy Technology Co. Ltd. The electrolytes used in the batteries are received from Shenzhen Capchem Technology Co., Ltd. and Suzhou Duoduo Chemical Technology Co. Ltd. Various commercial cathodes, such as $LiFePO_4$ (LFP), $LiCoO_2$ (LCO), and $LiNi_{0.8}Co_{0.1}Mn_{0.1}O_2$ (NCM811), are provided by Capchem and Canrd. The chemicals involved in the experiment are purchased from commercial companies and listed in Table 4.1. The chemicals are directly used as received without further treatment if there is no specification.

Table 4.1 Chemicals used in experiments

Chemical	Purity	Brand
Concentrated sulfuric acid (H_2SO_4)	98%	Sigma-Aldrich
Nitric acid (HNO_3)	65%	Sigma-Aldrich
Acetic acid (HAc)	99.5%	Acros

Ethanol absolute (EtOH)	99.5%	Merk
3-(trimethoxysilyl) propyl methacrylate (MPTS)	99.9%	Sigma-Aldrich
2-(methacryloyloxy) ethyl trimethylammonium chloride (METAC)	80%	Sigma-Aldrich
Potassium persulfate (KPS)	99%	Uni-Chem
Ammonium tetrachloropalladate ($(NH4)_2PdCl_4$)	97%	Alfa Aesar
Nickel sulfate hexahydrate ($NiSO_4 \cdot 6H_2O$)	99.7%	Alfa Aesar
Tri-sodium citrate dihydrate ($C_6H_5Na_3O_7 \cdot 2H_2O$)	99.5%	Fisher Chemicals
Lactic acid ($C_3H_6O_3$)	90%	Acros
Borane-dimethylamine complex (DMAB)	98%	Alfa Aesar
Ammonia solution ($NH_3 \cdot H_2O$)	25%	VWR Chemicals

4.1.2 Polymer-Assisted Metal Deposition (PAMD) for Metallization

Pre-treatment of carbon cloth (CC): The CC is totally immersed in a solution of concentrated H_2SO_4 and HNO_3 (v/v = 3:1). After ultrasonication at 80°C for 4 hours, CC is rinsed with deionized (DI) water. Then, the CC is soaked in the clean DI water overnight, and the water is changed once a day for one week to remove the H_2SO_4 and HNO_3 completely. Finally, the CC with good hydrophilicity is obtained.

Silanization of CC: The silanization process is performed to graft the C=C double bonds onto the carbon fiber surface. Firstly, 190 mL EtOH, 8 mL DI water, 2 mL HAc, and 8 mL of MPTS are prepared and well mixed to obtain the silanization solution. Later, the acid-treated CC substrate is placed into the as-prepared silanization solution for 1 hour at room temperature. The silanized CC is prepared after rinsing with DI water and drying in an oven.

Polymerization of CC: The free radical polymerization procedure is carried out to form a desirable polymer brush layer onto the CC fibers by opening the functional groups of C=C bonds. Here, 400 mg KPS is introduced in the mix solution of 40 mL METAC and

160 mL DI water, and dissolved thoroughly. The silanized substrate is soaked in the above solution for 2 hours at 85 ℃. Later, the polymerized CC is obtained after rinsing with DI water.

Catalyst adsorption of CC: The catalyst adsorption is operated to load Pd^{2+} onto the polymerized CC through an ion exchange process. Specifically, the polymerized CC is placed into the 0.5 M catalyst solution of $(NH_4)_2PdCl_4$, then the container is covered with tin foil for a light-blocking reaction. After 30 minutes, the catalyzed CC is gained after rinsing with DI water.

Electroless deposition (ELD): The ELD process is conducted by placing the catalyzed CC in a nickel (Ni)-based plating solution, which contains solution A (Ni salt) and solution B (reducing agent). During the process of deposition, the loading catalytic moieties on the CC substrate can serve as catalytic sites to reduce and deposit Ni metal on the fiber surface. Specifically, solution A consists of $NiSO_4 \cdot 6H_2O$ (200 g/L), $C_6H_5Na_3O_7 \cdot 2H_2O$ (100 g/L), and $C_3H_6O_3$ (50 g/L), while solution B comprises 0.75 g/L DMAB. Before the ELD process, the pH of solution A should be adjusted to a value of ~7.5 by adding $NH_3 \cdot H_2O$. Later, the catalyzed CC is placed in solution A, and then solution B is added dropwise. The ELD process is performed for 30 minutes. After rinsing and drying, the Ni coated CC (Ni-CC) is obtained.

4.1.3 Surface Modification by Thermal Evaporation

Thermal evaporation is a widely used vapor deposition technology, with the advantages of a facile process, high purity, and good compactness. Specifically, the deposition material evaporates or sublimates into gaseous particles and is quickly transported from the evaporation source to the substrate surface. The gaseous particles attach to the substrate surface to form nuclei, then grow, and finally form a continuous film through the contact and merging of adjacent stable nuclei. As such, the thermal evaporation (JSD-600) is employed for surface modification of substrates. For example, the antimony (Sb) with a high Li affinity is modified on a target substrate by thermal

evaporation to introduce the lithiophilicity. The thickness can be well adjusted by tuning the evaporation rate and time.

4.2 Cell Assembly

4.2.1 Coin Cell Assembly

The coin cell assembly process is carried out in an Ar-filled glove box with low H_2O and O_2 content (<1 ppm). Electrodes with different substrates are assembled into CR2025-type or CR2032-type coin cells, depending on the thickness of the electrode. The configuration of the coin cell is shown in Figure 4.1.

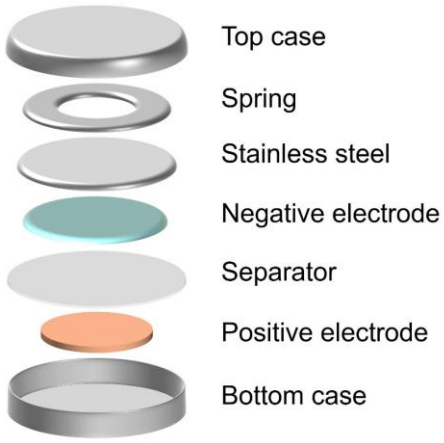

Figure 4.1 Schematic illustration of coin cell configuration.

The prepared electrodes are punched into a circular shape and thoroughly dried overnight. Firstly, the positive electrode is placed on the bottom battery case, and then a certain amount of electrolyte is dripped in, covered with a Celgard 2325 separator. Later, the negative electrode, a stainless steel (1 mm), and a hollow-shaped spring (1.1 mm) are placed in turn. Subsequently, the top battery case is covered for encapsulation. Finally, the MSK-110 machine is employed to crimp the coin cell for subsequent testing.

4.2.2 Pouch Cell Assembly

The pouch cell assembly process is carried out in an Ar-filled glove box with low H_2O and O_2 content (<1 ppm). The configuration of the pouch cell is shown in Figure 4.2. The prepared electrodes are cut into a rectangular shape and thoroughly dried overnight. The Ni tab and Al tab are attached to the negative electrode and positive electrode, respectively, for current collection. The Celgard 2325 is adopted as a separator and the Al laminated composite film serves as a packaging shell. The negative electrode, Celgard 2325 separator, and positive electrode are stacked in sequence and fixed in the Al laminated composite film with battery-used tape. After injecting the electrolyte, the MSK-115A machine is employed for vacuum-sealing of the assembled electrodes to obtain the pouch cell for subsequent testing.

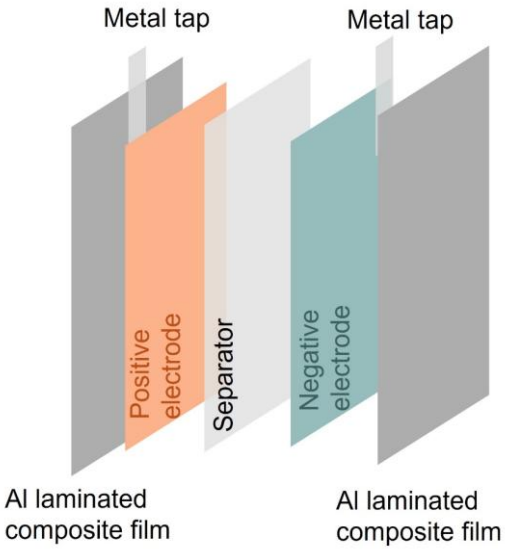

Figure 4.2 Schematic illustration of pouch cell configuration.

4.3 Characterization

4.3.1 Electrochemical Characterization

Galvanostatic charge-discharge test: The galvanostatic charge-discharge test is used to characterize the electrochemical properties of the assembled batteries, such as cyclability, stability, rate performance, etc. The test equipment is a battery test system

(Neware, BTS-4008), and the step conditions are set according to the type of battery. Taking the Li||Li symmetric battery as an example, the discharge and charge times are set to be the same under constant current, corresponding to the deposition/stripping process of Li with the same capacity. Since the theoretical redox potential of Li to Li is 0 V and remains unchanged, the theoretical battery voltage of the Li||Li symmetric battery should be 0 V. However, due to factors such as electrochemical polarization, concentration polarization, and ohmic polarization, the Li||Li symmetric battery has a voltage hysteresis phenomenon, which makes its redox potential often deviate from 0 V. With the continuous generation of Li dendrites and dead Li during cycle, this voltage hysteresis will gradually intensify until the battery short circuits. Therefore, the electrochemical stability, interface performance, and cycle life of the prepared negative electrode can be revealed by galvanostatic charge-discharge test of the Li||Li symmetric battery.

Electrochemical impedance spectroscopy (EIS): EIS is performed on a CHI660E electrochemical workstation with an amplitude voltage of 2 mV and a frequency range of 100 kHz to 100 mHz. It is a non-destructive and effective method that can measure the impedance at a series of frequency with varying AC signals. Based on the response and the corresponding plot, the kinetic behavior of the battery can be studied, including interfacial resistance, charge transfer resistance, and ion diffusion.

4.3.2 Structural Characterization

Scanning electron microscopy (SEM): The morphological investigation of the samples is characterized by SEM (Tescan VEGA3) and field-emission SEM (Tescan MAIA3). Air-sensitive samples are prepared in a glove box and fixed to the sample stage with conductive tape. Then, the samples are sealed and quickly transferred into the SEM chamber to minimize their exposure time in the air. SEM is an effective means to analyze and detect the surface morphology of materials. The principle is that when a high-energy focused electron beam bombards the surface of a material, secondary

electron scattering will occur. These scattered electron signals are collected, processed and imaged to obtain the morphological information. In addition, by embedding an X-ray energy dispersive spectrometer (EDS), key information such as the type, content, and distribution of elements on the surface of the material can also be obtained.

X-ray photoelectron spectroscopy (XPS): The surface composition and elemental state of samples are analyzed by XPS (Thermo Fisher Scientific Nexsa). When irradiated by an X-ray beam, electrons will escape from the surface atoms of the sample and generate photoelectrons. Combined with the electron energy analysis device, the number and kinetic energy of photoelectrons are measured to perform qualitative and quantitative analysis of surface elements.

X-ray diffraction (XRD): The crystalline structures of samples are evaluated by XRD (Rigaku Smart Lab 9kW) with an excitation source of Cu Kα ($\lambda = 1.54$ Å). Air-sensitive samples are prepared in the glove box and packaged with polyimide tape to eliminate adverse factors such as oxidation. When X-rays are irradiated onto crystalline material, X-rays with a wavelength close to the atomic spacing of the crystalline material will diffract in the periodically arranged atomic array, showing inherent characteristic spectral lines and diffraction angles. As such, the crystal information of samples can be analyzed by comparing the diffraction peaks with standard PDF cards.

4.3.3 Mechanical Flexibility Characterization

A homemade motion stage coupled with a four-probe test system (Keithley 2400 Sourcemeter) is used to evaluate the mechanical flexibility of the samples. Firstly, two sides of the pouch cell are clamped on the homemade motion stage with a target bending radius. Later, the bending procedure is set by controlling the moving distance and times of the motion stage. Meanwhile, the pouch cell is connected to the four-probe test system, which can measure the resistance of the sample under repeated bending conditions. As such, the bending tolerance and mechanical flexibility of the samples can be revealed based on the real-time change of resistance.

4.4 Metrics of the Batteries

4.4.1 Capacity

Theoretical capacity: The theoretical capacity of an electrode refers to the amount of capacity given by total active materials participating in the battery reaction, which can be calculated by the number of charge carriers (n), the faraday constant (F), and the molecular weight of active material (Mw). The equation is listed below, and the unit is mAh g^{-1}. For example, the Mw of $LiFePO_4$ is 157.756 g mol^{-1}, the n is determined to be 1, and the F is 96487 C mol^{-1}, thereby receiving a theoretical capacity of 170 mAh g^{-1}.

$$C = \frac{nF}{3.6M_w}$$

Actual capacity: Actual capacity refers to the amount of release capacity in a battery under practical discharge conditions.

4.4.2 N/P Ratio

The N/P ratio refers to the capacity ratio of the negative electrode to the positive electrode in the battery. In lithium metal batteries, the N/P ratio can be adjusted according to experimental requirements. The smaller the N/P ratio, the more significant the improvement in energy density. When the N/P ratio is 0, the system comes as an anode-free battery.

4.4.3 Charge Rate (C-rate)

The C-rate is a measure of charging speed, which refers to the current density required for the battery to be charged to its capacity within a specified time. It is numerically equal to the charging current divided by the capacity. For example, when the capacity of a battery is 100 mAh and the charging current density is 50 mA, then the C-rate is

determined to be 0.5 C, and the battery is fully charged in 2 hours. When the C-rate is increased to 1 C, the battery is fully charged in 1 hour. Thus, the larger the C-rate, the faster the battery charges.

4.4.4 Depth of Discharge (DOD)

The DOD is used to describe the degree of discharge of a battery during cycling. It represents the proportional relationship between the discharge capacity and the total capacity of the battery. For example, if the DOD of a battery is 50%, it means that the battery will be discharged half of its total capacity.

4.4.5 Energy Density

Volumetric energy density: The volumetric energy density (E_v, Wh L^{-1}) refers to the energy released by a battery per unit volume.

$$E_v = \frac{Discharge\ capacity\ \times Voltage}{Volume} = \frac{Discharge\ energy}{Volume}$$

Gravimetric energy density: The gravimetric energy density (E_g, Wh L^{-1}) refers to the energy released by a battery per unit weight.

$$E_g = \frac{Discharge\ capacity\ \times Voltage}{Weight} = \frac{Discharge\ energy}{Weight}$$

Chapter 5 A Thin, Stable, and Flexible Janus Lithium-Textile Anode for Long-Life and High-Energy Lithium Metal Battery

Adopting thin lithium (Li) metal anodes (LMAs) in Li metal batteries (LMBs) has shown great promise in enhancing energy density. However, the electrochemical stability of thin LMAs remains poor. In this chapter, a stable and thin LMA through selective wetting of molten Li on a Janus structured conductive textile, is introduced. As such, a thin Janus Li-textile anode with a thin Li coating (~50 μm) on one side of the textile framework is rapidly fabricated [190]. It is found that the upper buffering space and Janus design are significantly effective in suppressing dendrite growth, which contributes to a remarkably strengthened stability and ultralong lifespan of the thin LMAs-based batteries. Additionally, an impressive flexibility in the as-assembled pouch cell is also demonstrated.

5.1 Introduction

Over the past decade, significant efforts have been dedicated to the development of lithium metal batteries (LMBs) due to the growing need for batteries with higher energy density [10, 45, 191]. Uncontrolled growth of metallic dendrites on lithium metal anodes (LMAs) during the charge/discharge cycles, however, remains a huge challenge [15, 16]. To address this issue, various strategies have been proposed [19, 21-23, 26, 27, 128, 192, 193], such as reasonable electrolyte design, reliable artificial solid electrolyte interface (SEI) formation, and feasible three-dimensional (3D) current collector construction. Nevertheless, most of the aforementioned strategies heavily rely on a great excessive amount of Li, which is a critical yet unresolved matter.

In the laboratory research, the as-adopted commercially available cathodes typically show capacities varying from 1 to 4 mAh cm^{-2}. In comparison, the as-used anodes of

Li foil are commonly thick (400~750 μm in thickness), holding a high areal capacity of 80 to 150 mAh $cm^{-2.}$ As such, it indicates the largely-oversized Li in the cell configuration (20 to 100 fold excess). This substantial excess of Li considerably diminishes battery performances with much-decreased energy density, low Li utilization, and misleading results. Meanwhile, it also brings about inevitably increased battery cost as well as unnecessary resource waste. Therefore, thinning LMAs is fundamentally crucial for developing practical LMBs with enhanced energy density [13, 55].

Currently, there are primarily four approaches to produce thin LMAs with a thickness of no more than 50 μm (with areal capacity ≤10 mAh cm^{-2}) [28]. The physical vapor deposition (PVD) and electrochemical plating (ECP) can be selected to precisely control the amount and thickness of target thin LMAs [18, 168, 194-197]. From the aspect from practical applications, the PVD and ECP techniques involve a time-consuming and resource-wasting process with high production cost, rendering them unsuitable for industrial use. In terms of mechanical rolling and thermal infusion, they are facile strategies to rapidly develop the thin LMAs. Specifically, the mechanical rolling is the most commonly used method for developing thin Li foils due to its straightforwardness and facile operation [173-176]. As for the thermal infusion method, it is also employed to fabricate thin LMAs by simply introducing the molten Li into the thermally stable framework [32, 171, 198-201]. However, the as-fabricated thin LMAs by these two methods always exhibit poor electrochemical stability with very limited cycling lifespan. For example, using an ultrathin Li anode made through the rolling process only endured 60 cycles in full cells [169], while a battery using an ultrathin Li alloy anode produced by stamping lasts for just 25 cycles [171]. In other words, despite advancements, achieving excellent cycling stability for thin LMAs remains a key bottleneck to be solved.

In this chapter, a thin, stable, and flexible LMA is introduced through a novel strategy of selective wetting is introduced [190]. We developed a Janus conductive textile

framework, which possesses different Li affinity on two sides. As such, a Janus Li-textile anode with a thin Li coating (~50 μm) on the Li-affinitive side can be rapidly fabricated when contacting with molten Li. The fabrication, structural characterization, and electrochemical properties of the batteries using the Janus Li-textile anode are investigated and discussed carefully. Result finds that the Janus Li-textile anode contributes to realizing high-performance LMBs for practical applications due to its significantly strengthened cycling stability and superior mechanical flexibility.

5.2 Experiment

5.2.1 Materials Preparation

Preparation of Janus Conductive Textile: The conductive textile of Ni coated carbon cloth (Ni-CC) was fabricated by treating commercially available carbon cloth (CC) via polymer-assisted metal deposition (PAMD) as introduced in Chapter 4. Then, an ultrathin 100 nm antimony (Sb) layer was deposited on one side of Ni-CC via thermal evaporation. After heating, the Sb on the conductive textile (Sb-Ni-CC) was converted to NiSb alloy, thus achieving the Janus conductive textile (NiSb-CC) with a lithiophobic Ni side and a lithiophilic NiSb side.

Fabrication of Janus Li-Textile Anode: Exposing the NiSb side of the Janus conductive textile with the molten Li, the Janus Li-textile anode was then developed, yielding a thin Li coating layer (~50 μm) coating on one side of the Janus conductive textile. By controlling the contacting time between the Janus conductive textile host and the molten Li, the Li loading amount on the Janus conductive textile can be well adjusted.

Preparation of Homogeneous Anode: Given that the wettability of Li on Ni coated textile was poor, thermal infusion of molten Li on the conductive textile was carried out under a higher temperature of 400 °C and a longer heating time. As such, the homogeneous anode was fabricated after the conductive textile host was totally infused

with Li.

5.2.2 Cell Assembly

The Ni-CC and NiSb-CC were punched into a circular shape with 16 mm in diameter. After the thermal infusion, the symmetric cells were assembled. And the commercial LFP and LCO were used as cathodes in the full cells. For the pouch cell assembly, the Al laminate composite foil was used to seal the cell. The electrolyte used in symmetric cells and LFP-based full cells was an ether-based electrolyte, which consisted of 1 M lithium bis(trifluoromethanesulfonyl)imide (LiTFSI) in a mixture of 1,3-dioxolane/1,2-dimethoxyethane (DOL/DME, 1/1 in volume) with 2 wt.% lithium nitrates ($LiNO_3$). The ester-based electrolyte was utilized in high-voltage LCO-based full cells, concluding 1 M lithium hexafluorophosphate (LiPF6) in ethylene carbonate/diethyl carbonate (EC/DEC) with fluorinated ethylene carbonates (FEC). Detailed procedures for cell assembly can be found in chapter 4.

5.2.3 Characterizations

The galvanostatic tests and cycling performance of the batteries were evaluated by the Neware battery testing system. The energy density was calculated based on the mass of cell components, including the current collectors, electrodes, and separator. Detailed characteristics have been introduced in chapter 4.

5.3 Results and Discussion

5.3.1 Selective-Wetting Preparation of Janus Li-Textile Anode

The thermal infusion of molten Li into thermally-stable hosts is a facile way to prepare LMAs nowadays. As shown in Figure 5.1a, a Janus conductive textile host which is composed of a lithiophobic nickel (Ni) side and a lithiophilic nickel antimonide (NiSb) side was designed. Once contacting with the molten Li, it only wet the bottom

lithiophilic side while the upper lithiophobic remained a pristine textile structure with a totally Li-free feature. As such, a thin coating layer of Li (~50 μm) was rapidly formed on the textile framework and the mass loading of the Li was only ~3 mg cm^{-2}. Compared to the homogeneous anodes (with the whole framework totally covered with molten Li) fabricated by the conventional thermal infusion method, the amount of Li loading of the Janus anode exhibited a significant reduction of over 80% (Figure 5.1c). Consequently, the projective energy density of as-developed LMBs using thin Janus LMAs can achieve a meaningful enhancement of more than 50% (Figure 5.1d).

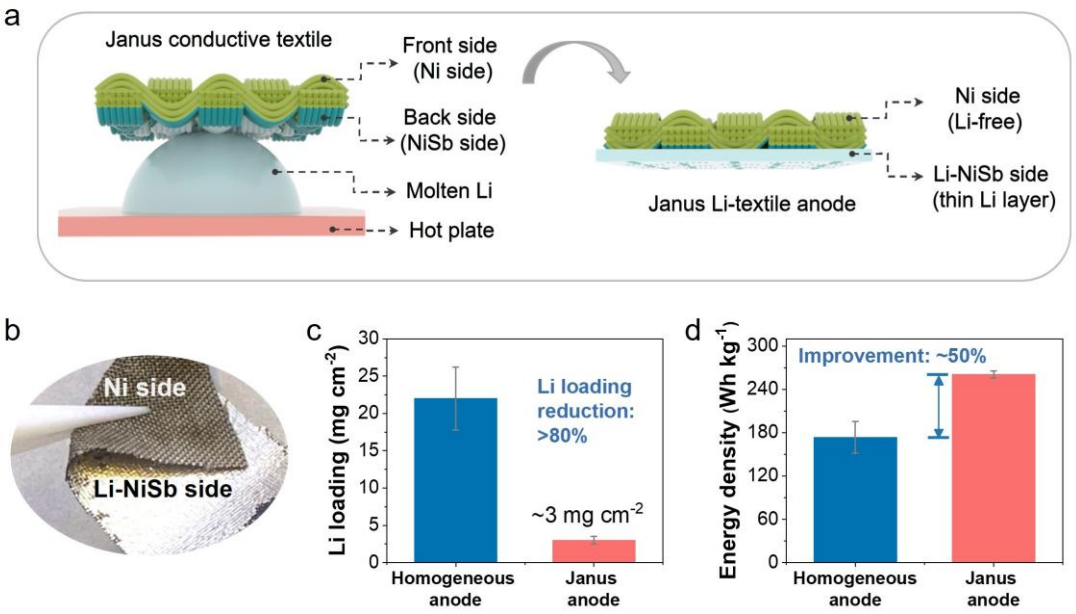

Figure 5.1. (a) Scheme illustration of selective-wetting mechanism to fabricate the Janus Li-textile anode coated with a thin Li metal layer. (b) Digital image of Janus anus Li-textile anode. (c) Li loading and (d) energy density comparison between homogeneous anode and Janus anode.

5.3.2 Structural Characterization of Janus Conductive Textile

Figure 5.2a shows the fabrication process for the Janus conductive textile host. Carbon cloth (CC)was used as the starting 3D textile substrate. We deposited a homogeneous layer of nickel (Ni) on the textile to obtain the Ni coated CC (Ni-CC) through the

method of PAMD. We then thermally evaporated antimony (Sb) on one side of the Ni-CC, followed by a heating process to convert the Sb into nickel antimony (NiSb) alloy. The conversion of the Sb to NiSb alloy was aimed at alleviating the huge volume expansion of Sb during the process of lithiation and delithiation, and enhancing the interfacial adhesion between Sb coating layer and the conductive textile host. As such, we obtained the Janus conductive textile of NiSb-CC comprising a lithiophobic Ni side and a lithiophilic NiSb side.

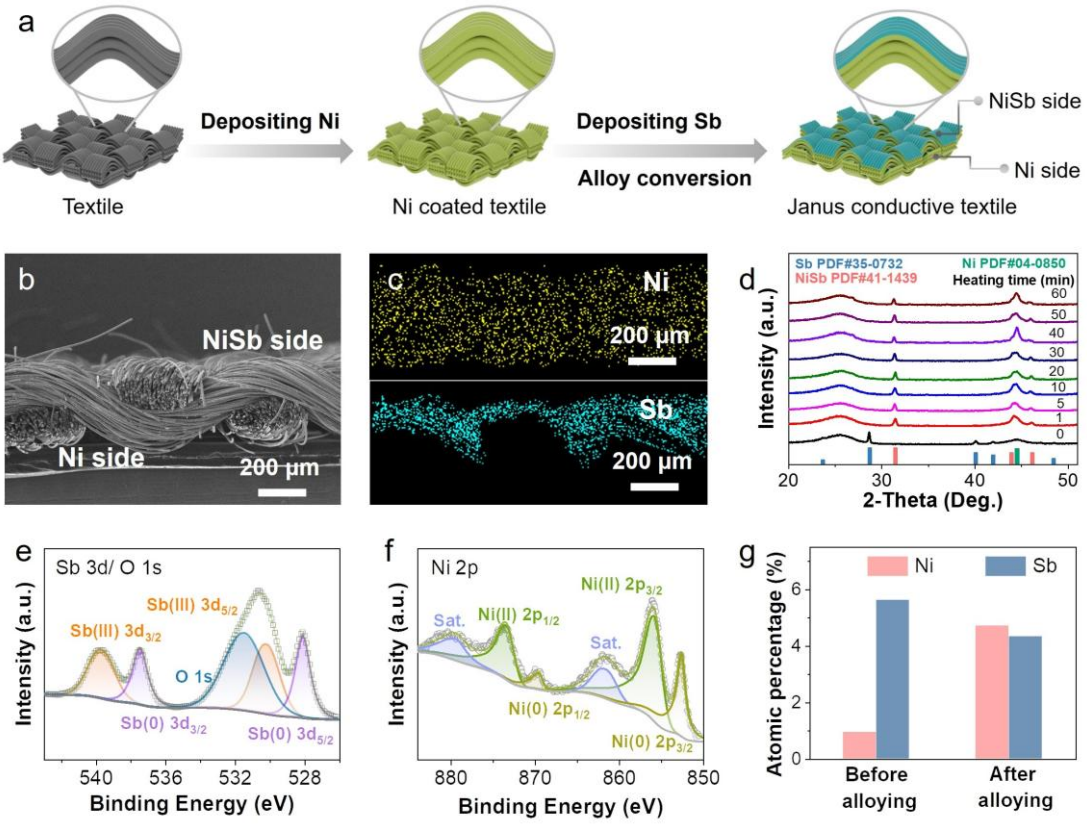

Figure 5.2 (a) Schematic illustration of the fabrication process, (b) morphology, (c) elemental mappings of the Janus conductive textile. (d) XRD spectrum of the Janus conductive textile after heating. (e, f) XPS of Sb 3d/O 1s, and Ni 2p of the Janus conductive textile host. (g) Atomic percentages of Ni and Sb of the conductive textile host before and after the heating.

Additionally, cross-section morphology and elemental mapping of the Janus conductive

textile were given in Figures 5.2b and 5.2c. The result showed that the distribution of Ni was uniform while the Sb was only on the treated side of the textile, indicating two different surfaces of the framework. The heating time for alloy conversion ranging from 1 min to 60 min was investigated by XRD spectrum. In Figure 5.2d, new peaks at 31.4° and 46.2° assigned to NiSb were found when only heating for 1 min, indicating the rapid conversion of NiSb alloy. The surface compositions of the Janus conductive textile before and after heating were further explored by XPS. Before heating, the atomic percentage of Sb (5.63%) on the surface was much larger than that of Ni (0.95%). After heating for alloy conversion, the atomic ratio of Ni and Sb was close to 1:1 (Figure 5.2g). And signals related to NiSb alloy, such as Sb (0) $3d_{5/2}$, Sb (0) $3d_{3/2}$, Ni (0)$2p_{3/2}$ and Ni (0) $2p_{1/2}$ could be easily found on surface of the textile host (Figure 5.2e and 5.2f). Additionally, the TEM image of NiSb morphology is shown in Figure 5.3a. The lattice with the spacing of 0.206 nm was revealed (Figure 5.3b), which corresponded to the (102) plane of the hexagonal NiSb alloy. In a word, we demonstrated that the deposited Sb on the Ni-CC was completely converted into NiSb alloy after heating.

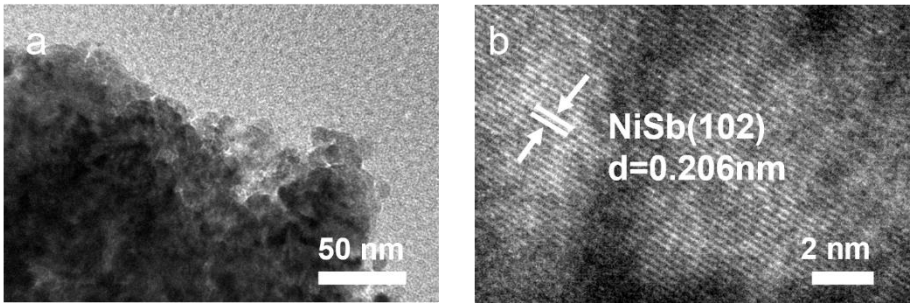

Figure 5.3 (a) Low-magnification and (b) high-resolution transmission electron microscope (TEM) image of the NiSb.

5.3.3 Raid Fabrication for Janus Li-Textile Anode

As mentioned, the framework of the Janus conductive textile owned two different surfaces, which were especially designed to construct the difference in Li affinity for selective wetting. Firstly, the Li nucleation behavior on Janus conductive textile was

investigated (Figure 5.4a and 4c). It could be observed that the front Ni side of the sample was free of Li deposits. In contrast, the fibers with NiSb layer on the bottom side were almost fully covered with Li seeds (Figure 5.4b and 4d). The result indicated that the Li tended to nucleate at the bottom side of the Janus conductive textile because the NiSb owned good affinity to Li. Secondly, with modification of NiSb, the nucleation overpotential of NiSb-CC was lower than Ni-CC (Figure 5.5), since the Li could form an alloy with Sb, thus reducing the nucleation barrier.

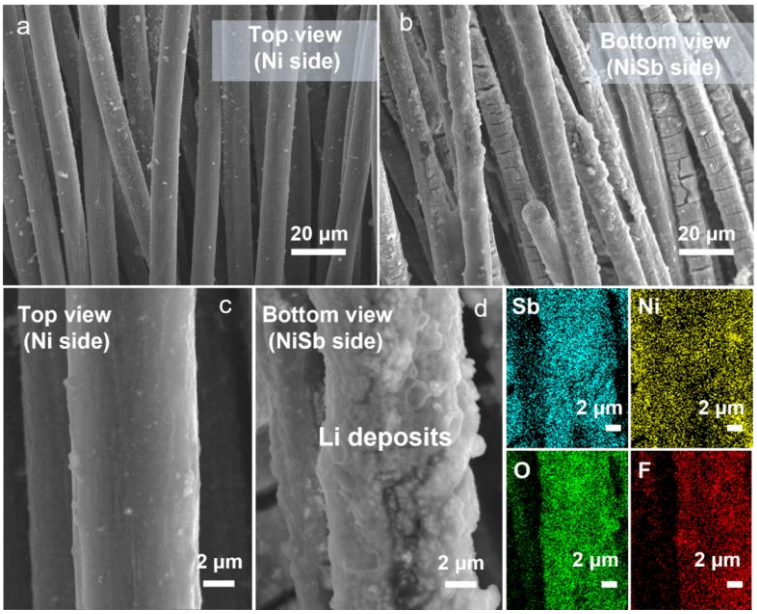

Figure 5.4 (a, c) Top view and (b, d) bottom view of nucleation behavior of the Janus conductive textile after electrodeposition under 0.025 mA cm^{-2} with the capacity of 0.1 mAh cm^{-2}.

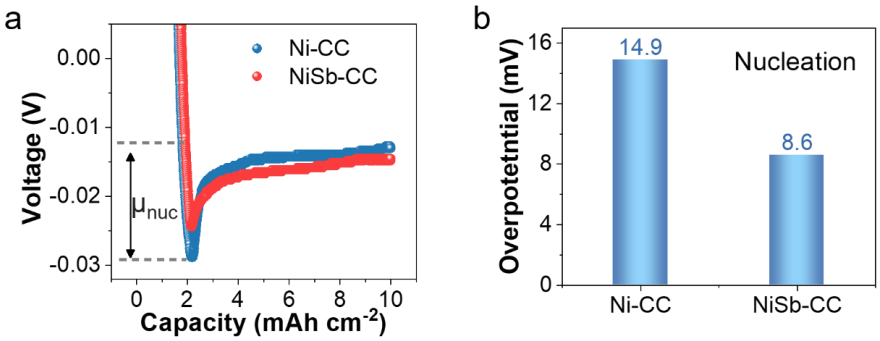

Figure 5.5 The (a) voltage profile and (b) nucleation overpotential of Ni-CC and NiSb-

CC.

To further demonstrate the difference in Li affinity of the framework, we directly placed a Li foil on top of two sides of the Janus conductive textile. After heating, the Li foil on the NiSb side could wet the framework while the Li on Ni side presented a poor wettability as illustrated in Figure 5.6a and 5.6b. In this case, we utilized this kind of Li-affinity difference of the framework to realize the selective wetting of the molten Li in the framework.

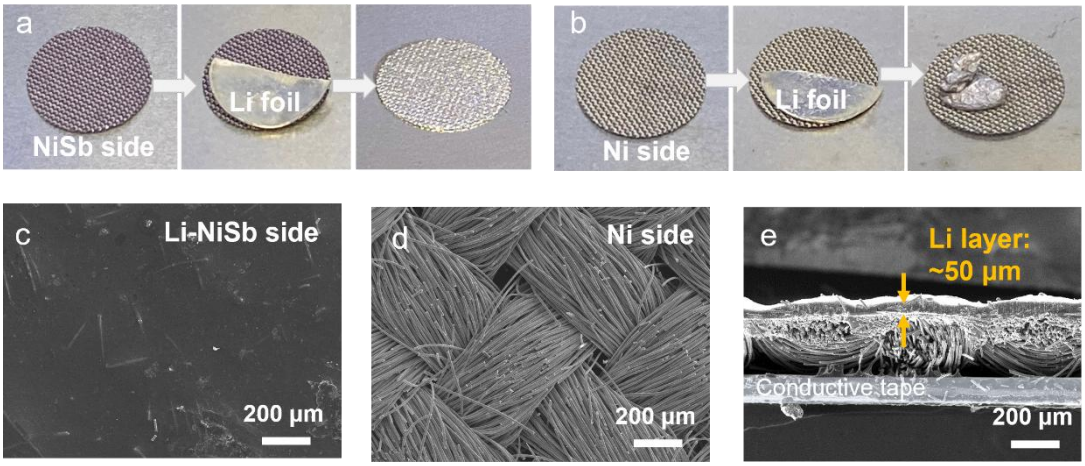

Figure 5.6 Wetting performance of Li on (a) NiSb side and (b) Ni side of the Janus conductive textile under the same heating time. SEM images of Janus Li-textile anode, (c) back side of Li-NiSb, (d) front Ni side maintaining original textile structure, and (e) cross section of Janus anode with ~50 μm Li coating.

Specifically, we put the NiSb side of NiSb-CC on the top surface of the molten Li, then the Janus Li-textile electrode with ultrathin Li coating can be easily obtained within 30 seconds. Then, by controlling the placing time, the loading of Li on the Janus conductive textile can be well adjusted. As observed from the SEM image, the bottom side of the framework was filled with Li while the upper surface remained the perfect fabric structure (Figure 5.6c and 5.6d). The cross-section of the Janus Li-textile anode was also given in Figure 5.6e, showing a uniform and thin Li layer of ~50 μm coated on one side of the framework.

As for Ni-CC, the wettability of Li on this framework was poor. Here, the thermal infusion method to fabricate the homogeneous anode of Li-Ni-CC was carried out under a higher temperature of 400 °C and a longer heating time. The top-view and cross-section morphologies of the homogeneous anode were shown in Figure 5.7. It was found that the Ni-CC framework was fully covered with Li, and the thickness of the homogeneous anode was thick (~350 μm).

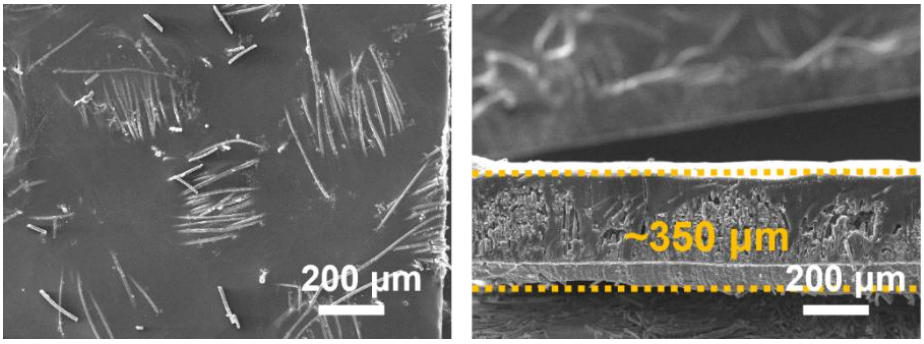

Figure 5.7 Top view and cross section of the homogeneous anode.

5.3.4 Long-Term cycling performances of Janus Li-Textile Anode

The electrochemical performance of the as-developed thin Janus Li-textile anode was investigated. Here, we adopted a 50 μm-thick Li foil and a homogeneous anode of Li-Ni-CC to serve as the control samples. Both the Li foil and the homogeneous anode exhibited a large overpotential of over 100 mV (1 mA cm^{-2}, 1 mAh cm^{-2}) and potent profile fluctuations at the beginning of the cycling test as shown in the dashed frame of Figure 5.8a. The cell of Li foil shorted after only 150 hr cycling. The homogeneous anode cell showed a decreased overpotential after 100 hr cycling but then regained an enormous profile fluctuation after 400 hr cycling, indicating the formation of mossy Li.

In contrast, the Janus anode exhibited a steady voltage profile with a flat plateau and a small overpotential of ~18 mV as revealed in the insets. It also showed a prolonged cycling life of more than 3,000 hr, indicating a significant improvement in the cycling stability of the thin LMA. Additionally, a good rate capability was observed in the Janus

anode (Figure 5.8b).

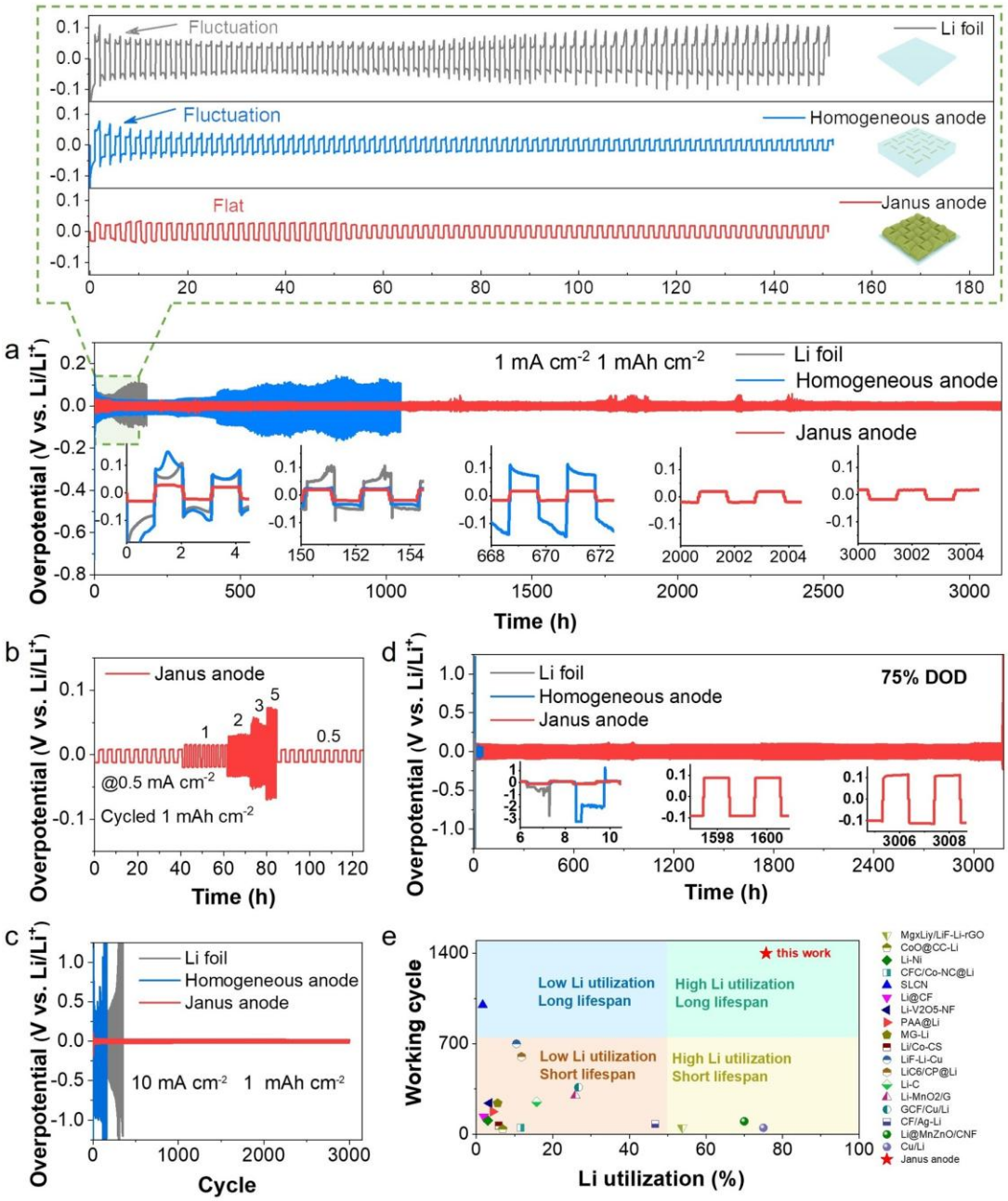

Figure 5.8 (a) Cycling performance of the different anode-based symmetric cells. The dashed frame shows the early voltage profile, and corresponding configuration of three types of anodes are given. (b) Rate performance of the Janus Li-textile anode. Comparison of electrochemical stability in symmetric cells using different anodes under a high current density of 10 mA cm^{-2} (c) and under 1 C rate at 75% DOD (d). (e) Comparison our Janus anode with previously reported LMAs fabricated by thermal

infusion in terms of Li utilization and working cycle [33, 41, 164, 201-211].

When the current density increased to 10 mA cm^{-2}, both the thin Li foil and the homogeneous anode cells entered failure with no more than 100 hr cycling (Figure 5.8c). The Janus anode maintained outstanding electrochemical stability under an ultrahigh rate of 10 C; the overpotential remained steady at 23 mV despite cycling 3,000 times. Moreover, under a high DOD of 75% at high current density (10 mAh cm^{-2}, 10 mA cm^{-2}), the Janus anode still displayed an ultrastable cycling performance over 3,000 h as depicted in Figure 5.8d. The detailed voltage profiles at the initial, middle, and late stages revealed excellent cyclic stability and dendrite-free behavior. From this investigation, the Janus Li-textile anode evidently outperformed the state-of-the-art, thermal-infusion-processed LMAs [33, 41, 164, 201-211], in terms of working cycles and involved Li utilization during cycling (Figure 5.8e).

In an attempt to delve deeper into the exploration for differences in cyclic performance, the symmetric cells were disassembled after the 1^{st}, 50^{th}, and 500^{th} cycle for observing the morphology evolution. As illustrated in Figure 5.9a and Figure 10, colossal Li dendrites were observed on the surface of the Li foil and homogeneous anode at the 50^{th} plating. After 500 cycles, a large amount of dead Li and obvious volume expansion were found on the homogeneous anode. Specifically, the thickness of the homogeneous anode increased from ~350 μm to ~400 μm. Model 1 (Figure 5.9a) clarifies the top deposition mode of the homogeneous anode. Since the Li-coated side is close to the separator, the plating/stripping preferentially occurs on the top surface of the homogeneous anode due to the shorter Li-ion diffusion pathway, finally leading to the uncontrollable dendrite growth.

The surface of the Janus anode, on the other hand, was free from Li metal deposits, maintaining its smooth fiber surface and porous textile structure at the 500th plating (Figure 5.9b). The thickness of the Li layer in the Janus anode remained consistent at ~50 μm before and after the cycling test, indicating zero-volume expansion. Model 2

(Figure 5.9b) explains the bottom deposition mode of the Janus anode. Because of the poor affinity of the upper Ni side to Li, the additional Li metal prefers to deposit on the bottom lithiophilic side, thus significantly mitigating the growth of metallic dendrites on the anode's top surface. Moreover, the upper porous textile framework provides a large space to accommodate the Li deposits, alleviate the immense volume expansion, and stabilize the SEI layer during plating/stripping.

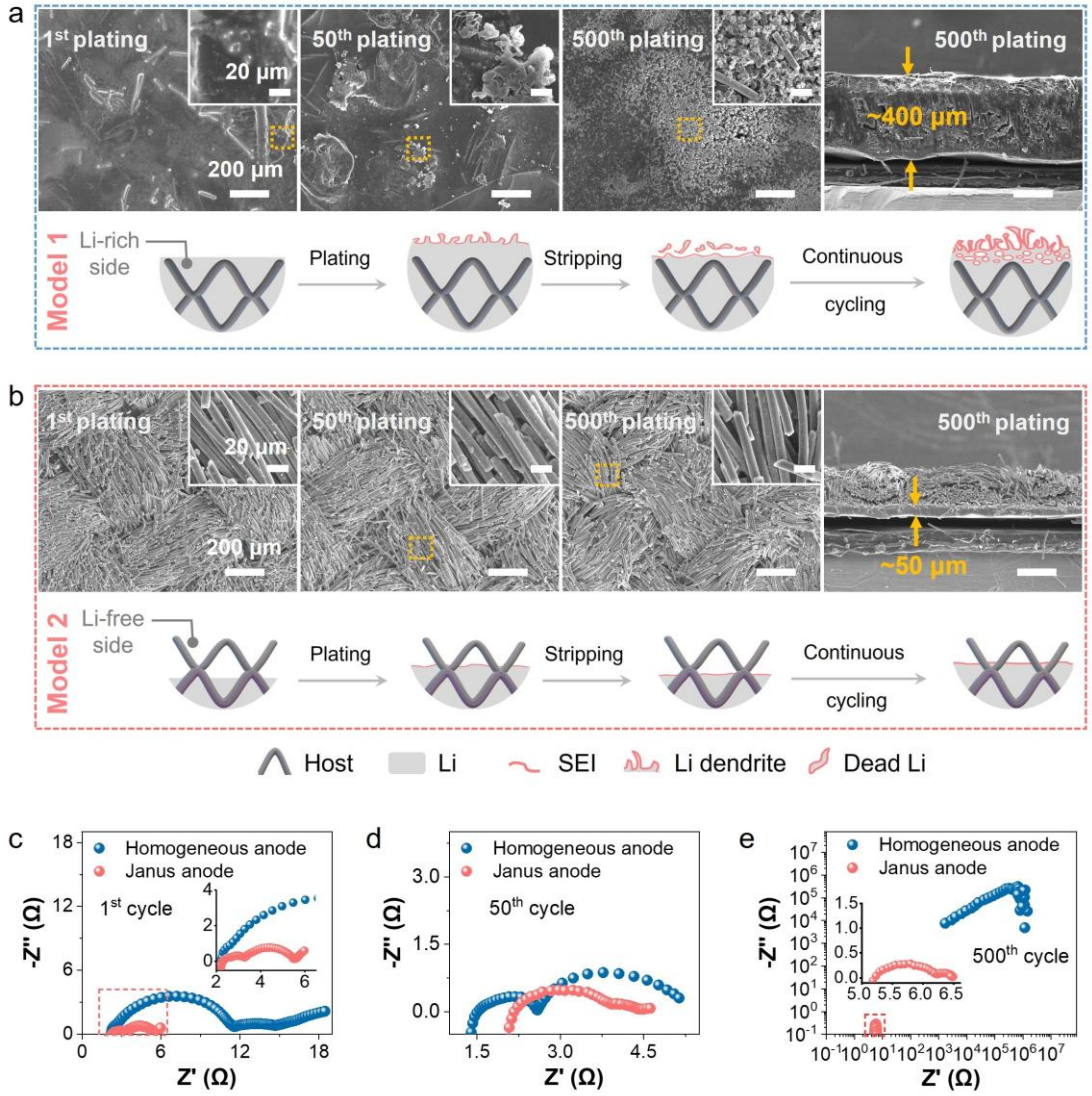

Figure 5.9 The morphology evolution and impedance evaluation of different anodes. (a) The morphology evolution of the homogeneous anode at the 1st, 50th, and 500th plating under 1 mAh cm^{-2} and 1mA cm^{-2}; Model 1 depicts the dendritic growth on the homogeneous anode. (b) The morphology evolution of the Janus anode at the 1st, 50th,

and 500th plating; Model 2 describes the smooth deposition on the Janus anode. (c-e) The impedance evaluation of the homogeneous anode and the Janus anode at the 1st cycle (c), 50th cycle (d), and 500th cycle (e).

To further reveal the reaction kinetics and mechanism, the interfacial properties of the symmetric cells at different cycles were evaluated by electrochemical impedance spectroscopy (EIS). The two semicircles that appeared at the high frequency and low frequency of the Nyquist plot are assigned to the interfacial resistance and charge transfer resistance, respectively. After the 1st cycle, the symmetric cell using the Janus anode displayed two smaller semicircles than those of the homogeneous anode (Figure 5.9c). The interfacial resistance of the Janus anode cell maintained a stable value from 3.2 Ω to 3.9 Ω during the progress of 50 cycles (Figure 5.9d). The homogeneous anode cell also showed a similar decrease from 11.5 Ω to 2.6 Ω. An extremely high and disordered impedance (Figure 5.9e) was found in the homogeneous anode cell after the 500th cycle because of the accumulated thick SEI layer. In contrast, the value in the Janus anode cell was slightly increased to 6.2 Ω despite 500 cycles. This result may be attributed to the stable SEI layer and fast reaction kinetics facilitated by the upper textile framework of the Janus Li-textile anode.

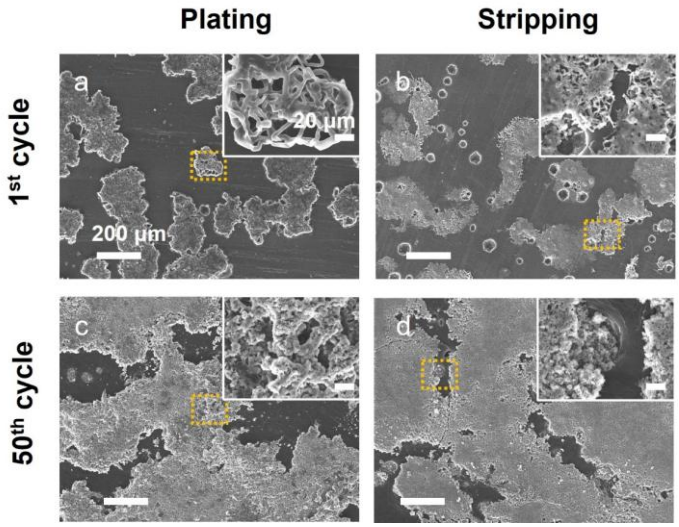

Figure 5.10 The plating and stripping morphologies of Li foil after the 1st (a, b) and the 50th cycle (c, d).

To sum up, the Janus anode possesses the following powerful advantages, enabling itself with prolonged cycling performance and superior stability. The Li-affinity difference of the textile framework induces a desirable oriented bottom-up deposition, which can fundamentally overcome the issue of dendrite growth on the top surface, thus greatly prolonging the working lifespan. In addition, the upper buffering textile skeleton acts as a significant role in regulating the Li ion diffusion kinetics, suppressing the huge volumetric change of Li metal during repeated plating/stripping, and protecting the Li/electrolyte interface. The resulting rapid reaction kinetics, zero-volume expansion, and stable interfacial property endow the Janus anode with better electrochemical performance, outstanding structural stability, and cycling stability. Consequently, the combination of the Janus configuration and thin Li layer offers great insights into developing advanced thin Li composite anodes.

5.3.5 Long-Life and High-Energy LMBs using Janus Anodes

The stability of the Janus Li-textile anode in the LMBs was carefully studied by pairing with Li-containing cathodes, including lithium cobalt oxide (LCO) and lithium iron phosphate (LFP). As shown in Figure 5.11a, the LCO//Janus anode cell exhibited an impressive long-life performance of 2,000 cycles with an outstanding cyclic capacity retention of 99.94% per cycle at the rate of 1 C (1.8 mA cm^{-2}, 1.8 mAh cm^{-2}). The LMB equipping with the Janus anode showed a record-extended cycling lifespan when compared with the battery adopting the Li foil as the anode, which just sustained several cycles. The undesirable cycling stability and intolerable rate capability of the Li foil were also observed in the rate study (Figure 5.11d). As given by galvanostatic charge/discharge (GCD) profiles (Figure 5.11b), the capacity of the initial cycle between the LMBs using homogeneous anode and Janus anode showed little difference. However, the capacity of LCO//homogeneous anode drastically dropped by 48% from 1.45 mAh cm^{-2} to 0.76 mAh cm^{-2} after 600 cycles. In contrast, the LCO//Janus anode cell demonstrated a superior capacity retention of 85% at the first 600 cycles. Apart from the overwhelming advantages of prolonged working life and enhanced capacity

retention, a higher DOD and improved energy density (> 30%) were also realized in the LMB using the Janus anode (Figure 5.11c).

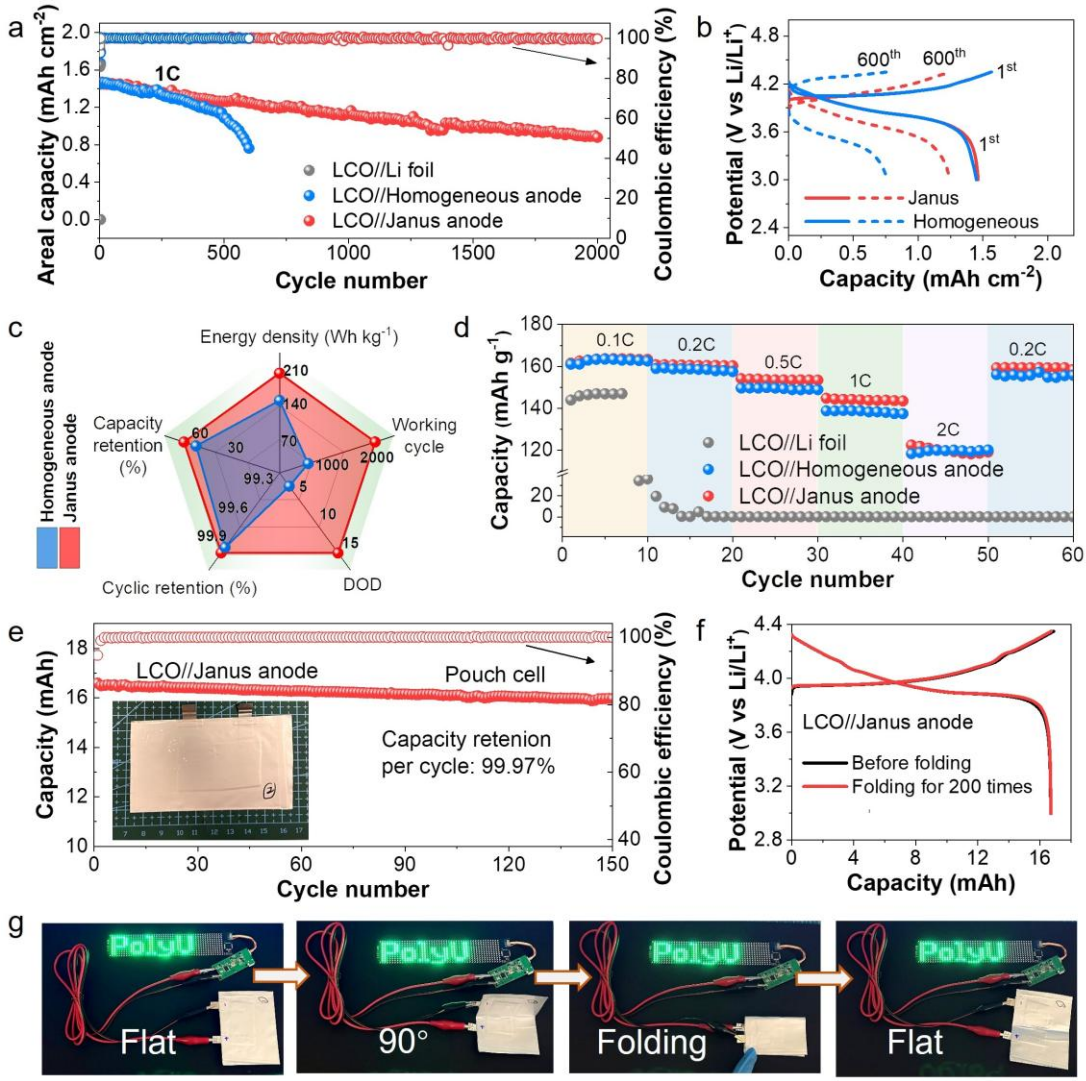

Figure 5.11 The LMBs with enhanced electrochemical stability and improved energy density. (a) Cycling stability of the LCO//Li foil, LCO//homogeneous anode and LCO//Janus anode at the 1 C rate of 1.8 mA cm^{-2} under the working voltage of 3.0-4.35 V. (b) GCD profiles at the 1st and 600th cycle. (c) Comprehensive comparison of LMBs using the homogeneous anode and Janus anode in terms of energy density, working cycle, DOD, cyclic retention, and capacity retention. (d) Rate performance of the full cells based on different anodes. e) Cycling durability of the pouch cell of LCO//Janus anode. (f) GCD profiles the pouch cell before and after 200 cycles of folding. (g)

Flexibility demonstration of the pouch cell.

To further reveal the practicality of the Janus anode, a high areal capacity cathode material of LFP was used in the LMB. The LFP//Janus anode cell, prepared with a low N/P ratio of 3.8, not only delivered a practical areal capacity of ~2.7mAh cm^{-2}, but also enabled a prolonged working life of 950 cycles at a 1/3 C rate (Figure 5.12a). After cycling 400 times, the LFP//Janus anode presented an outstanding capacity retention of 91.8%. The LMBs based on the Li foil and homogeneous anode, however, housed poor cyclic stability with rapid capacity deterioration, both of which failed to achieve long-life cycling (Figure 5.12a and 5.12c). Note that the intrinsic void spaces existing in the textile host would be beneficial for the electrochemical performance with inevitably reduced energy density. Expectedly, by strictly controlling the intake of the molten Li in the textile host, the reduction in energy density can be effectively mitigated. As a result, the battery adopting the Janus anode presented a moderate energy density of 261 Wh kg^{-1}, which was over 30% enhancement compared with the cell using a homogeneous anode (Figure 5.12b).When further increasing the current density, the LFP//Janus anode still exhibited a superior capacity retention of 89.8% after 300 cycles at 1 C rate (Figure 5.12c) and better rate capability (Figure 5.12d).

Finally, the pouch cell of LCO//Janus anode was assembled with a total capacity over 16 mAh, which delivered an outstanding capacity retention of 99.97% per cycle (Figure 5.11e). Desirable electrochemical stability and folding tolerance were demonstrated in Figure 5f, where the GCD profiles perfectly overlapped after folding 200 times. Impressive flexibility was also revealed as it could normally power the LED array despite bending at 90 degree or even totally folding (Figure 5.11g). Therefore, the Janus anode fabricated by selective wetting can facilitate the intrinsic cycling stability, outstanding lifespan, and desirable flexibility required for the advanced anode, promising great potential in the next generation of LMBs.

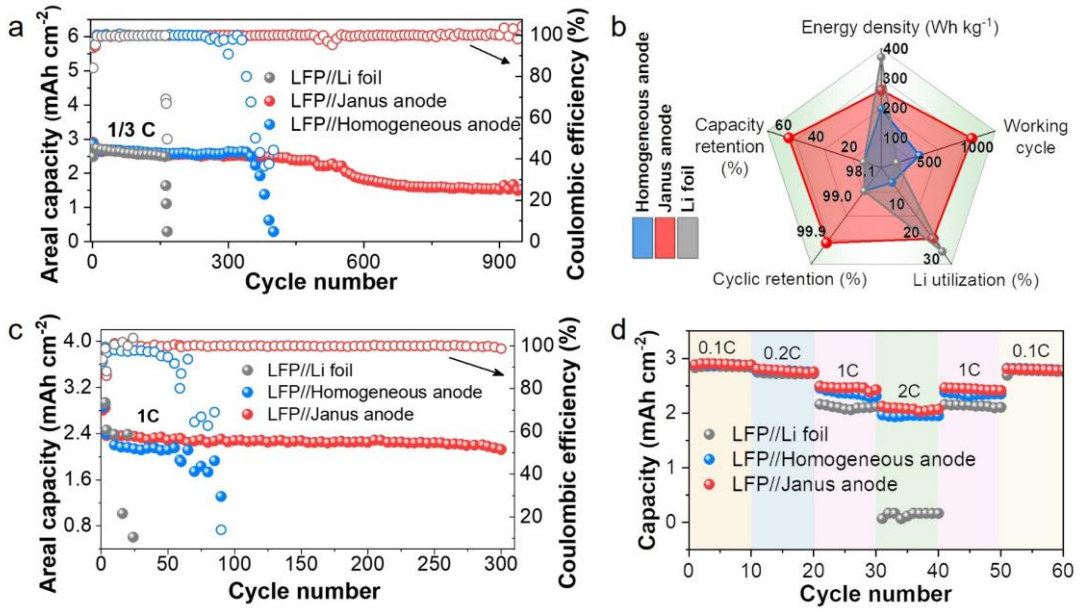

Figure 5.12 Cycling durability of the LFP//Li foil, LFP//homogeneous anode, and LFP//Janus anode at 1/3 C (a) and 1 C rate (c), comprehensive comparison of these LMBs based on energy density, working cycle, DOD, cyclic retention, and capacity retention (b), and rate capability based on different anodes (d).

5.4 Conclusion

In summary, we have proposed a facile yet effective strategy of selective wetting that realized the rapid fabrication of the stable Janus Li-textile anode with a thin Li coating layer (~50 μm). In the symmetric cell study, the Janus anode cell showed an ultrastable electrochemical performance with a prolonged cycling life of over 3,000 hr even under a high DOD (10 mAh cm^{-2}, 10 mA cm^{-2}). It was probably attributed to its Janus lithiophobic-lithiophilic textile host and upper buffering space, which could guide an oriented Li deposition, promote the Li plating/stripping kinetics and maintain a stable electrode interface, thus achieving significant improvements in cycling stability and working lifespan. The LCO//Janus anode cell delivered a long-term lifespan of 2,000 cycles with superior cyclic retention over 99.9% at the 1 C rate. When paired with the LFP cathode, the LFP//Janus anode cell also displayed a prolonged cycling life of 950 cycles, and improved energy density by over 30%. Finally, the outstanding

electrochemical stability and impressive flexibility were further revealed in the pouch cell. To conclude, the facile strategy of selective wetting is a convenient, credible, and promising method for achieving the thin LMAs toward high-performance LMBs.

Chapter 6 Sandwiched Lithium Metal Anodes for High-Energy and Highly-Flexible Lithium Metal Batteries

Achieving high flexibility while maintaining high energy density remains a challenge in batteries featuring thin lithium (Li) metal anodes (LMAs). To solve this challenge, in this chapter, we focus on the development of a thin, ultralight, and flexible LMA to enable the lithium metal battery (LMB) with both high energy density as well as high flexibility. Typically, a thin Li strip is designed to be sandwiched between two ultralight fabric layers. Such incorporation of the superlight fabric layers minimizes unnecessary weight within the battery, while the sandwiched structure simultaneously endows the thin LMA with superior electrochemical stability and exceptional flexibility. The sandwiched composite Li anode (SW Li), exhibits a significant weight reduction of over 60% in contrast to foil-based thin LMAs, thus theoretically receiving energy density improvement of more than 13%. Additionally, the SW Li possesses good origami capability and high bending tolerance, enduring 10,000 times at a bending radius of 1.5 mm. Furthermore, SW Li battery not only delivers enhanced electrochemical stability with a high specific energy of 309 Wh kg^{-1}, but also presents outstanding flexibility with a remarkably high figure of merit for flexible battery (163.8), outperforming the state-of-the-art flexible batteries.

6.1 Introduction

The remarkable importance of utilizing a thin lithium (Li) metal anode (LMA) in the battery system has been pointed out and demonstrated in our work chapter 5. However, achieving high energy and high flexibility in lithium metal batteries (LMBs) incorporating thin LMAs remains a formidable challenge.

The majority of studies of thin LMAs reported to date have used either low cathode loading or heavy current collectors [171, 212-215], leading to uncompetitive energy density that fails to meet the requirements of practical applications. For instance, a thin

LMA developed through electroplating was coupled with a low-loading LiFePO4 (~4 mg cm^{-2}) to achieve a promising lifespan, which was at the cost of energy density [212]. Meanwhile, the Cu foil as a current collector and support for thin LMAs is disadvantageous due to its considerable density (8.96 g cm^{-3}), which constitutes more than 15 wt% of the total battery weight. Consequently, the reported battery energy remains limited, falling short of commercial viability despite practical cathodes being employed. Achieving high energy density in the thin LMA-based batteries necessitates pushing nearly all parameters to their limits, including adopting realistic conditions such as high-capacity cathode (≥3 mAh cm^{-2}), limited negative to positive areal capacity ratio (N/P), ultralight current collectors, and lean electrolyte.

Apart from acquiring high energy density, it is also essential to achieve good flexibility of batteries to meet the requirement of flexible electronics, e.g., bendable phone and roll-up display [45, 61]. However, thin LMAs usually suffer from mechanical fragility and poor flexibility. In this regard, integrating 3D porous carbon-/polymer-based hosts with thin LMAs offers a promising solution to simultaneously enhance electrochemical stability and mechanical flexibility [216-219]. A pioneering work is the development of a flexible carbon fabric-based lithium-sulfur battery, which demonstrated superior cycling stability and remarkable bending tolerance [24]. However, the pursuit of flexibility in most studies typically compromises energy density due to the introduction of heavy and thick inactive hosts. Furthermore, approaches designed to develop flexible composite thin LMAs, such as electrochemical deposition and molten infusion [24, 30, 32], still lack scalability for large-area production. Therefore, acquiring high flexibility yet maintaining high energy density in thin LMA-based batteries through a facile method remains a bottleneck to be solved.

In this chapter, we report a thin, ultralight, and highly flexible sandwiched Li (SW Li) anode for energy-dense flexible LMBs. We incorporate ultralight insulating and conductive fabrics to sandwich the thin Li strip through mechanical rolling, effectively minimizing superfluous weight while enhancing the anode's stability and flexibility.

Notably, the SW Li exhibits a mass loading of only ~4.3 mg cm^{-2}, achieving a 62.6% reduction in weight and a 13.6~14.8% improvement in energy density compared to a traditional thin Li electrode using Cu foil as the current collector. Moreover, the mechanical support provided by the fabric layers endows the SW Li with exceptional flexibility, allowing it to be folded into an origami shape and bent for 10000 times at a radius of 1.5 mm. The electrochemical studies show that the SW Li could be compatible with various high-loading commercial cathodes, contributing to achieving a practical high whole-cell energy density of over 300 Wh kg^{-1}. Meanwhile, the high-energy SW Li battery also exhibits outstanding dynamic bending tolerance even when subjected to repeated bending at a small radius of 1 mm, resulting in a significantly high figure of merit for flexible battery (fb_{FOM}) of 163.8.

6.2 Experiment

6.2.1 Materials Preparation

Fabrication of SW Li Anode: An ultrathin lithiophilic Sb layer with a thickness of 100 nm was evaporated to one side of the commercially available PI fabric to obtain the Sb coated PI (PI-Sb) fabric. Then, another side of the PI fabric was further modified with 1 μm-thick Cu via thermal evaporation (JSD-600) to receive the conductive Cu coated PI-Sb (Cu-PI-Sb) fabric. Later, the thin SW Li anode was easily fabricated by sandwiching thin Li foil between insulating PI-Sb fabric and conductive Cu-PI-Sb fabric through mechanical rolling. Typically, the calendaring thickness of the SW Li could be well-controlled by adjusting the gap distance between the two rollers. After rolling, the Li layer thickness in the SW Li changed from ~50 μm to ~40 μm due to the ductility of Li.

Fabrication of Cu/Li/PI Anode and Cu/Li Anode: Similarly, the Cu/Li/PI anode was prepared by sandwiching thin Li between PI fabric and Cu foil through the same procedure. In the case of the Cu/Li anode, thin Li was stacked and rolled between a

sacrificial polypropylene (PP) film and Cu foil. When accomplishing the rolling process, the PP film was peeled off to obtain the Cu/Li anode.

6.2.2 Cell Assembly

Half cells were assembled by pairing the pouched substrates with the counter electrode of 400 μm Li. Half cells were assembled by using the prepared anodes. Full cells were assembled by stacking the prepared anodes, Celgard 2325 separator, and high-loading cathodes in the 2025-type coin cells. The pouch cells were also prepared, and the detailed process could refer to chapter 4.

6.2.3 Characterizations

The galvanostatic tests and cycling performance of the batteries were evaluated by the Neware battery testing system. The Aurbach protocol in a half cell for CE calculation was carried out. A fixed amount of Li metal (10 mAh cm^{-2}) was deposited, and then subjected to 100 cycles (1 mA cm^{-2}, 1 mAh cm^{-2}) followed by complete stripping. The energy density was calculated based on the mass loading of all the cell components, including the current collectors, anode, cathode, electrolyte, and separator. Detailed characterizations for the electrodes and batteries could refer to chapter 4.

6.3 Results and Discussion

6.3.1 Fabrication, Design Principle, and Properties of Sandwiched Li (SW Li)

As illustrated in Figure 6.1a, we fabricated a thin, lightweight, and flexible SW Li by sandwiching the Li foil between two ultralight polyimide (PI)-based fabrics through a facile rolling process. In our design, the lithiophilic antimony (Sb) modified PI (PI-Sb) fabric was employed as the top buffering layer to stabilize the anode while the conductive Cu coated PI-Sb (Cu-PI-Sb) fabric was adopted as the superlight current collector of the SW Li. Apart from minimizing the unnecessary weight of the electrode

and enhancing the electrochemical stability, the upper and bottom fabric layers also provide a robust mechanical support, endowing SW Li with exceptional flexibility.

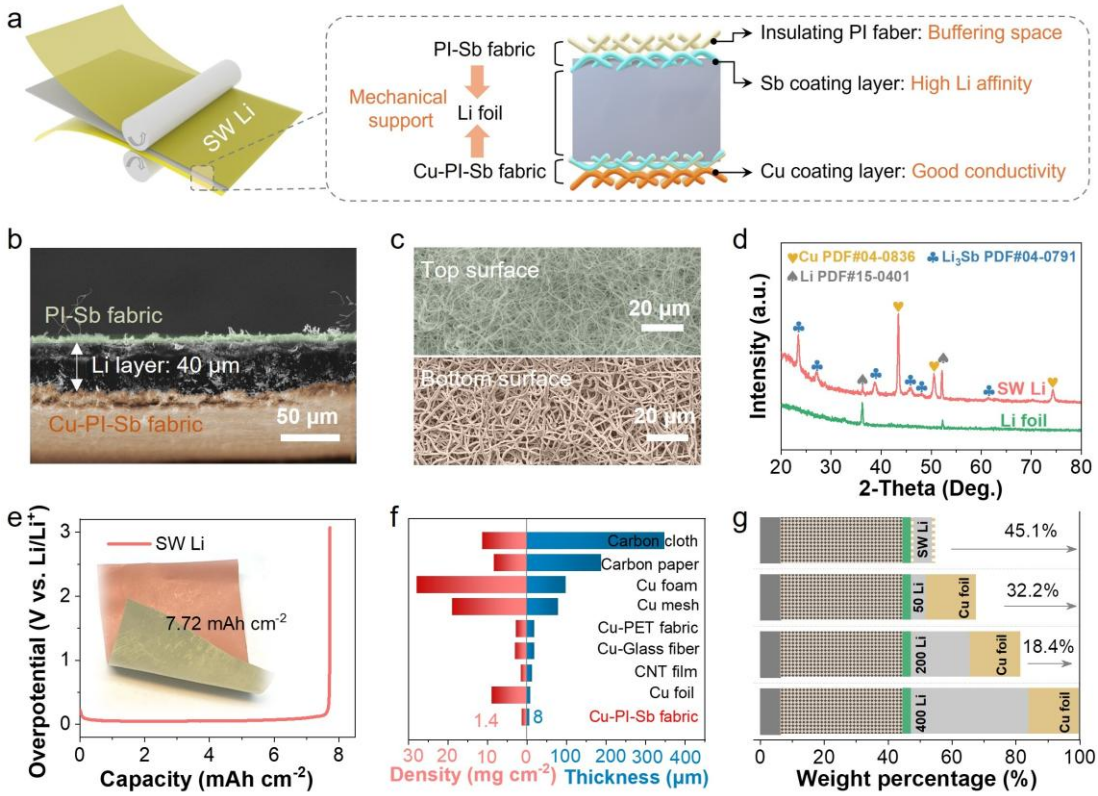

Figure 6.1 (a) Schematic illustration of the one-step rolling fabrication process and design principle of the SW Li. (b) Cross-sectional SEM image of the SW Li, where the Li layer is only 40 μm. (c) The top and bottom surface of the SW Li. (d) XRD spectrum of bare Li foil and SW Li.(e) Stripping profile of the SW Li for capacity determination, and the inset shows the optical images of the SW Li (5 × 6 cm). (f) Comparison of the Cu-PI-Sb fabric with different types of collector collectors in terms of density and thickness. (g) Comparison of the cell configuration weight of Li metal batteries using different anodes. The 400 Li, 20 Li, and 50 Li represents 400 μm-thick Li, 200 μm-thick Li, and 50 μm-thick Li, respectively.

As shown in Figure 6.1b, the SW Li composed of three layers, was 55 μm in total, where the thickness of the middle Li layer changed from 50 to 40 μm after rolling because of its ductility. Two sides of the Li layer were distributed with the Sb elements

as indicated in the mapping result (Figure 6.2). The top and bottom fabric surfaces of the SW Li are given in Figure 6.1c. Due to the coating of Cu, the diameter of the nanofibers on the bottom side was larger than that on the top side.

In the X-ray diffraction (XRD) spectrum, additional pronounced peaks assigned to Cu and Li_3Sb alloy were found in the SW Li compared to bare Li foil (Figure 6.1d). It is verified that the Sb coated on the fibers was converted into the Li-Sb alloy during the rolling process to achieve the SW Li. The Li_3Sb alloy not only shows good Li^+ affinity with strong Li^+ adsorption (1.04 eV), but also exhibits a low energy barrier of Li^+ diffusion (0.09 eV) [125, 220], which can regulate the Li deposition behavior and promote rapid Li^+ transportation, thereby benefiting anode stabilization. The as-fabricated freestanding SW Li possessed a stripping capacity of 7.72 mAh cm-2 (Figure 6.2e). It theoretically corresponded to 38.6 μm-thick Li, which was consistent with the observed thickness of the Li layer.

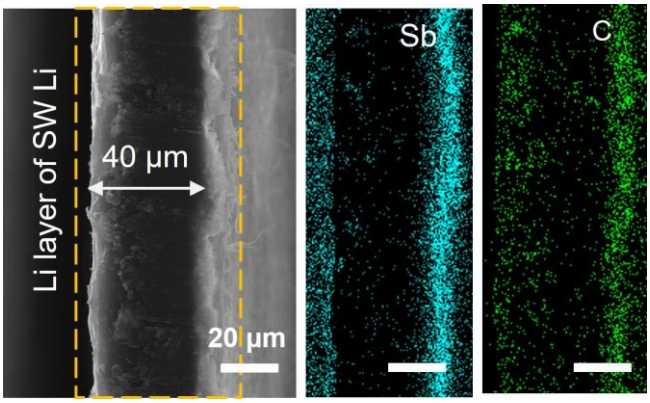

Figure 6.2 The SEM image and the mapping of the middle Li layer of the SW Li.

Notably, the Cu-PI-Sb fabric was 8 μm in thickness and 1.4 mg cm^{-2} in density (Figure 6.1f, Figure 6.3), which was thinner and lighter than commonly used Cu foil (10 μm, 8.9 mg cm^{-2}) and most of the 3D current collectors. As such, our SW Li also showed an ultralight nature of 4.3 mg cm^{-2}, realizing a 62.6% weight reduction in contrast to the 50 μm-thick Li/Cu electrode. When the thin Li (50 μm) is substituted for the thick Li (400 μm), the weight of the cell configuration could be reduced by 32.2% (Figure 6.1g).

Significantly, the whole-cell weight could be further minimized by 12.9% when replacing the 50 μm-thick Li/Cu electrode with our lightweight SW Li. As a consequence, the projective energy densities of the batteries equipping with the SW Li would achieve a remarkable improvement by 13.6~14.8% and 47.7~51.9% when compared to those batteries employing the 50 μm-thick Li/Cu electrode and 400 μm-thick Li/Cu electrode, respectively.

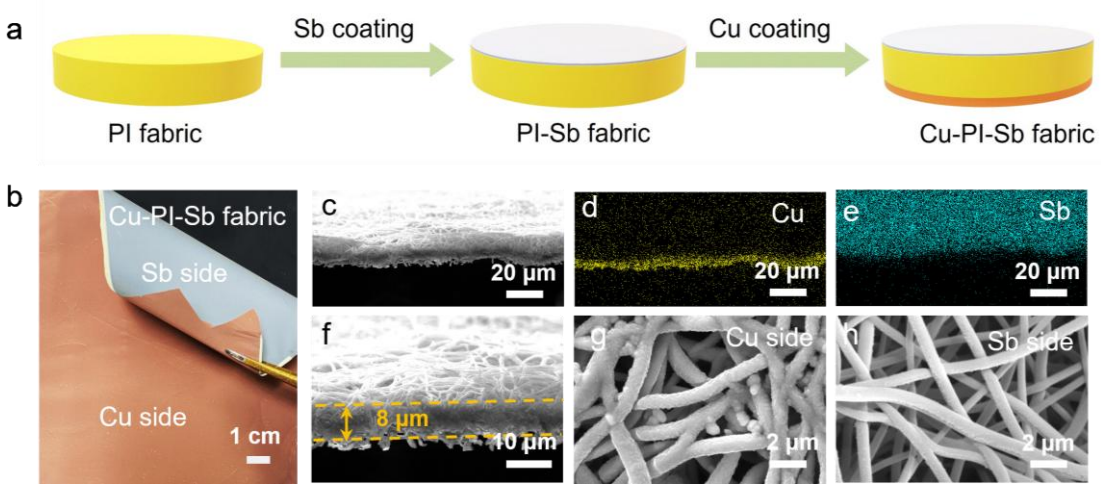

Figure 6.3 (a) The fabrication process of Cu-PI-Sb fabric. (b) Digital image of the Cu-PI-Sb fabric. The cross-sectional images of the Cu-PI-Sb (c, f), and corresponding elemental mapping of Cu (d), and Sb (e). Surface morphologies of Cu side (g) and Sb side (h) of the Cu-PI- Sb fabric.

6.3.2 Cycling Stability and Durability of SW Li

A high average Coulombic efficiency (CE) of 99.1% was reached on the Cu-PI-Sb fabric (Figure 6.4). It suggests a good reversibility of Li metal on the Cu-PI-Sb fabric, which is suitable to act as a current collector for hosting Li. The SW Li comprised of PI-Sb, Li foil, and Cu-Li-PI promotes a well-regulated Li deposition behavior, where the Li deposits could be confined underneath the top layer assisted by the interfacial Li-Sb alloy.

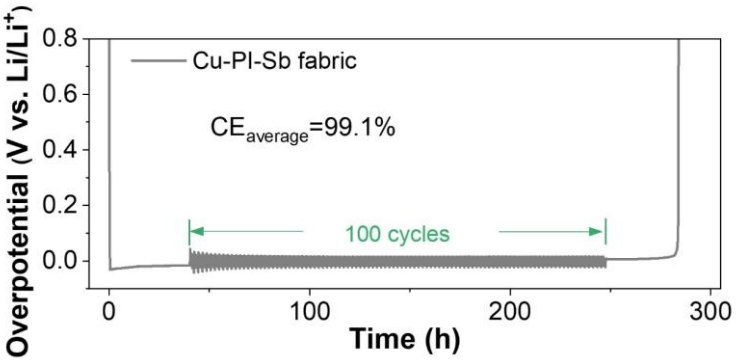

Figure 6.4 (a) Plating/stripping curves of Li on the Cu-PI-Sb fabric for CE determination.

As shown in Figure 6.5, a dense Li deposition with a capacity of 5 mAh cm^{-2} was found on the SW Li, where the top layer was free of Li deposits and dendrites. In this regard, the SW Li shows good potential for long-life cycling. To evaluate the long-term electrochemical stability of the SW Li, the galvanostatic cyclic test of symmetric cells was then conducted. For better comparison, thin Li foils were rolled with Cu foil (Cu/Li), or rolled between Cu foil and PI fabric (Cu/Li/PI), to serve as the control samples.

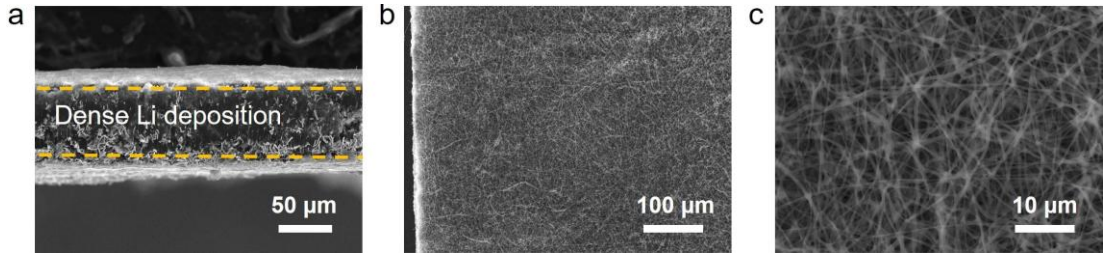

Figure 6.5 The (a) cross-sectional morphology and (b, c)top surface of the SW Li after 5 mAh cm^{-2} Li deposition. The thickness of middle Li layer changes from initial ~40 μm to ~65 μm, indicating a dense Li deposition.

In Figure 6.6a, the symmetric SW Li cell presented a much lower voltage hysteresis (~15 mV) and a prolonged cycling lifespan of more than 750 hr at a depth of discharge (DOD) of 12.5% (1 mA cm^{-2}, 1 mAh cm^{-2}). In sharp contrast, the Cu/Li cell exhibited

a poor electrochemical stability of only ~200 hr with a random yet drastic voltage vibration, indicating the severe growth of Li dendrites. A considerable increase in overpotential (>160 mV) was found in the symmetric Cu/Li/PI cell within 250 hr, implying that uncontrollable dendrites still formed on top of the electrode surface. The SW Li-based symmetric cell also displayed a better rate capability, showing a stable and flat voltage profile without fluctuation (Figure 6.6b).

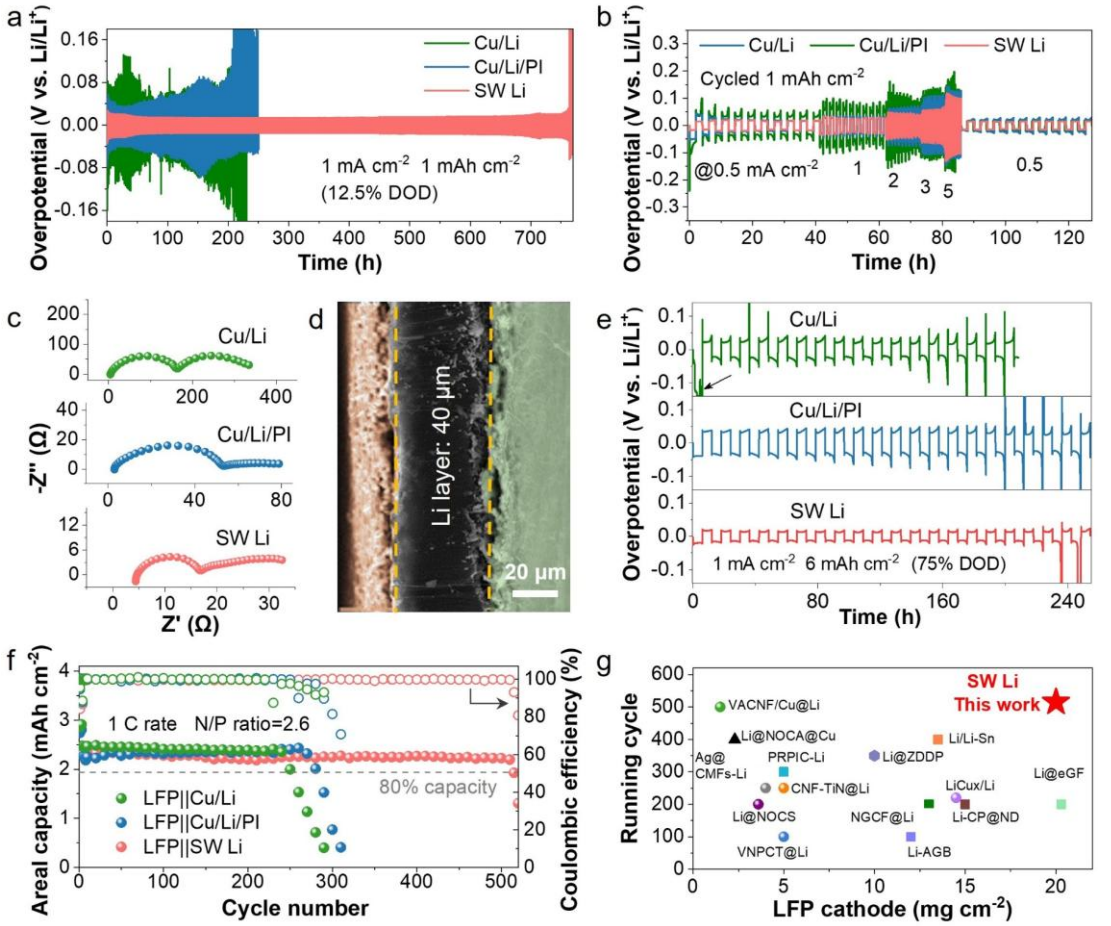

Figure 6.6 (a) Cycling stability of symmetric cells based on Cu/Li, Cu/Li/PI, and SW Li at a DOD of 12.5%. (b) Comparison of rate capability of symmetric cells using various anodes. (c) Nyquist plots of symmetric cells before cycling. (d) The structural morphology of the SW Li after 50 cycles. (e) Voltage profiles of symmetric cells at a high DOD of 75%. (f) Cycling durability of the LFP-based full cells pairing with different anodes at the 1 C rate of 3 mA cm^{-2}. (g) Comparison of LFP loading and running cycle between our SW Li battery and reported state-of-the-art Li metal batteries

using the thin Li metal as anodes [30, 32, 172, 177, 212-215, 221-226].

As shown in Figure 6.6c, the electrochemical impedance spectroscopy (EIS) evidenced a smaller charge transfer resistance of 16.7 Ω for the SW Li cell in contrast to cells of Cu/Li (165.1 Ω) and Cu/Li/PI (53.5 Ω). It reveals better charge distribution and faster Li ion diffusion kinetics of the SW Li anode due to the synergy effect of the fabric framework and Li-Sb interfacial alloy layer. Moreover, the SW Li could maintain good structural stability without volumetric expansion and dendritic growth after 50 plating/stripping cycles (Figure 6.6d). Even under a high DOD of 75%, the SW Li still showed a stable cyclic life up to 220 hr with a much-reduced voltage polarization of 20 mV (Figure 6.6e).

The cyclability and durability of our SW Li were also investigated in full cells by pairing a commercial lithium iron phosphate (LFP, 3 mAh cm^{-2}) cathode. Realistic conditions of a low N/P ratio of 2.6 and a high current density of 1 C rate were adopted. Impressively, the LFP||SW Li cell delivered a practical capacity of 2.4 mAh cm^{-2} at 1 C rate and demonstrated a well-extended lifespan of 500 cycles with an outstanding capacity retention of 92% (Figure 6.6f and Figure 6.7a). By contrast, batteries using Cu/Li and Cu/Li/Pi as anodes dropped to 80% capacity after 250 cycles and 280 cycles, respectively, then entered a quick failure as revealed by charge/discharge profiles (Figure 6.7b and 6.7c). The SW Li endowed itself with significantly improved cycling stability, which could sustain a long-term cycling life under a high LFP loading (Figure 6.6g), outperforming most of the reported thin LMAs [30, 32, 172, 177, 212-215, 221-226].

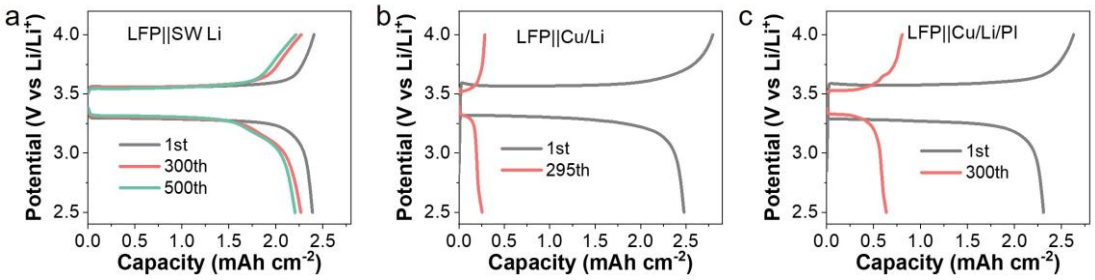

Figure 6.7 The voltage profiles of (a) LFP||Cu/Li, (b) LFP||Cu/Li/PI, and (c) LFP||SW Li under different cycles.

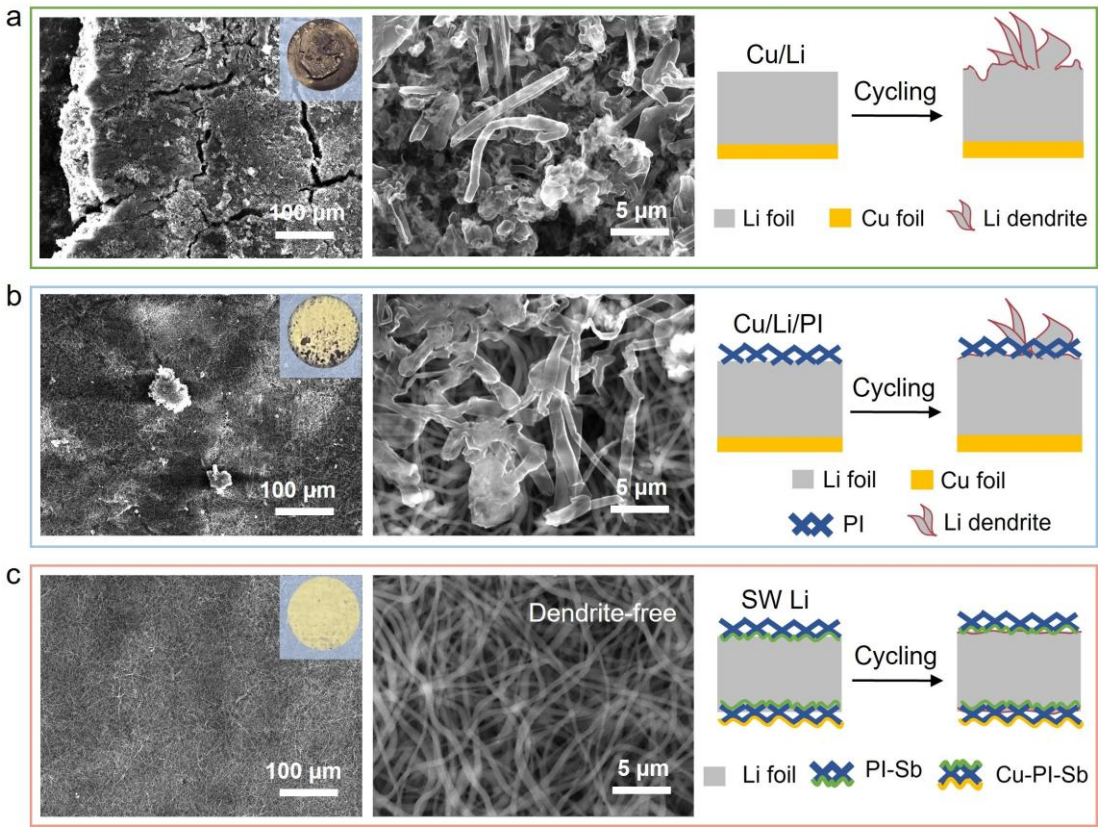

Figure 6.8 Top-view morphologies of various cycled anodes of Cu/Li (a), Cu/Li/PI (b), and SW Li (c) when paired with the high-loading cathode. The insets are the digital images of the corresponding cycled anodes. The cycling models are also given respectively, where the Cu/Li and Cu/Li/PI anode show the uncontrollable dendritic growth on top of the electrode after repeatedly cycling, while the SW Li anode exhibits a favorable dendrite-free surface by guiding Li deposition underneath the top fabric framework.

To better understand the superior stabilization enabled by the SW Li anode, we visualized the top-view morphologies of different anodes after 20 cycles. As shown in Figure 6.8a, the top surface of the cycled Cu/Li anode became rough and rugged with isolated chunks of dead Li, massive cracks, and obvious dendritic Li. The Cu/Li/PI

anode exhibited an improved cycled surface with less accumulated dead Li due to the upper buffering PI framework, which could facilitate a homogenous Li ion distribution. However, uneven Li deposits pierced the PI fabric, eventually forming dendrites on top of the Cu/Li/PI anode (Figure 6.8b). The cycling models of Cu/Li and Cu/Li/PI both describe the deteriorated surface with dendrite formation after repeated cycling, which could be the main cause of the poor cycling stability. In comparison, the cycled SW Li anode maintained an intact, tidy, and smooth fabric surface with a dendrite-free feature (Figure 6.8c). The interfacial Li-Sb alloy of SW Li could contribute to the oriented Li deposition and facilitate the rapid Li ion transportation. Consequently, the Li deposition was adjusted to the underneath of the top layer of the SW Li, which effectively suppressed the growth of dendrites on the surface, as shown in the cycling model (Figure 6.8c). The structural integrity and electrochemical stability in the SW Li were thus significantly enhanced.

6.3.3 Practical High-Energy LMBs Enabled by SW Li

To showcase the practicability of our SW Li, high-loading commercial cathodes of $LiCoO_2$ (LCO) and $LiNi_{0.8}Co_{0.1}Mn_{0.1}O_2$ (NCM811) were used with a 4.4 V high cut-off voltage and controlled electrolyte (5μl mAh^{-1}). The LCO-based batteries using different anodes started with a very similar discharge capacity of 3.2 mAh cm^{-2} at 0.1 C (Figure 6.9a and 6.9b). After 120 cycles at the rate of 1 C (Figure 6.9a), the SW Li cell presented a better capacity retention of 78.7% than batteries using Cu/Li (69.4%) and Cu/Li/PI (74.2%). Meanwhile, the LCO||SW Li battery maintained a superior average CE of 99.73% during 150 cycles. In addition, the NCM811-based batteries using anodes of Cu/Li, Cu/Li/PI, and SW Li both delivered a high capacity of 4.2 mAh cm^{-2} with almost overlapped voltage profiles (Figure 6.9d). However, under such a low N/P ratio of 1.9, the Cu/Li battery and Cu/Li/PI battery showed a faster capacity deterioration with retention of only 54.5% and 65.2% after cycling 100 times at a 0.5 C rate (Figure 6.9c). In contrast, the NCM811||SW Li battery still presented a prolonged lifespan and retained a capacity of 3.2 mAh cm^{-2} at the 100th cycle, displaying a

superior retention of 84.2%. These results strongly demonstrate the effectiveness of the SW Li anode in improving cycling stability.

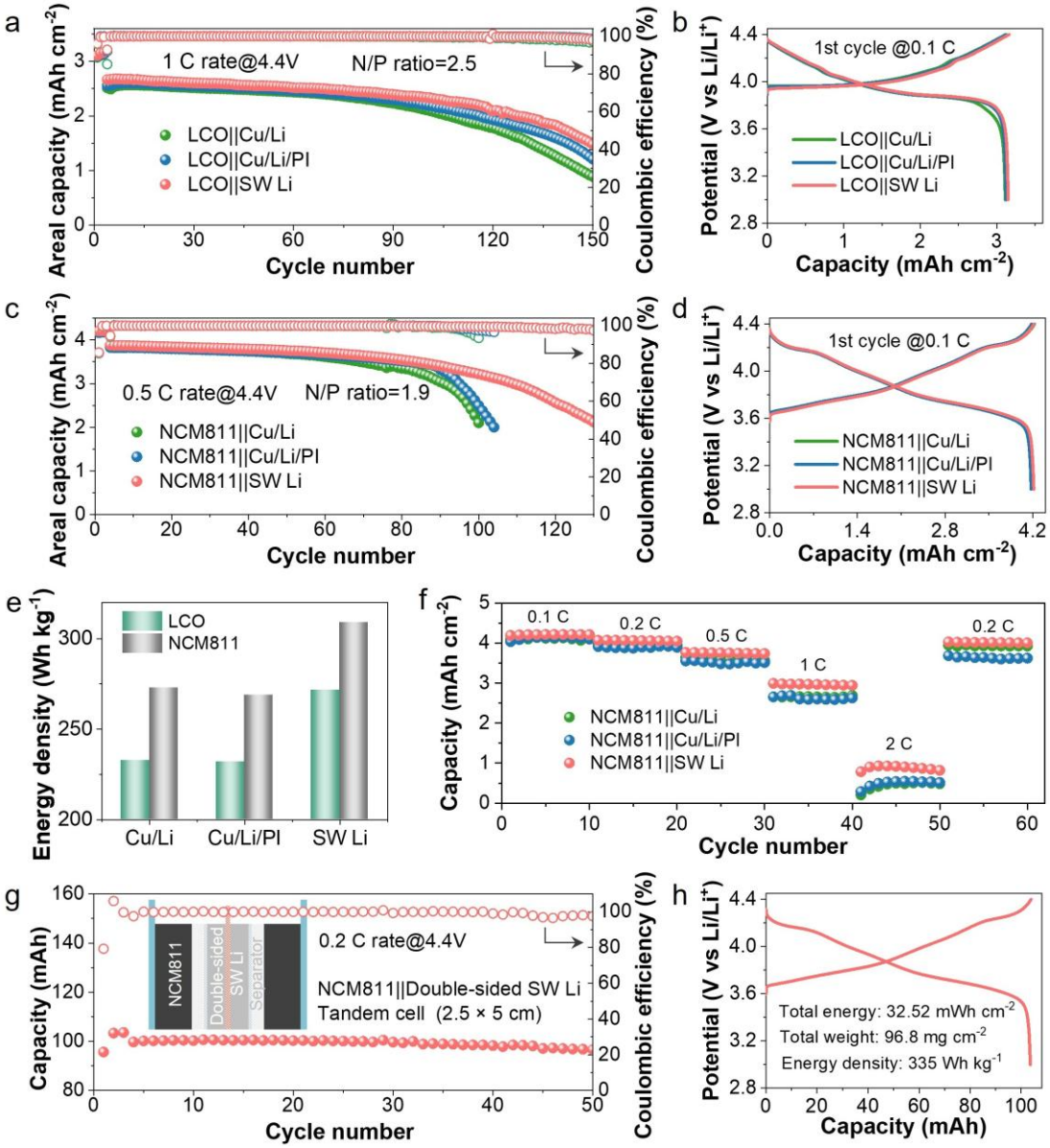

Figure 6.9 Electrochemical stability and voltage profiles of the LMBs pairing various anodes with the high-voltage and high-loading cathodes of (a, b) LCO and (c, d) NCM811. (e) Comparison of the gravimetric energy density of different full-battery systems using various anodes. (f) Rate performance of full cells. (g) Cycling performance and (h) GCD profile of the tandem pouch cell using the double-sided SW Li. The inset shows the schematic configuration of the tandem cell made of the double-sided SW Li and one pair of NCM811.

More importantly, the Li metal batteries realized a significant enhancement in energy density by 13.3~17.1% when substituting the Cu/Li and Cu/Li/PI with our ultralight SW Li anode (Figure 6.9e). For example, the whole-cell energy density of NCM811||SW Li reached a practical value of 309 Wh kg^{-1}, which was superior to Cu/Li battery (273 Wh kg^{-1}) and Cu/Li/PI battery (267 Wh kg^{-1}). Furthermore, the SW Li battery manifested a better rate capability with a current density ranging from 0.1 C to 2 C (Figure 6.9f). Later, a tandem cell prototype was fabricated with lean electrolyte (2.8 μl mAh^{-1}) and a low N/P ratio of 1.9. Specifically, we adopted a double-sided SW Li as anode and a pair of NCM811 (2.5×5 cm) as cathode. The tandem cell presented a stable cycling lifespan of 50 cycles with superior capacity retention of 96.2% (Figure 6.9g). Meanwhile, the tandem cell with a total capacity of 103.6 mAh achieved an excellent energy density of 335 Wh kg^{-1} (Figure 6.9h).

6.3.4 Highly-flexible LMBs realized by SW Li

It is verified that the SW Li could be folded into an origami boat as shown in Figure 6.10a. In addition, the SW Li sustained a stable resistance without significant change at a bending radius of 2.5 mm and 1.5 mm for 10000 times, indicating its excellent flexibility and superior bending tolerance (Figure 6.10a). However, the bare Li foil failed quickly after being bent 277 times at a small radius of 1.5 mm, exposing its mechanical fragility. In this regard, the lightweight and flexible SW Li anode has great potential to achieve advanced batteries with high energy and high flexibility.

As a proof of concept, high-loading NCM811-based single-layer pouch cells (N/P ratio=1.9, E/C ratio=5 μl mAh^{-1}) with a size of 4 cm^2 were assembled to compare the flexibility by investigating the electrochemical stability under dynamic flexing. Upon a charging/discharging cycle, the pouch cell would be bent 1800 times at a small bending radius of 1.5 mm.

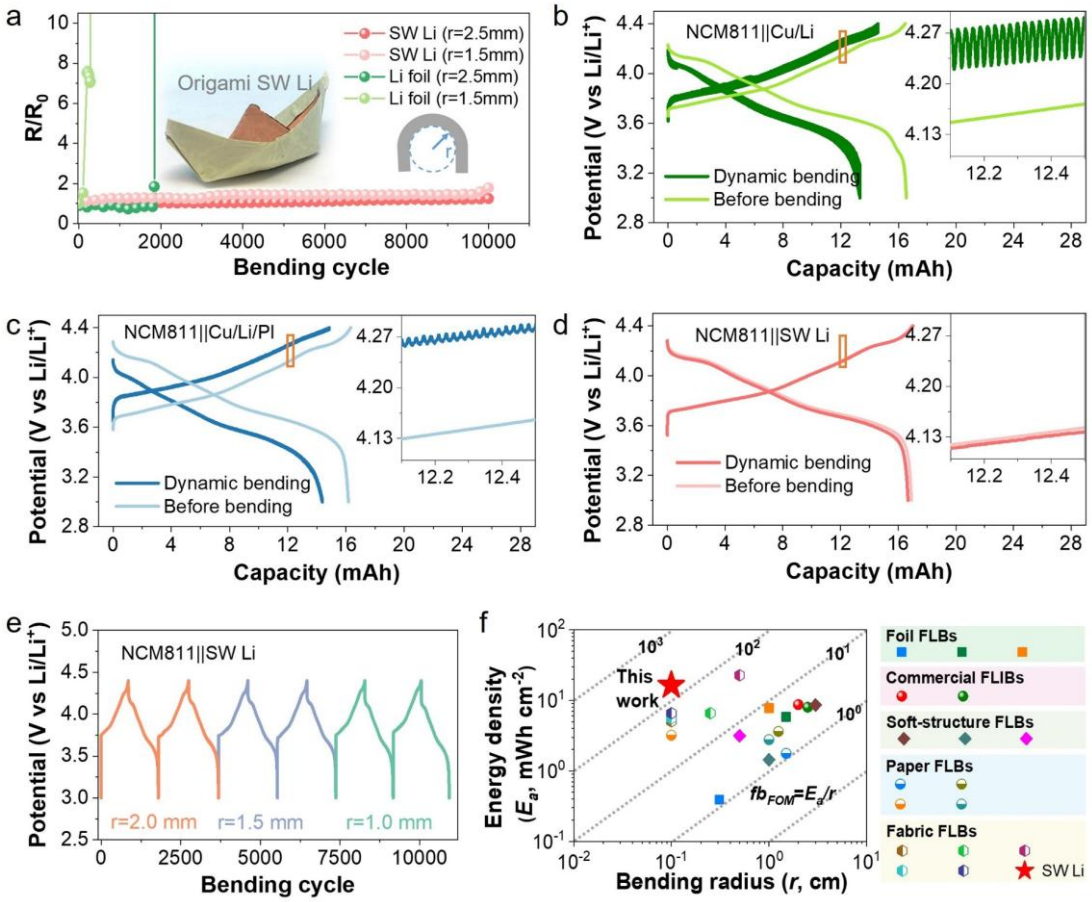

Figure 6.10 (a) Resistance change of SW Li and bare Li metal foil under different bending radius. The inset shows the origami-shaped SW Li, indicating a good flexibility of the SW Li. The GCD profiles of pouch cells of (b) NCM811||Cu/Li, (c) NCM811||Cu/Li/PI, and (d) NCM811||SW Li under flat and dynamic bending state at 0.2 C rate. Inset is the zoom-in profile of the frame. The bending radius is 1.5 mm, and a total 1800 bends is performed during the charging/discharging process. (e) Charge/discharge curves of flexible LMB of NCM811||SW Li as a function of bending cycles at different curvature radii of 2 mm, 1.5 mm, and 1 mm. (f) Comparison of the figure of merit for flexible battery (fb_{FOM}, Ea/r) [24, 47, 178, 190, 227-238].

In Figure 6.10b, the pouch cell using the Cu/Li anode could maintain a normal and stable GCD profile before bending. However, the voltage output of this pouch cell fluctuated dramatically during the dynamic bending process as indicated in the magnified profile, while the total capacity deteriorated from 16.5 mAh to 13.3 mAh

after completing 1800 bends (Figure 6.10b). When using the Cu/Li/PI as an anode, the pouch cell under dynamic bending state still suffered from a large capacity loss of 11% despite the fluctuation in voltage profile becoming smaller (Figure 6.10c). These results imply that the pouch cells adopting anodes of Cu/Li and Cu/Li/PI both have undesirable dynamic stability and poor mechanical flexibility.

In sharp contrast, during dynamic flexing, the GCD curve of the SW Li-based pouch cell remained smooth and stable, almost overlapping with the pristine voltage profile (Figure 6.10d). Moreover, the NCM811||SW Li pouch cell with an energy density of 309 Wh kg^{-1} maintained a high capacity retention of 98.7% after dynamic bending. Besides, it could also normally work with a steady signal output even when subjected to an extremely small bending radius of 1.0 mm (Figure 6.10e), indicating an outstanding flexibility of the cell. The extraordinary flexibility was also demonstrated in the LCO||SW Li pouch cell.

To fairly benchmark the performance of flexible batteries, the figure of merit of flexible battery (fb_{FOM}) is especially introduced as an indicator [43]. The fb_{FOM} considers the areal energy (Ea) and bending radius (r) of curvature of the cell, which can quantitatively evaluate the battery performance and properly reflect the applicability of laboratory research in industrial applications. The commercial flexible lithium ion batteries (FLIBs) and reported advanced flexible lithium batteries (FLBs) based on soft-structural design or soft-material selection, reached the fb_{FOM} values of no more than 70 (Table 6.1). Impressively, the flexible SW Li battery achieved a high fb_{FOM} of 163.8, significantly surpassing the state-of-the-art flexible batteries (Figure 6.10f and Table 6.1). Therefore, our SW Li made a great advancement in the field of thin LMAs, which could not only meaningfully improve energy density, but also effectively enhance mechanical flexibility, showing great feasibility in practical applications.

Table 6.1 Comparison of our flexible SW Li battery with the state-of-the-art flexible Li-based batteries [24, 47, 178, 190, 227-239].

Type	Batteries	Areal capacity (mAh cm^{-2})	Energy density (Wh kg^{-1})	Areal energy (*Ea*, mWh cm^{-2})	Bending radius (*r*, cm)	FOM
Foil-based FLBs	Thin-film LIB [227]	0.1	NA	0.39	0.31	1.3
	Patterned LIB [228]	1.5	169	5.82	1.5	3.9
	GPE-based LMB [229]	2.0	NA	7.76	1.0	7.8
Commercial FLBs	Jenax Inc. LIB [230]	2.3	NA	8.70	2.0	4.4
	Panasonic Corp. LIB [231]	2.1	108	7.98	2.5	3.2
Soft-structure FLBs	Wave-like LIB [232]	2.2	56	8.60	3.0	2.9
	Layered LCO battery [233]	0.6	NA	1.44	1.0	1.4
	All-in-one LMB [234]	1.5	NA	3.15	0.5	6.3
Paper-based FLBs	S@CNT battery [239]	0.8	NA	1.76	1.5	1.2
	RGO/NC@Li battery [238]	1.7	NA	3.62	1.25	2.9
	GO-GPE based LIB [235]	1.3	69	3.19	0.1	31.9
	CA-CNT based LIB [236]	1.2	98	2.76	1.0	2.8
Fabric-based FLBs	Fabric Li-S battery [24]	2.4	230	5.04	0.1	50.4
	Hybrid LIMB [237]	1.9	167	6.59	0.25	26.4
	ZeroVE-Li battery [47]	5.8	284	22.74	0.5	45.6
	GF based battery [178]	1.4	225	5.57	0.1	55.7
	Janus Li battery [190]	1.7	140	6.59	0.1	65.9
	SW Li battery (This work)	4.2	301	16.38	0.1	163.8

6.4 Conclusion

In conclusion, we have reported a thin SW Li (55 μm, ~8 mAh cm^{-2}) with merits of

lightweight, high stability, and good flexibility, contributing to realizing high-energy yet highly-flexible LMBs. Despite introducing two fabric layers, the density of the SW Li (4.3 mg cm^{-2}) was only 37.4% of the traditional thin Cu/Li electrode, thereby theoretically enhancing the energy density by 13.6~14.8%. The SW Li anode was compatible with different high-loading commercial cathodes (LFP, LCO, NCM811), showing improved electrochemical stability due to the fabric framework and Li-Sb interfacial alloy. Moreover, the NCM811||SW Li battery achieved a practical energy density of 309 Wh kg^{-1}. Importantly, the SW Li electrode received exceptional flexibility, which could maintain a stable performance after 10000 bends at a radius of 1.5 mm. The corresponding pouch cell demonstrated high flexibility, which could normally work even under a harsh bending condition (radius=1 mm). Consequently, our flexible and high-energy SW Li battery achieved a remarkably high fb_{FOM} of 163.8, outperforming the commercial flexible batteries (fb_{FOM} <5) and reported state-of-the-art flexible batteries (fb_{FOM} <70). This thin, ultralight, and flexible SW Li achieved by one-step mechanical rolling paves the way for developing advanced thin LMAs towards high-energy-density and highly-flexible LMBs.

Chapter 7 Ultrathin Interphase Layer for High-Performance Anode-Free Lithium Metal Batteries

Thinning the thickness of lithium (Li) metal to zero can maximize the energy density and enhance the safety of Li metal batteries (LMBs). However, anode-free LMBs using bare Cu foil as an electrode often suffer from poor cycling stability. In this chapter, a simple and effective strategy of the ultrathin interphase layer is introduced to modify Cu foil for the preparation of high-performance anode-free LMBs. This surface modification significantly enhances the plating behavior with more uniform and dense Li deposition. The cycling performance of the anode-free batteries using the modified Cu as electrode, and high-loading LFP and NCM811 as cathodes, is carefully investigated.

7.1 Introduction

As mentioned, adopting thin lithium (Li) metal anodes (LMAs) shows great promise in boosting the energy density of LMBs. Typically, when the thickness of Li is reduced to zero, the anode-free LMB is thus developed, which shows overwhelming merits in aspects of energy density, production convenience, and economic adaptability [36, 240, 241]. Normally, the Cu foil with zero-excess Li is adopted as an electrode to pair with the Li-contained cathode. Given that there is no available Li reservoir from the Cu side to compensate for inevitable and irreversible capacity loss, the practical use of anode-free LMBs is still hindered by poor cycling reversibility and limited cycling lifespan [35, 242].

To solve these challenges, great progress has been made [240, 243-246], particularly in electrolyte engineering [138, 167, 247, 248], to effectively enhance the Coulombic efficiency (CE) of anode-free batteries with strengthened cycling reversibility. For instance, Zhang et al. engineered the ether-based locally high-concentration electrolyte with a trace amount of additive (LiDFOB, 0.02 mol L^{-1}) for anode-free batteries [249].

As a result, the anode-free LMBs could improve capacity retention from 57.3% to 80.3% after 50 cycles when paired with a practical high NCM811 cathode with a voltage up to 4.4V. Besides, a dual additives ($LiAsF_6$ and FEC) was reported to enhance the cycling stability of NMC||Cu anode-free batteries in commercially available carbonate-based electrolyte [250], where the average CE was improved to 98.3% over 100 cycles. Nevertheless, most of these studies were conducted on the bare Cu foil, which showed a lithiophobic nature and a large thermodynamic mismatch with Li, thus making it more susceptible to inducing dendrite growth with poor cycling stability.

Adopting porous substrates to replace planar Cu foil has been explored to stabilize anode-free LMBs [245, 251-253]. They are capable of regulating Li deposition behavior by effectively reducing localized current density and accommodating volume expansion. However, the 3D porous substrate shows larger weight and volume, and it will inevitably absorb more electrolyte as well as consume more Li, leading to a compromised energy density and electrochemical performance. Engineering an interfacial layer between anode and electrolyte, is another effective approach to mitigate dendrite growth in anode-free batteries [244, 254]. The applied interphase layer can engage in the formation of SEI by releasing desirable components, while it also acts as a protective layer to alleviate severe side reactions[119, 125, 255-258]. For instance, a polymeric film of PVDF was employed on the Cu current collector to facilitate the homogeneous Li deposition behavior, thus benefiting from achieving prolonged lifespan in the half-cell study [254]. Nevertheless, the as-developed interphase layers were either thick or required a complex synthesis process [119, 254, 255]. In this regard, stabilizing the anode-free LMBs through a facile yet effective method without sacrificing energy density and electrochemical performance remains a critical bottleneck.

As revealed in the previous two chapters, the feasibility of antimony (Sb) in regulating Li deposition has been demonstrated. It exhibits a good affinity for Li, and the resulting Li-Sb alloy layer can promote the rapid transport of Li ions at the interface. Notably,

the planar Cu foil is selected as the substrate instead of using porous textile or fabric framework. As mentioned, the porous substrate with high specific surface area inevitably accelerates electrolyte depletion and exacerbates Li loss through continuous formation of the SEI layer on interconnected fibrous networks. Additionally, the weight or volume of the porous substrate may also further compromise the energy density of the anode-free configurations. Hence, in this chapter, an ultrathin interphase layer (50 nm) of antimony (Sb) is modified on the Cu surface for stabilizing anode-free LMBs. Through a feasible and simple thermal evaporation method, the surface modification with ultrathin Sb is developed, which can minimize the impact of the ultrathin layer on energy density. The morphological investigation of Li deposition and electrochemical properties of anode-free LMBs is conducted and discussed carefully. Results find that the modified Cu foil showed a prolonged cycling life of 400 cycles with an impressive average CE of ~99.3%. The NCM811||CuSb anode-free batteries also demonstrated a remarkable energy density of 425 Wh kg^{-1}, and improved cycling stability at a practical high areal capacity of over 4 mAh cm^{-2}.

7.2 Experiment

7.2.1 Materials Preparation

Fabrication of Sb modified Cu foil (CuSb): An ultrathin lithiophilic Sb layer with a thickness of 50 nm was evaporated to one side of the commercially available Cu foil to obtain the Sb coated Cu (CuSb) foil.

7.2.2 Cell Assembly

The electrolyte used in this chapter was a mixture of LiFSI, DME, and HFE with the molar ratio of 1: 1.8: 2. Half cells were assembled by pairing the pouched current collectors with the counter electrode of 400 μm Li. Anode-free LMBs cells were assembled by stacking the prepared current collectors of Cu or CuSb foil, Celgard 2325 separator, and high-loading cathodes of LFP and NCM811 in the 2025-typed coin cells.

To pursue a higher energy density, the thinner Cu foil (8 μm) and lean electrolyte (< 3 g Ah^{-1}) were adopted in the pouch cell. A detailed procedure has been introduced in chapter 4.

7.2.3 Characterizations

The galvanostatic tests and cycling performance of the batteries were evaluated by the Neware battery testing system. The energy density was calculated based on the mass of cell components, including the current collectors, electrodes, and separator. Detailed characterizations have been introduced in chapter 4.

7.3 Results and Discussion

7.3.1 Ultrathin Interphase Layer for Dendrite Suppression

Here, the commercially available Cu foil was modified with an ultrathin Sb layer (50 nm) through a facile process of thermal evaporation. As pointed out and demonstrated in previous chapters, the Sb has a good affinity to Li, which could form an alloy with Li. The as-developed Li-Sb alloy has great potential in regulating and smoothing Li deposition [125, 220]. Importantly, the Li-Sb alloy can not only reduce interfacial resistance, but also facilitate rapid Li ion transportation. Meanwhile, it provides a stable interface for Li nucleation and deposition. As such, the ultrathin Sb layer was selected to modify the Cu foil towards high-performance anode-free LMBs.

In Figures 7.1a and 7.1b, the morphologies of bare Cu foil were given, which had some defects with uneven surface. After modifying with an ultrathin Sb layer, the surface morphology and roughness of CuSb did not show significant changes (Figure 7.1c). As observed from the zoomed-in SEM image (Figure 7.1d), there were nanoparticles coating on the surface. EDX mapping was then carried out. Signals related to elemental species of Cu and Sb were clearly found on the surface of CuSb foil (Figure 7.2), indicating the successful modification of Sb on the Cu foil. According to the EDX

spectrum, the atomic percentages of Cu, Sb, and O elements on the CuSb surface were 82.37%, 9.56%, and 8.07%, respectively. Since the coating thickness was very thin and the CuSb sample was directly exposed to the air when finishing the evaporation, it was inevitable to introduce the element of O on the sample.

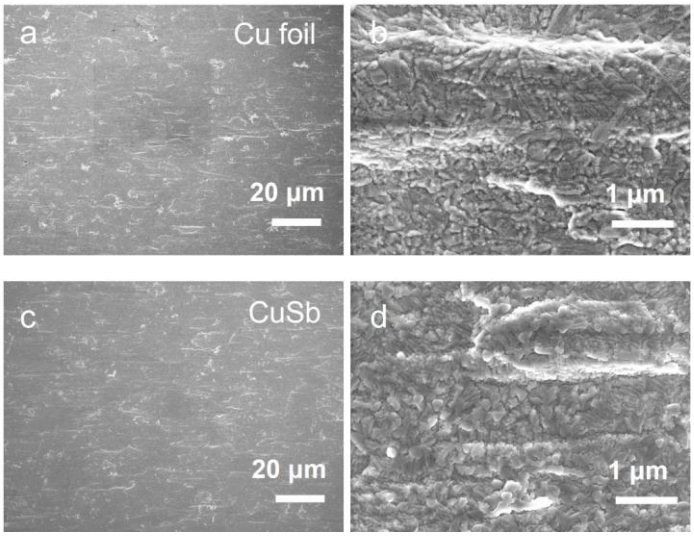

Figure 7.1 Top view morphologies of (a, b) Cu foil and (c, d) CuSb foil. (b) and (d) are the corresponding zoom in images, respectively.

Before the investigation of Li deposition behavior, we compared the surface roughness and modulus on Cu foil and CuSb foil at the initial discharge state. Noted that the formation of SEI was prior to the Li deposition, the discharge voltage was set to 0 V. The surface roughness of the Cu foil was shown in Figure 7.3a, which exhibited an average surface roughness (Ra) of 103 nm. In Figure 7.3b, the distribution of the modulus on the Cu foil was uneven with the average modulus of only 297 MPa. Since there was no cycling and no Li deposits on the Cu, the SEI was very incomplete and fragile, leading to a very low modulus value on the Cu foil. As such, the surface roughness could be regarded as the bulky roughness instead of the SEI layer.

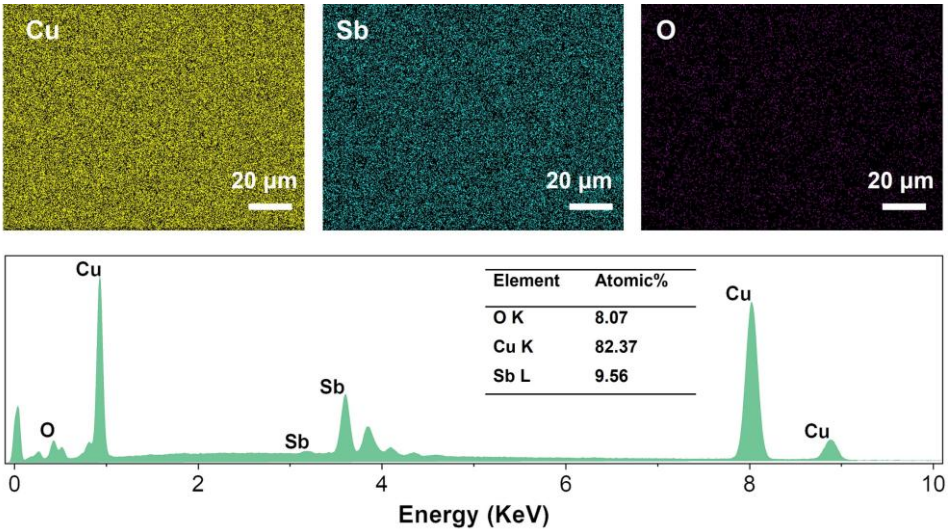

Figure 7.2 Corresponding EDX mapping and spectrum of the CuSb foil.

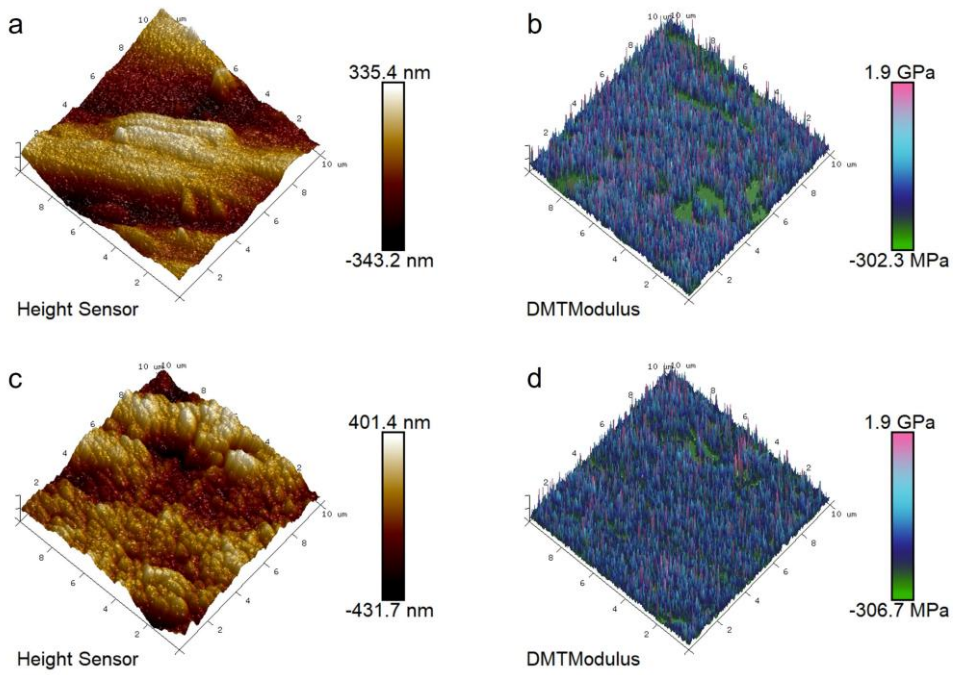

Figure 7.3 Comparison of surface roughness (a, c) and DMT modulus (b, d) of Cu foil and the CuSb foil after discharge to 0 V, respectively.

The surface roughness of the CuSb foil shown in Figure 7.3c was different from the Cu foil due to the coating layer of Sb nanoparticles, which was consistent with the SEM observation. The Ra for the CuSb foil was 97.4 nm, slightly lower than that of the Cu foil, revealing a more uniform surface. Additionally, the distribution of modulus on the

CuSb foil was also more uniform with an average modulus of 426 MPa (Figure 7.3d). Clearly, Cu foil with an ultrathin modified layer could promote a uniform deposition surface and an even formation of the initial SEI layer with a strengthened modulus.

Later, morphological investigations of Li deposition behavior on different current collectors were conducted. Obvious Li dendrites were covered on the top of Cu foil (Figure 7.4a and 7.4b) after depositing 1 mAh cm^{-2} Li at a current density of 0.5 mA cm^{-2}. When further depositing the capacity of 4 mAh cm^{-2}, the Li deposits were still inhomogeneous and uncompact (Figure 7.4c and 7.4d).

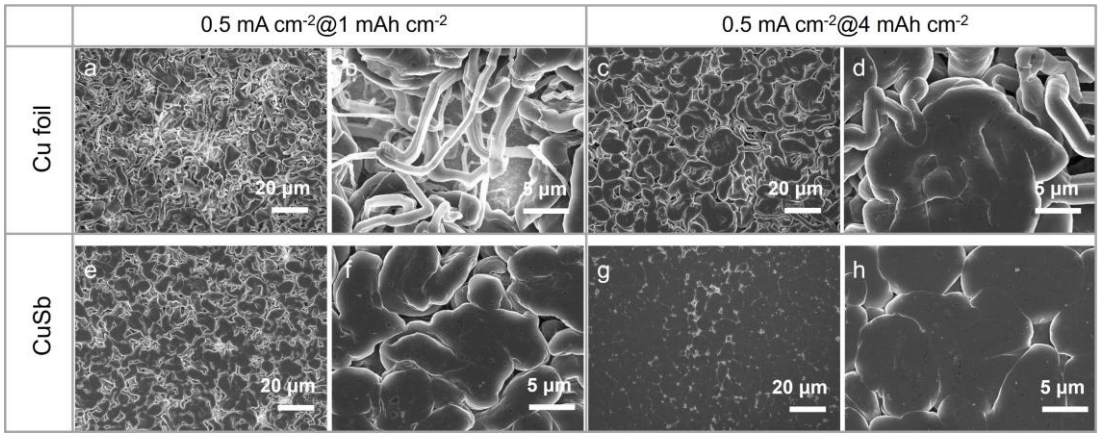

Figure 7.4 Morphologies of Li deposition on (a-d) Cu foil and (e-h) CuSb foil with the capacities of 1 mAh cm^{-2} and 4 mAh cm^{-2} at a low current density of 0.5 mA cm^{-2}.

In sharp contrast, the CuSb foil demonstrated a more uniform and compact Li deposition at the capacity of 1 mAh cm^{-2} as shown in Figures 7.4e and 7.4f. Meanwhile, it was found that the Li deposits on the CuSb foil were in the form of large granules rather than filaments on the Cu foil. Moreover, at a higher capacity of 4 mAh cm^{-2}, a very dense and smooth Li deposition was observed on the CuSb foil (Figures 7.4g and 7.4h). It suggests that the modification layer on the Cu foil can effectively suppress the dendrite formation, contributing to a uniform, dense, and smooth deposition morphology. Such improvement on deposition morphology is crucial for enhancing the electrochemical stability of anode-free LMBs.

The Li deposition morphologies at a higher current density of 2 mA cm^{-2} were further investigated. The deposition on Cu foil became rough and porous with a pronounced dendrite structure (Figure 7.5a). As for the CuSb foil, it could maintain a uniform deposition with large Li granules (Figure 7.5b), further demonstrating the effectiveness of the Sb modification in promoting a stable and uniform Li deposition.

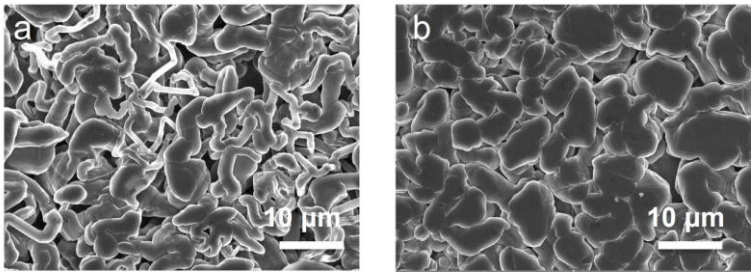

Figure 7.5 Deposition morphologies on (a) Cu foil and (b) CuSb foil with the capacity of 4 mAh cm^{-2} at a high current density of 2mA cm^{-2}.

7.3.2 Cycling Stability of Modified Cu Foil

To evaluate the coulombic efficiency (CE) of Li on current collectors of Cu foil and CuSb foil, half cells were assembled and cycled at a capacity of 1 mAh cm^{-2} and a current density of 1 mA cm^{-2} with the charging voltage up to 0.6 V. The Cu foil could stably cycle for 270 cycles with an average initial CE of 99.2%, then the voltage profile fluctuated due to structural damage or dendrite formation (Figure 7.6a). In comparison, the CuSb foil exhibited a prolonged cycling life of 400 cycles with an average CE of 99.3% (Figure 7.6a), indicating a much improved cycling stability.

The voltage profiles of the first cycle are shown in Figure 7.6b. In the discharging curve, there existed a voltage plateau at ~0.735 V, which was attributed to the new phase formation of Li-Sb alloy. Such alloy formation causes extra consumption of Li, leading to a lower initial CE of 92.24% compared to 96.64% for Cu foil. And there was no significant difference in the following cycle life. Despite the decreased ICE, the CuSb foil presented a better electrochemical stability and longer lifespan. Additionally, the

ultrathin Sb layer on the Cu foil could reduce the nucleation barrier, leading to a lower nucleation barrier of 24.1 mV in contrast to 50.8 mV for Cu foil (Figure 7.6c).

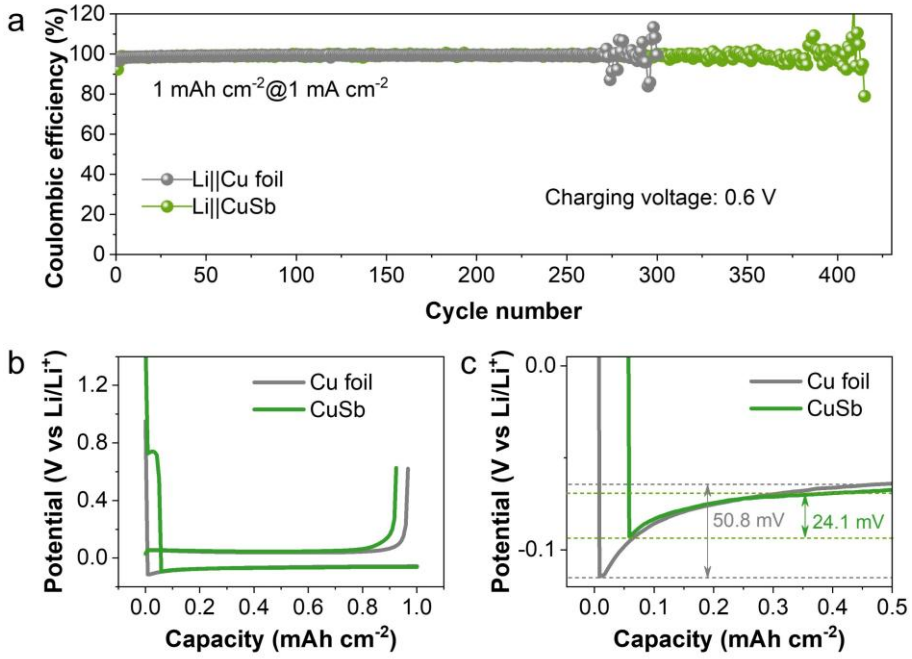

Figure 7.6 (a) Cycling reversibility of Li on the Cu foil and CuSb foil with the charging voltage up to 0.6 V. (b) The voltage profile of the first cycle, and (c) the corresponding enlarge profile for comparison of nucleation potential.

Here, an XRD test was carried out to understand the structural stability of the interphase Li-Sb layer. In Figure 7.7a, peaks related to Cu and Sb could be clearly found on the CuSb foil, which were in accordance with the Cu PDF#04-0836 and Sb PDF#35-0732. Specifically, during the first plating process, the Sb ultrathin layer on the Cu would form Li-Sb alloy, and Li deposition occurs when the discharging voltage below 0 V. During the stripping process, the charging voltage was controlled at 0.6 V so that only the Li deposits would be stripped while Li-Sb alloy could remain unchanged. In this regard, it could avoid the dilemma of volume expansion and peeling off during repeated alloying and dealloying. The peaks belonged to Li_3Sb alloy on CuSb foil after the 1st plating, the 20th plating, and the 20th stripping were evidently observed, and they could perfectly overlap (Figure 7.7b). It demonstrates that the interphase Li-Sb alloy remains

stable after cycling due to the voltage control. As such, this stable Li-Sb alloy interphase layer can provide us with a favorable interface for deposition.

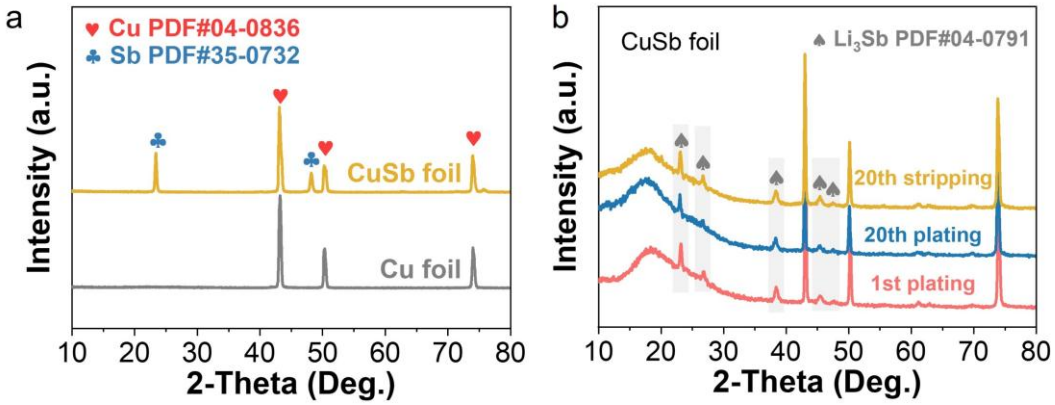

Figure 7.7 (a) XRD pattern of Cu foil, CuSb foil, and (b) cycled CuSb foil after the 1st plating, the 20th plating, and 20th stripping.

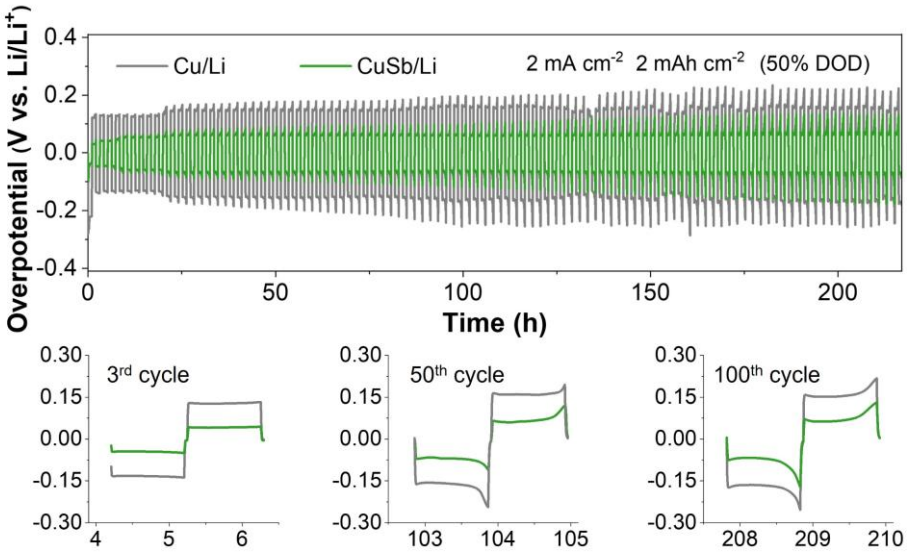

Figure 7.8 Cycling performance of symmetric cells using Cu/Li electrode and CuSb/Li electrode at a DOD of 50%.

Later, a fixed amount of Li (4 mAh cm^{-2})was deposited on the Cu foil and CuSb foil to obtain the Cu/Li electrode and CuSb/Li electrode. Symmetric cells were then assembled at a high depth of discharge (DOD) of 50% at 1 C rate (2 mA cm^{-2}). Cycling

performance and detailed voltage profiles at different cycles are presented in Figure 7.8. The CuSb/Li showed much reduced overpotential than that of the cell using Cu foil during 200 hr cycling, further demonstrating a better cycling stability enabled by the interphase layer.

7.3.3 High-Energy and Life-Prolonged Anode-Free LMBs

To investigate the practicability of the CuSb foil, high-loading commercial cathodes of LFP (3.0 mAh cm $^{-2}$) and NCM811 (4.2 mAh cm^{-2}) were adopted for anode-free LMBs. The LFP-based anode-free batteries were cycled at 0.5 C rate with a working window between 2.5~4.2V. The NCM811-based anode-free batteries were also cycled at 0.5 C rate and the working window was 3~4.4V.

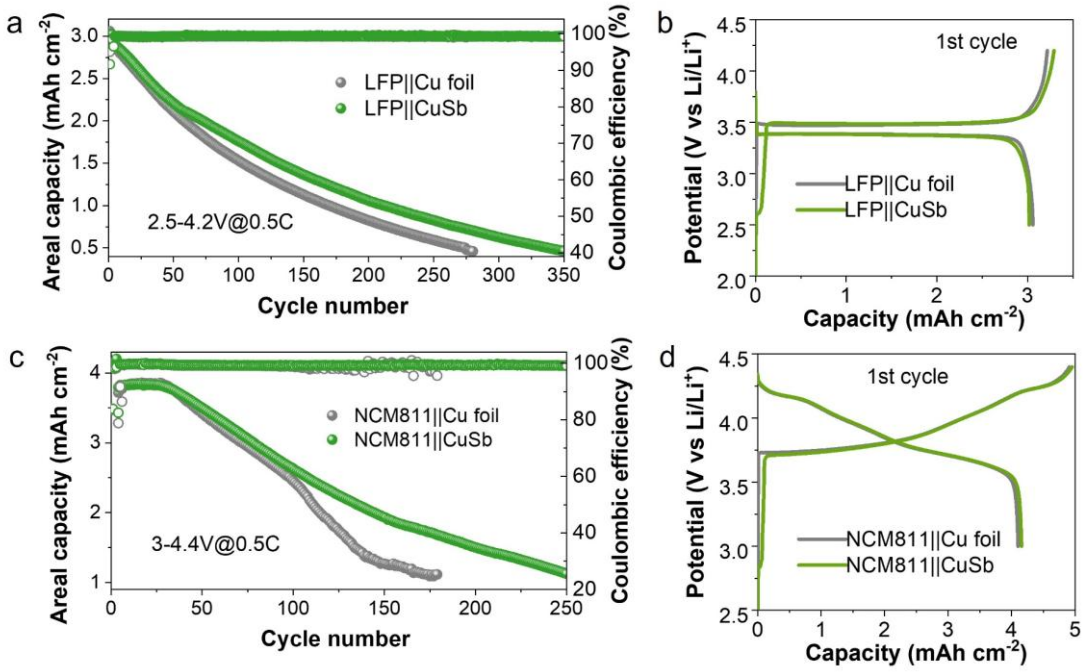

Figure 7.9 Electrochemical performance and voltage profiles of anode-free LMBs pairing various high-loading anodes of (a, b) LFP and (c, d) NCM811 at the 0.5 C rate.

As shown in Figure 7.9a, the LFP||Cu foil anode-free batteries showed a working life of 280 cycles with capacity retention of 99.3% per cycle. The anode-free LMB of LFP||CuSb foil exhibited a slightly lower initial capacity (3.02 mAh cm^{-2} vs. 3.06 mAh

cm^{-2} for Cu foil) and a clear decrease in ICE, from 95.1% to 91.2%. As discussed, the formation of Li-Sb on the interface consumed a certain amount of Li, resulting in a lower ICE than bare Cu foil. However, the CuSb foil still demonstrated effectiveness in cycling stability and lifespan. Specifically, a prolonged cycling life of 350 cycles and an improved capacity retention of 99.5% per cycle were found in the LFP||CuSb foil anode-free battery, showing the feasibility of an ultrathin interphase layer in advancing battery performance.

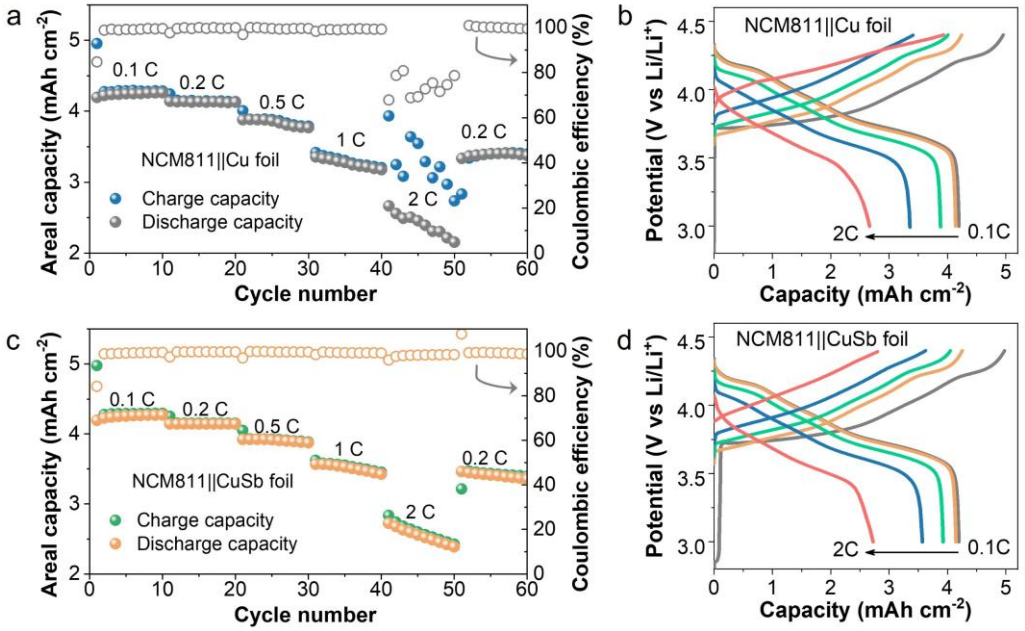

Figure 7.10 Rate performance and voltage profiles of anode-free LMBs based on (a, b) Cu foil and (c, d) CuSb foil.

When adopting the NCM811 (4.2 mAh cm^{-2}) as cathode (Figure 7.9d), the anode-free LMBs using the CuSb foil showed a comparable ICE (83.9% vs. 83.6% for Cu foil), since NCM811 possessed a higher areal capacity in this case and was not as stable as the LFP cathode. Notably, the NCM811||Cu foil showed faster capacity decay at 0.5 C rate, dropping to 1.23 mAh cm^{-2} after 150 cycles, with capacity retention of only 33.1% (Figure 7.9c). In contrast, the NCM811||CuSb foil anode-free battery maintained a higher capacity of 1.93 mAh cm^{-2} with retention of 50.7% after 150 cycles (Figure 7.9c). Additionally, CuSb foil-based anode-free LMBs displayed an extended cycling life

from 170 cycles to 270 cycles with significantly improved average CE of 99.4% while the value in NCM811||Cu foil cell was 98.9%. These results strongly demonstrated the feasibility of the CuSb foil in improving cycling stability and prolonging cycling lifespan. The anode-free LMB of NCM811||CuSb foil also presented a better rate performance especially at higher C rates, than the anode-free cell using the Cu foil (Figure 7.10). It can be attributed to the fast Li ions transport enabled by the Li-Sb alloy layer, which possesses a much lower Li diffusion barrier.

Finally, a prototype of anode-free pouch cell (2.5×4 cm) featuring a high-areal-capacity NCM811 (4.2 mAh cm^{-2}) was fabricated. The anode-free pouch cell of NCM811||CuSb foil with a total capacity of 41.5 mAh presented a stable cycling of 100 cycles at a high rate of 0.5 C (Figure 7.11). The capacity retention could still maintain 50.4% after 100 cycles. Specifically, cell failure was primarily attributed to (i) progressive accumulation of irreversible capacity loss from parasitic side reactions, (ii) continuous electrolyte depletion due to SEI reconstruction, and (iii) interfacial degradation caused by Li-Sb alloy layer. As such, despite the encouraging cycling life of 100 cycles in the anode-free battery, its long-term stability requires further enhancement. Additionally, the anode-free pouch cell based on CuSb foil achieved a practically high energy density of 425.4 Wh kg^{-1} (Figure 7.11b). Overall, such a simple approach of surface medication provides a novel insight into developing high-performance anode-free LMBs.

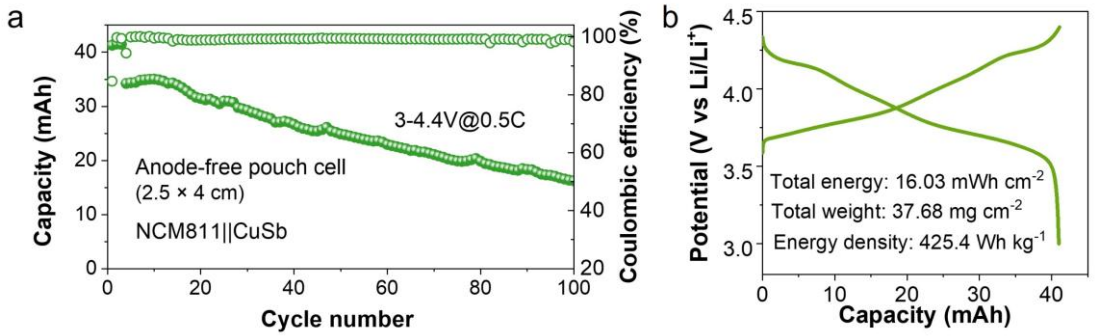

Figure 7.11 (a) Cycling performance and (b) voltage profile of the anode-free pouch cell of NCM811||CuSb foil.

7.4 Conclusion

In conclusion, a feasible strategy of ultrathin interphase layer modified on Cu foil was developed to achieve high-performance anode-free LMBs. Specifically, thermal evaporation of a 50 nm-thick Sb layer on Cu foil significantly improved the Li deposition behavior. Morphological studies showed that the CuSb foil achieved denser and more uniform Li deposition at different current densities and capacities compared to Cu foil. In the half-cell study, the cycling life of CuSb foil was extended from 270 cycles to 400 cycles with an impressive average CE of ~99.3%. Additionally, the anode-free LMBs using CuSb foil and high-loading cathodes (LFP and NCM811) also showed improved cycling stability and prolonged lifespan at 0.5 C rate. In addition, the NCM811||CuSb anode-free pouch cell with a practical high areal capacity of 4.2 mAh cm^{-2} was assembled, which could deliver a remarkable energy density of 425 Wh kg^{-1} and maintain a stable cycling for 100 cycles. This simple modification strategy provides a feasible and effective way to advance anode-free LMBs, showing great promise in practical applications.

Chapter 8 Conclusions and Outlook

8.1 Conclusions

In this thesis, we demonstrated the fabrication of advanced thin LMAs through material selection, structural design, and lithiophilic modification via facile and feasible processing technologies. Such advanced thin LMAs can contribute to the realization of high-performance LMBs. Firstly, a thin LMA with the Janus structure and top buffering textile space was designed through facile selective wetting, which significantly improved the long-term cycling stability and mechanical flexibility of the LMBs. Secondly, a thin, lightweight, and flexible LMA with the incorporation of ultralight fabrics and sandwiched configuration was proposed to achieve highly-flexible LMBs while maintaining high energy density. Finally, a simple strategy of surface modification was applied to the Cu foil for the preparation of stable anode-free LMBs with remarkably high energy density. The feasibility of these thin LMAs was carefully investigated. Meanwhile, the related electrochemical performances and mechanical properties of the thin LMA-based batteries were also studied.

In chapter 5, a thin Janus Li-textile anode was designed for the achievement of long-life and flexible LMBs. A thin Li layer (~50 μm) was rapidly developed on one side of the Janus conductive textile through a novel strategy of selective wetting, which was facile and efficient. As such, a porous upper textile skeleton could be maintained, which could offer effective buffering space and provide an oriented deposition, thus realizing the dendrite suppression with the strengthened stability and lengthened lifespan in the Janus Li-based batteries. Consequently, the symmetric cells showed an ultralong lifespan of 3000 hr even at a high DOD of 75% while the full cells also achieved an extended working life of 2000 cycles with outstanding cycling retention of 99.94% per cycle. Meanwhile, the pouch cell based on the Janus Li-textile anode also exhibited an impressive bending tolerance, revealing good mechanical flexibility.

In chapter 6, a stable, ultralight, and flexible thin LMA was developed through a facile one-step process of mechanical rolling, which can contribute to the realization of highly flexible LMAs while further promoting a high energy density. Specifically, a thin Li strip was sandwiched between two superlight fabrics. The combination of superlight substrate and sandwiched protective structure enables the as-developed sandwiched Li (SW Li) anode with both merits of lightweight, good stability, and high flexibility. Therefore, the full cell using the SW Li demonstrated a well-extended lifespan of 500 cycles at 1 C rate with an outstanding capacity retention of 92%. Moreover, LMBs adopting SW Li not only delivered an improved energy of 309 Wh kg^{-1}, but also showed outstanding flexibility with a remarkably high figure of merit for flexible battery of 163.8, outperforming the state-of-the-art flexible batteries.

In chapter 7, a simple yet effective strategy of surface modification was proposed to achieve high-performance anode-free LMBs. The ultrathin interphase layer (50 nm) modified on the Cu substrate facilitated a significantly improved Li deposition behavior, which was beneficial for the improvement of cycling stability and lifespan. The modified Cu foil showed a prolonged cycling life of 400 cycles with an impressive average CE of ~99.3%. The anode-free batteries using the modified Cu also demonstrated improved cycling stability at a 0.5 C rate and a practically high areal capacity of over 4 mAh cm^{-2}. Under a realistic condition, the anode-free pouch cell based on the modified Cu can maintain stable cycling for 100 cycles, delivering a remarkable energy density of 425 Wh kg^{-1}.

In summary, the feasibility of developing thin LMAs in advancing LMBs through facile strategies has been explored in this project. It shows that the combination of textile material and thin Li under a rational structural design can significantly promote the electrochemical stability as well as the mechanical flexibility. Moreover, the selection of ultralight fabric layer and sandwiched configuration can further enhance the high energy density when pursuing good flexibility in thin LMA-based batteries. Furthermore, thinning Li to zero with the modified Cu foil as electrode can maximize

the energy density of batteries with improved cycling stability. Therefore, it is effective and promising to utilize advanced thin LMAs to pave the way for high-performance LMBs with high energy density, outstanding flexibility, and excellent electrochemical stability.

8.2 Outlook

In this research, we mainly focus on the development of advanced anode electrodes with thin Li or even Li-free for high-performance LMBs. Despite the progress made, efforts are still needed for further improvements and development in the future. Several important aspects for future development are as follows:

1. The thin Janus Li-textile anode can enable the LMBs with excellent electrochemical stability and ultralong-life cycles. However, the involved textile framework of carbon cloth is quite thick and has a considerable mass load, which significantly limits the whole-cell energy density. Attempts for reconstructing carbon cloth substrate with thinner thickness as well as lighter weight are desirable for further improvement on the energy density. In addition, more suitable, and reliable substrates should also be considered.

2. Superlight polymeric non-woven fabric was adopted to host thin LMAs to achieve energy-dense flexible LMBs. Nevertheless, this non-woven nanofiber framework requires a substantial amount of electrolyte absorption for normal cycling, making it challenging to further enhance the energy density. Innovative structural design of fabrics with porosity engineering and surface chemistry may be beneficial for reducing unnecessary electrolyte uptake. Advanced fabrication techniques, such as electrospinning, to achieve regulated fibers with alignment design, may also contribute to minimizing excess electrolyte absorption.

3. The introduction of lithiophilic material of Sb to modify the surface of Cu foil can effectively regulate the Li deposition behavior, which is beneficial to improving

cycling stability and lifespan. However, there exists the issue of volume expansion during the alloying process with Li. Besides, inevitably capacity loss is caused at the first cycle to form the Li-Sb alloy. It is necessary to explore feasible solutions to suppress the volume expansion, and adopt advanced prelithiation methods to compensate for the capacity loss to further improve the electrochemical stability and longevity of LMBs.

4. In this thesis, we only focused on the development of thin, stable, and flexible LMAs. However, the realization of flexible LMBs for practical applications also requires innovative cathode design. The cathode should combine the heavy active material loading with the smart structural design to enhance mechanical flexibility without sacrificing the energy density. In addition, integrating novel manufacturing technologies, such as 3D printing or roll-to-roll processing, may be beneficial to promoting the development of flexible cathodes.

5. While significant research efforts have been dedicated to advancing thin LMAs, critical safety concerns of the batteries remain underexplored. The integration of solid-state electrolytes (SSEs) in the flexible LMBs becomes essential, which can eliminate liquid leakage risks and enhance structural compliance. To enable the realization of high-energy, flexible, and safe LMBs, future efforts should prioritize the development of ultrathin SSEs incorporating smart interface design through innovative strategies. Additionally, establishing robust multiscale interfacial adhesion between SSEs, LMAs, and cathodes is imperative to ensure electrochemical stability under cyclic bending.

References

[1] R.F. Service, TECHNOLOGY: Electronic Textiles Charge Ahead, Science 301 (2003) 909-911.

[2] W. Gao, H. Ota, D. Kiriya, K. Takei, A. Javey, Flexible Electronics toward Wearable Sensing, Acc Chem Res 52 (2019) 523-533.

[3] W. Gao, S. Emaminejad, H.Y.Y. Nyein, S. Challa, K. Chen, A. Peck, H.M. Fahad, H. Ota, H. Shiraki, D. Kiriya, D.H. Lien, G.A. Brooks, R.W. Davis, A. Javey, Fully integrated wearable sensor arrays for multiplexed in situ perspiration analysis, Nature 529 (2016) 509-514.

[4] D.H. Kim, N. Lu, R. Ma, Y.S. Kim, R.H. Kim, S. Wang, J. Wu, S.M. Won, H. Tao, A. Islam, K.J. Yu, T.I. Kim, R. Chowdhury, M. Ying, L. Xu, M. Li, H.J. Chung, H. Keum, M. McCormick, P. Liu, Y.W. Zhang, F.G. Omenetto, Y. Huang, T. Coleman, J.A. Rogers, Epidermal electronics, Science 333 (2011) 838-843.

[5] J.R. Miller, Valuing Reversible Energy Storage, Science 335 (2012) 1312.

[6] B. Dunn, H. Kamath, J.M. Tarascon, Electrical Energy Storage for the Grid: A Battery of Choices, Science 334 (2011) 928-935.

[7] J. He, C. Lu, H. Jiang, F. Han, X. Shi, J. Wu, L. Wang, T. Chen, J. Wang, Y. Zhang, H. Yang, G. Zhang, X. Sun, B. Wang, P. Chen, Y. Wang, Y. Xia, H. Peng, Scalable production of high-performing woven lithium-ion fibre batteries, Nature 597 (2021) 57-63.

[8] F. Duffner, N. Kronemeyer, J. Tübke, J. Leker, M. Winter, R. Schmuch, Post-lithium-ion battery cell production and its compatibility with lithium-ion cell production infrastructure, Nat Energy 6 (2021) 123-134.

[9] M. Li, J. Lu, Z. Chen, K. Amine, 30 Years of Lithium-Ion Batteries, Adv Mater (2018) e1800561.

[10] D. Lin, Y. Liu, Y. Cui, Reviving the lithium metal anode for high-energy batteries, Nat Nanotechnol 12 (2017) 194-206.

[11] J.M. Tarascon, M. Armand, Issues and challenges facing rechargeable lithium

batteries, Nature 414 (2001) 359-367.
[12] J.B. Goodenough, K.S. Park, The Li-ion rechargeable battery: a perspective, J Am Chem Soc 135 (2013) 1167-1176.
[13] J. Liu, Z. Bao, Y. Cui, E.J. Dufek, J.B. Goodenough, P. Khalifah, Q. Li, B.Y. Liaw, P. Liu, A. Manthiram, Y.S. Meng, V.R. Subramanian, M.F. Toney, V.V. Viswanathan, M.S. Whittingham, J. Xiao, W. Xu, J. Yang, X.-Q. Yang, J.-G. Zhang, Pathways for practical high-energy long-cycling lithium metal batteries, Nat Energy 4 (2019) 180-186.
[14] W. Xu, J. Wang, F. Ding, X. Chen, E. Nasybulin, Y. Zhang, J.-G. Zhang, Lithium metal anodes for rechargeable batteries, Energy Environ Sci 7 (2014) 513-537.
[15] X.B. Cheng, R. Zhang, C.Z. Zhao, Q. Zhang, Toward Safe Lithium Metal Anode in Rechargeable Batteries: A Review, Chem Rev 117 (2017) 10403-10473.
[16] F. Ding, W. Xu, G.L. Graff, J. Zhang, M.L. Sushko, X. Chen, Y. Shao, M.H. Engelhard, Z. Nie, J. Xiao, X. Liu, P.V. Sushko, J. Liu, J.G. Zhang, Dendrite-free lithium deposition via self-healing electrostatic shield mechanism, J Am Chem Soc 135 (2013) 4450-4456.
[17] S. Kim, J.S. Kim, L. Miara, Y. Wang, S.K. Jung, S.Y. Park, Z. Song, H. Kim, M. Badding, J. Chang, V. Roev, G. Yoon, R. Kim, J.H. Kim, K. Yoon, D. Im, K. Kang, High-energy and durable lithium metal batteries using garnet-type solid electrolytes with tailored lithium-metal compatibility, Nat Commun 13 (2022) 1883.
[18] J.H. Kim, K. Go, K.J. Lee, H.S. Kim, Improved Performance of All-Solid-State Lithium Metal Batteries via Physical and Chemical Interfacial Control, Adv Sci 9 (2022) e2103433.
[19] X.-Q. Zhang, X.-B. Cheng, X. Chen, C. Yan, Q. Zhang, Fluoroethylene Carbonate Additives to Render Uniform Li Deposits in Lithium Metal Batteries, Adv Funct Mater 27 (2017).
[20] D. Luo, L. Zheng, Z. Zhang, M. Li, Z. Chen, R. Cui, Y. Shen, G. Li, R. Feng, S. Zhang, G. Jiang, L. Chen, A. Yu, X. Wang, Constructing multifunctional solid electrolyte interface via in-situ polymerization for dendrite-free and low N/P ratio

lithium metal batteries, Nat Commun 12 (2021) 186.

[21] Y. Liu, D. Lin, P.Y. Yuen, K. Liu, J. Xie, R.H. Dauskardt, Y. Cui, An Artificial Solid Electrolyte Interphase with High Li-Ion Conductivity, Mechanical Strength, and Flexibility for Stable Lithium Metal Anodes, Adv Mater 29 (2017).

[22] M. Guan, Y. Huang, Q. Meng, B. Zhang, N. Chen, L. Li, F. Wu, R. Chen, Stabilization of Lithium Metal Interfaces by Constructing Composite Artificial Solid Electrolyte Interface with Mesoporous TiO2 and Perfluoropolymers, Small 18 (2022) e2202981.

[23] H. Zhang, X. Liao, Y. Guan, Y. Xiang, M. Li, W. Zhang, X. Zhu, H. Ming, L. Lu, J. Qiu, Y. Huang, G. Cao, Y. Yang, L. Mai, Y. Zhao, H. Zhang, Lithiophilic-lithiophobic gradient interfacial layer for a highly stable lithium metal anode, Nat Commun 9 (2018) 3729.

[24] J. Chang, J. Shang, Y. Sun, L.K. Ono, D. Wang, Z. Ma, Q. Huang, D. Chen, G. Liu, Y. Cui, Y. Qi, Z. Zheng, Flexible and stable high-energy lithium-sulfur full batteries with only 100% oversized lithium, Nat Commun 9 (2018) 4480.

[25] H. Gan, J. Wu, H. Chen, R. Li, H. Liu, Guiding lithium deposition in tent-like nitrogen-doped porous carbon microcavities for stable lithium metal anodes, J Mater Chem A 8 (2020) 13480-13489.

[26] C. Guan, W. Zhao, Y. Hu, Q. Ke, X. Li, H. Zhang, J. Wang, High-Performance Flexible Solid-State Ni/Fe Battery Consisting of Metal Oxides Coated Carbon Cloth/Carbon Nanofiber Electrodes, Adv Energy Mater 6 (2016).

[27] D. Jin, J. Park, M.H. Ryou, Y.M. Lee, Structure-Controlled Li Metal Electrodes for Post-Li-Ion Batteries: Recent Progress and Perspectives, Adv Mater Interfaces 7 (2020).

[28] W. Wu, W. Luo, Y. Huang, Less is more: a perspective on thinning lithium metal towards high-energy-density rechargeable lithium batteries, Chem Soc Rev 52 (2023) 2553-2572.

[29] J. Lee, S.H. Jeong, J.S. Nam, M. Sagong, J. Ahn, H. Lim, I.D. Kim, Toward thin and stable anodes for practical lithium metal batteries: A review, strategies, and

perspectives, EcoMat 5 (2023).
[30] H. Chen, Y. Yang, D.T. Boyle, Y.K. Jeong, R. Xu, L.S. de Vasconcelos, Z. Huang, H. Wang, H. Wang, W. Huang, H. Li, J. Wang, H. Gu, R. Matsumoto, K. Motohashi, Y. Nakayama, K. Zhao, Y. Cui, Free-standing ultrathin lithium metal–graphene oxide host foils with controllable thickness for lithium batteries, Nat Energy 6 (2021) 790-798.
[31] M. He, L. G. Hector Jr, F. Dai, F. Xu, S. Kolluri, N. Hardin, M. Cai, Industry needs for practical lithium-metal battery designs in electric vehicles, Nat Energy 9 (2024) 1199–1205.
[32] J. Du, W. Wang, M. Wan, X. Wang, G. Li, Y. Tan, C. Li, S. Tu, Y. Sun, Doctor-Blade Casting Fabrication of Ultrathin Li Metal Electrode for High-Energy-Density Batteries, Adv Energy Mater 11 (2021).
[33] C. Niu, H. Pan, W. Xu, J. Xiao, J.G. Zhang, L. Luo, C. Wang, D. Mei, J. Meng, X. Wang, Z. Liu, L. Mai, J. Liu, Self-smoothing anode for achieving high-energy lithium metal batteries under realistic conditions, Nature Nanotechnology 14 (2019) 594-601.
[34] Z. Xie, Z. Wu, X. An, X. Yue, J. Wang, A. Abudula, G. Guan, Anode-free rechargeable lithium metal batteries: Progress and prospects, Energy Storage Mater 32 (2020) 386-401.
[35] S. Nanda, A. Gupta, A. Manthiram, Anode-Free Full Cells: A Pathway to High-Energy Density Lithium-Metal Batteries, Adv Energy Mater 11 (2020).
[36] J. Qian, B.D. Adams, J. Zheng, W. Xu, W.A. Henderson, J. Wang, M.E. Bowden, S. Xu, J. Hu, J.G. Zhang, Anode-Free Rechargeable Lithium Metal Batteries, Adv Funct Mater 26 (2016) 7094-7102.
[37] J. Liu, H. Jia, D. Nguyen, J. Liu, C. Fang, Fabricating ultralight and ultrathin copper current collectors for high-energy batteries, eScience 4 (2024).
[38] W. Wu, D. Ning, J. Zhang, G. Liu, L. Zeng, H. Yao, M. Wang, L. Deng, L. Yao, Ultralight lithiophilic three-dimensional lithium host for stable high-energy-density anode-free lithium metal batteries, Energy Storage Mater 63 (2023).

[39] C. H. Zhang, Y.J. Guo, S.-J. Tan, Y.-H. Wang, J.-C. Guo, Y.-F. Tian, X.-S. Zhang, B.-Z. Liu, S. Xin, J. Zhang, L.-J. Wan, Y.-G. Guo, An ultralight, pulverization- free integrated anode toward lithium- less lithium metal batteries, Sci Adv 10 (2024) eadl4842.

[40] Z. Luo, Y. Cao, G. Xu, W. Sun, X. Xiao, H. Liu, S. Wang, Recent advances in robust and ultra‐thin Li metal anode, Carbon Neutralization 3 (2024) 647-672.

[41] J. Chang, H. Hu, J. Shang, R. Fang, D. Shou, C. Xie, Y. Gao, Y. Yang, Q.N. Zhuang, X. Lu, Y.K. Zhang, F. Li, Z. Zheng, Rational Design of Li-Wicking Hosts for Ultrafast Fabrication of Flexible and Stable Lithium Metal Anodes, Small 18 (2022) e2105308.

[42] A. Masias, N. Felten, R. Garcia-Mendez, J. Wolfenstine, J. Sakamoto, Elastic, plastic, and creep mechanical properties of lithium metal, J Mater Sci 54 (2018) 2585-2600.

[43] J. Chang, Q. Huang, Z. Zheng, A Figure of Merit for Flexible Batteries, Joule 4 (2020) 1346-1349.

[44] J. Peng, G.J. Snyder, A figure of merit for flexibility, Science 366 690-691.

[45] J. Chang, Q. Huang, Y. Gao, Z. Zheng, Pathways of Developing High-Energy-Density Flexible Lithium Batteries, Adv Mater 33 (2021) e2004419.

[46] D. Li, C. Xie, Y. Gao, H. Hu, L. Wang, Z. Zheng, Inverted Anode Structure for Long‐Life Lithium Metal Batteries, Adv Energy Mater 12 (2022).

[47] C. Luo, H. Hu, T. Zhang, S. Wen, R. Wang, Y. An, S. Chi, J. Wang, C. Wang, J. Chang, Z. Zheng, Y. Deng, Roll-To-Roll Fabrication of Zero-Volume-Expansion Lithium-Composite Anodes to Realize High-Energy-Density Flexible and Stable Lithium-Metal Batteries, Adv Mater 34 (2022) e2205677.

[48] Y. Gao, C. Xie, Z. Zheng, Textile Composite Electrodes for Flexible Batteries and Supercapacitors: Opportunities and Challenges, Adv Energy Mater 11 (2020).

[49] D. Li, Y. Gao, C. Xie, Z. Zheng, Au-coated carbon fabric as Janus current collector for dendrite-free flexible lithium metal anode and battery, App Phys Rev 9 (2022) 011424.

[50] Y. Zhou, Y. Han, H. Zhang, D. Sui, Z. Sun, P. Xiao, X. Wang, Y. Ma, Y. Chen, A

carbon cloth-based lithium composite anode for high-performance lithium metal batteries, Energy Storage Mater 14 (2018) 222-229.

[51] B. Dunn, H. Kamath, J.-M. Tarascon, Electrical Energy Storage for the Grid: A Battery of Choices, Science 334 (2011) 928–935.

[52] G. Zubi, R. Dufo-López, M. Carvalho, G. Pasaoglu, The lithium-ion battery: State of the art and future perspectives, Renewable Sustainable Energy Rev 89 (2018) 292-308.

[53] S. Evers, L.F. Nazar, New approaches for high energy density lithium-sulfur battery cathodes, Acc Chem Res 46 (2012) 1135-1143.

[54] P.G. Bruce, S.A. Freunberger, L.J. Hardwick, J.M. Tarascon, Li-O_2 and Li-S batteries with high energy storage, Nat Mater 11 (2011) 19-29.

[55] P. Albertus, S. Babinec, S. Litzelman, A. Newman, Status and challenges in enabling the lithium metal electrode for high-energy and low-cost rechargeable batteries, Nat Energy 3 (2017) 16-21.

[56] M. Winter, B. Barnett, K. Xu, Before Li Ion Batteries, Chem Rev 118 (2018) 11433-11456.

[57] M.S. Whittingham, Lithium batteries and cathode materials, Chem Rev 104 (2004) 4271-4302.

[58] M.S. Whittingham, History, Evolution, and Future Status of Energy Storage, Proc. IEEE 100 (2012) 1518-1534.

[59] B. K., Historical development of secondary lithium batteries, Solid State Ionics 69 (1994) 173-183.

[60] A. Manthiram, Y. Fu, S.H. Chung, C. Zu, Y.S. Su, Rechargeable lithium-sulfur batteries, Chem Rev 114 (2014) 11751-11787.

[61] Y. Liang, C.-Z. Zhao, H. Yuan, Y. Chen, W. Zhang, J.-Q. Huang, D. Yu, Y. Liu, M.-M. Titirici, Y.-L. Chue, H. Yu, Q. Zhang, A review of rechargeable batteries for portable electronic devices, InfoMat 1 (2019) 6-32.

[62] F. Dai, M. Cai, Best practices in lithium battery cell preparation and evaluation, Commun Mater 3 (2022) 1-6.

[63] S.V. Gopinadh, V. Anoopkumar, M.J.N. Ansari, D. Srivastava, A.R. M., B. John, A. Samridh, P.S. Vijayakumar, T.D. Mercy, Lithium-Ion Pouch Cells: An Overview, in: P.P. Subha (Ed.), Energy Harvesting and Storage, M.K. Jayaraj
A. Antony, Energy Systems in Electrical Engineering, 2022, pp. 209-210.
[64] M. Ahmadian-Elmi, P. Zhao, Review of Thermal Management Strategies for Cylindrical Lithium-Ion Battery Packs, Batteries 10 (2024).
[65] S. Link, C. Neef, T. Wicke, Trends in Automotive Battery Cell Design: A Statistical Analysis of Empirical Data, Batteries 9 (2023).
[66] M. Cai, C. Sun, D.-h. Le, P.-y. Li, Y.-d. Huang, H.-Z. Chen, X.-h. Zhang, J.-c. Zheng, Recent advances in synthesis and modification of phosphate-based cathode materials, J Energy Storage 95 (2024).
[67] A. Manthiram, J.B. Goodenough, Layered lithium cobalt oxide cathodes, Nat Energy 6 (2021) 323-323.
[68] J. Wang, Y.S. He, J. Yang, Sulfur-based composite cathode materials for high-energy rechargeable lithium batteries, Adv Mater 27 (2015) 569-575.
[69] Z. Hao, Y. Wu, Q. Zhao, J. Tang, Q. Zhang, X. Ke, J. Liu, Y. Jin, H. Wang, Functional Separators Regulating Ion Transport Enabled by Metal - Organic Frameworks for Dendrite-Free Lithium Metal Anodes, Adv Funct Mater 31 (2021).
[70] Z. Hao, Q. Zhao, J. Tang, Q. Zhang, J. Liu, Y. Jin, H. Wang, Functional separators towards the suppression of lithium dendrites for rechargeable high-energy batteries, Mater Horiz 8 (2021) 12-32.
[71] M. Li, C. Wang, K. Davey, J. Li, G. Li, S. Zhang, J. Mao, Z. Guo, Recent progress in electrolyte design for advanced lithium metal batteries, SmartMat 4 (2023).
[72] H. Wang, Z. Yu, X. Kong, S.C. Kim, D.T. Boyle, J. Qin, Z. Bao, Y. Cui, Liquid electrolyte: The nexus of practical lithium metal batteries, Joule 6 (2022) 588-616.
[73] X. Zhao, C. Wang, H. Liu, Y. Liang, L.Z. Fan, A Review of Polymer-based Solid-State Electrolytes for Lithium-Metal Batteries: Structure, Kinetic, Interface Stability, and Application, Batteries Supercaps 6 (2023) 1-22.

[74] Q. Shi, C. Lu, Y. Cao, Y. Hao, A. Bachmatiuk, M.H. Rümmeli, Recent developments in current collectors for lithium metal anodes, Mater Chem Front 7 (2023) 1298-1311.

[75] S. Jin, Y. Jiang, H. Ji, Y. Yu, Advanced 3D Current Collectors for Lithium-Based Batteries, Adv Mater 30 (2018) e1802014.

[76] H. Zhang, G.G. Eshetu, X. Judez, C. Li, L.M. Rodriguez-Martinez, M. Armand, Electrolyte Additives for Lithium Metal Anodes and Rechargeable Lithium Metal Batteries: Progress and Perspectives, Angew Chem Int Ed 57 (2018) 15002-15027.

[77] Q. Fan, J. Zhang, S. Fan, B. Xi, Z. Gao, X. Guo, Z. Duan, X. Zheng, Y. Liu, S. Xiong, Advances in Functional Organosulfur-Based Mediators for Regulating Performance of Lithium Metal Batteries, Adv Mater 36 (2024) e2409521.

[78] Q. Wang, B. Liu, Y. Shen, J. Wu, Z. Zhao, C. Zhong, W. Hu, Confronting the Challenges in Lithium Anodes for Lithium Metal Batteries, Adv Sci 8 (2021) e2101111.

[79] M. Zhu, K. Xu, D. Li, T. Xu, W. Sun, Y. Zhu, Y. Qian, Guiding Smooth Li Plating and Stripping by a Spherical Island Model for Lithium Metal Anodes, ACS Appl Mater Interfaces 12 (2020) 38098-38105.

[80] X. Zheng, L. Huang, W. Luo, H. Wang, Y. Dai, X. Liu, Z. Wang, H. Zheng, Y. Huang, Tailoring Electrolyte Solvation Chemistry toward an Inorganic-Rich Solid-Electrolyte Interphase at a Li Metal Anode, ACS Energy Lett 6 (2021) 2054-2063.

[81] R. Zhang, X. Shen, X.-B. Cheng, Q. Zhang, The dendrite growth in 3D structured lithium metal anodes: Electron or ion transfer limitation?, Energy Storage Mater 23 (2019) 556-565.

[82] L. Zhang, T. Yang, C. Du, Q. Liu, Y. Tang, J. Zhao, B. Wang, T. Chen, Y. Sun, P. Jia, H. Li, L. Geng, J. Chen, H. Ye, Z. Wang, Y. Li, H. Sun, X. Li, Q. Dai, Y. Tang, Q. Peng, T. Shen, S. Zhang, T. Zhu, J. Huang, Lithium whisker growth and stress generation in an in situ atomic force microscope-environmental transmission electron microscope set-up, Nat Nanotechnol 15 (2020) 94-98.

[83] X. Zhang, A. Wang, X. Liu, J. Luo, Dendrites in Lithium Metal Anodes: Suppression, Regulation, and Elimination, Acc Chem Res 52 (2019) 3223-3232.

[84] D. Aurbach, E. Zinigrad, H. Teller, P. Dan, Factors Which Limit the Cycle Life of Rechargeable Lithium (Metal) Batteries, J Electrochem Soc 147 (2000) 1274−1279.

[85] R. Bhattacharyya, B. Key, H. Chen, A.S. Best, A.F. Hollenkamp, C.P. Grey, In situ NMR observation of the formation of metallic lithium microstructures in lithium batteries, Nat Mater 9 (2010) 504-510.

[86] S. Chandrashekar, N.M. Trease, H.J. Chang, L.S. Du, C.P. Grey, A. Jerschow, 7Li MRI of Li batteries reveals location of microstructural lithium, Nat Mater 11 (2012) 311-315.

[87] D. Lu, Y. Shao, T. Lozano, W.D. Bennett, G.L. Graff, B. Polzin, J. Zhang, M.H. Engelhard, N.T. Saenz, W.A. Henderson, P. Bhattacharya, J. Liu, J. Xiao, Failure Mechanism for Fast-Charged Lithium Metal Batteries with Liquid Electrolytes, Adv Energy Mater 5 (2015).

[88] C.M. Lopez, J.T. Vaughey, D.W. Dees, Morphological Transitions on Lithium Metal Anodes, J Electrochem Soc 156 (2009) A726-A729.

[89] Y.G. Qi, H.B., L.G. Hector Jr, A. Timmons, Threefold Increase in the Young's Modulus of Graphite Negative Electrode during Lithium Intercalation, J Electrochem Soc 157 (2010) A558.

[90] C.K. Chan, H. Peng, G. Liu, K. McIlwrath, X.F. Zhang, R.A. Huggins, Y. Cui, High-performance lithium battery anodes using silicon nanowires, Nat Nanotechnol 3 (2008) 31-35.

[91] D.A. Dornbusch, R. Hilton, S.D. Lohman, G.J. Suppes, Experimental Validation of the Elimination of Dendrite Short-Circuit Failure in Secondary Lithium-Metal Convection Cell Batteries, J Electrochem Soc 162 (2014) A262-A268.

[92] H.J. Chang, A.J. Ilott, N.M. Trease, M. Mohammadi, A. Jerschow, C.P. Grey, Correlating Microstructural Lithium Metal Growth with Electrolyte Salt Depletion in Lithium Batteries Using (7)Li MRI, J Am Chem Soc 137 (2015) 15209-15216.

[93] S. Li, M. Jiang, Y. Xie, H. Xu, J. Jia, J. Li, Developing High-Performance Lithium Metal Anode in Liquid Electrolytes: Challenges and Progress, Adv Mater 30 (2018) e1706375.

[94] A. Pei, G. Zheng, F. Shi, Y. Li, Y. Cui, Nanoscale Nucleation and Growth of Electrodeposited Lithium Metal, Nano Lett 17 (2017) 1132-1139.

[95] L. Zhang, C. Zhu, S. Yu, D. Ge, H. Zhou, Status and challenges facing representative anode materials for rechargeable lithium batteries, J Energy Chem 66 (2022) 260-294.

[96] J. Chazalviel, Electrochemical aspects of the generation of ramified metallic electrodeposits, Phys Rev A 42 (1990) 7355-7367.

[97] A. Kushima, K.P. So, C. Su, P. Bai, N. Kuriyama, T. Maebashi, Y. Fujiwara, M.Z. Bazant, J. Li, Liquid cell transmission electron microscopy observation of lithium metal growth and dissolution: Root growth, dead lithium and lithium flotsams, Nano Energy 32 (2017) 271-279.

[98] R.L. Sacci, N.J. Dudney, K.L. More, L.R. Parent, I. Arslan, N.D. Browning, R.R. Unocic, Direct visualization of initial SEI morphology and growth kinetics during lithium deposition by in situ electrochemical transmission electron microscopy, Chem Commun 50 (2014) 2104-2107.

[99] X. Chen, X.R. Chen, T.Z. Hou, B.Q. Li, X.B. Cheng, R. Zhang, Q. Zhang, Lithiophilicity chemistry of heteroatom-doped carbon to guide uniform lithium nucleation in lithium metal anodes, Sci Adv 5 (2019) eaau7728.

[100] X. Chen, Y.K. Bai, C.Z. Zhao, X. Shen, Q. Zhang, Lithium Bonds in Lithium Batteries, Angew Chem Int Ed 59 (2020) 11192-11195.

[101] D.R. Ely, R.E. García, Heterogeneous Nucleation and Growth of Lithium Electrodeposits on Negative Electrodes, J Electrochem Soc 160 (2013) A662-A668.

[102] K. Yan, Z. Lu, H.-W. Lee, F. Xiong, P.-C. Hsu, Y. Li, J. Zhao, S. Chu, Y. Cui, Selective deposition and stable encapsulation of lithium through heterogeneous seeded growth, Nat Energy 1 (2016).

[103] H.J.S. Sand, On the Concentration at the Electrodes in a Solution, with special reference to the Liberation of Hydrogen by Electrolysis of a Mixture of Copper Sulphate and Sulphuric Acid, Proc Phys Soc London 1 (1901) 45-79.

[104] M. Rosso, T. Gobron, C. Brissot, J. Chazalviel, S. Lascau, Onset of dendritic

growth in lithium/polymer cells, J Power Sources (2001) 804-806.

[105] K. Dong, Y. Xu, J. Tan, M. Osenberg, F. Sun, Z. Kochovski, D.T. Pham, S. Mei, A. Hilger, E. Ryan, Y. Lu, J. Banhart, I. Manke, Unravelling the Mechanism of Lithium Nucleation and Growth and the Interaction with the Solid Electrolyte Interface, ACS Energy Lett 6 (2021) 1719-1728.

[106] E. Peled, S. Menkin, Review—SEI: Past, Present and Future, J Electrochem Soc 164 (2017) A1703-A1719.

[107] M.D. Tikekar, S. Choudhury, Z. Tu, L.A. Archer, Design principles for electrolytes and interfaces for stable lithium-metal batteries, Nat Energy 1 (2016).

[108] P. Bai, J. Guo, M. Wang, A. Kushima, L. Su, J. Li, F.R. Brushett, M.Z. Bazant, Interactions between Lithium Growths and Nanoporous Ceramic Separators, Joule 2 (2018) 2434-2449.

[109] R. Akolkar, Mathematical model of the dendritic growth during lithium electrodeposition, J Power Sources 232 (2013) 23-28.

[110] K. Nishikawa, T. Mori, T. Nishida, Y. Fukunaka, M. Rosso, Li dendrite growth and Li+ ionic mass transfer phenomenon, J Electroanal Chem 661 (2011) 84-89.

[111] J. Steiger, D. Kramer, R. Mönig, Mechanisms of dendritic growth investigated by in situ light microscopy during electrodeposition and dissolution of lithium, J Power Sources 261 (2014) 112-119.

[112] J. Steiger, D. Kramer, R. Mönig, Microscopic observations of the formation, growth and shrinkage of lithium moss during electrodeposition and dissolution, Electrochim Acta 136 (2014) 529-536.

[113] M.S. Park, S.B. Ma, D.J. Lee, D. Im, S.G. Doo, O. Yamamoto, A highly reversible lithium metal anode, Sci Rep 4 (2014) 3815.

[114] W. Li, H. Zheng, G. Chu, F. Luo, J. Zheng, D. Xiao, X. Li, L. Gu, H. Li, X. Wei, Q. Chen, L. Chen, Effect of electrochemical dissolution and deposition order on lithium dendrite formation: a top view investigation, Faraday Discuss 176 (2014) 109-124.

[115] M.J. Wang, R. Choudhury, J. Sakamoto, Characterizing the Li-Solid-Electrolyte Interface Dynamics as a Function of Stack Pressure and Current Density, Joule 3 (2019)

2165-2178.

[116] D. Koo, B. Kwon, J. Lee, K.T. Lee, Asymmetric behaviour of Li/Li symmetric cells for Li metal batteries, Chem Commun 55 (2019) 9637-9640.

[117] F.N. Jiang, S.J. Yang, H. Liu, X.B. Cheng, L. Liu, R. Xiang, Q. Zhang, S. Kaskel, J.Q. Huang, Mechanism understanding for stripping electrochemistry of Li metal anode, SusMat 1 (2021) 506-536.

[118] Y. Liu, X. Xu, O.O. Kapitanova, P.V. Evdokimov, Z. Song, A. Matic, S. Xiong, Electro - Chemo - Mechanical Modeling of Artificial Solid Electrolyte Interphase to Enable Uniform Electrodeposition of Lithium Metal Anodes, Adv Energy Mater 12 (2022).

[119] Y. Gao, Z. Yan, J.L. Gray, X. He, D. Wang, T. Chen, Q. Huang, Y.C. Li, H. Wang, S.H. Kim, T.E. Mallouk, D. Wang, Polymer-inorganic solid-electrolyte interphase for stable lithium metal batteries under lean electrolyte conditions, Nat Mater 18 (2019) 384-389.

[120] M.S. Kim, J.-H. Ryu, Deepika, Y.R. Lim, I.W. Nah, K.-R. Lee, L.A. Archer, W. Il Cho, Langmuir–Blodgett artificial solid-electrolyte interphases for practical lithium metal batteries, Nat Energy 3 (2018) 889-898.

[121] Z. Yu, D.G. Mackanic, W. Michaels, M. Lee, A. Pei, D. Feng, Q. Zhang, Y. Tsao, C.V. Amanchukwu, X. Yan, H. Wang, S. Chen, K. Liu, J. Kang, J. Qin, Y. Cui, Z. Bao, A Dynamic, Electrolyte-Blocking, and Single-Ion-Conductive Network for Stable Lithium-Metal Anodes, Joule 3 (2019) 2761-2776.

[122] Z. Huang, S. Choudhury, N. Paul, J.H. Thienenkamp, P. Lennartz, H. Gong, P. M ü ller - Buschbaum, G. Brunklaus, R. Gilles, Z. Bao, Effects of Polymer Coating Mechanics at Solid - Electrolyte Interphase for Stabilizing Lithium Metal Anodes, Adv Energy Mater 12 (2021).

[123] Z. Huang, S. Choudhury, H. Gong, Y. Cui, Z. Bao, A Cation-Tethered Flowable Polymeric Interface for Enabling Stable Deposition of Metallic Lithium, J Am Chem Soc 142 (2020) 21393-21403.

[124] R.M. Gao, H. Yang, C.Y. Wang, H. Ye, F.F. Cao, Z.P. Guo, Fatigue-Resistant Interfacial Layer for Safe Lithium Metal Batteries, Angew Chem Int Ed 60 (2021) 25508-25513.

[125] A. Hu, W. Chen, X. Du, Y. Hu, T. Lei, H. Wang, L. Xue, Y. Li, H. Sun, Y. Yan, J. Long, C. Shu, J. Zhu, B. Li, X. Wang, J. Xiong, An artificial hybrid interphase for an ultrahigh-rate and practical lithium metal anode, Energy Environ Sci 14 (2021) 4115-4124.

[126] P. Liu, J. Zhang, L. Zhong, S. Huang, L. Gong, D. Han, S. Wang, M. Xiao, Y. Meng, Interphase Building of Organic-Inorganic Hybrid Polymer Solid Electrolyte with Uniform Intermolecular Li(+) Path for Stable Lithium Metal Batteries, Small 17 (2021) e2102454.

[127] Z. Yu, S. Seo, J. Song, Z. Zhang, S.T. Oyakhire, Y. Wang, R. Xu, H. Gong, S. Zhang, Y. Zheng, Y. Tsao, L. Mondonico, E.G. Lomeli, X. Wang, W. Kim, K. Ryu, Z. Bao, A Solution - Processable High - Modulus Crystalline Artificial Solid Electrolyte Interphase for Practical Lithium Metal Batteries, Adv Energy Mater 12 (2022).

[128] Y. Jie, X. Ren, R. Cao, W. Cai, S. Jiao, Advanced Liquid Electrolytes for Rechargeable Li Metal Batteries, Adv Funct Mater 30 (2020).

[129] S. Yuan, S. Weng, F. Wang, X. Dong, Y. Wang, Z. Wang, C. Shen, J.L. Bao, X. Wang, Y. Xia, Revisiting the designing criteria of advanced solid electrolyte interphase on lithium metal anode under practical condition, Nano Energy 83 (2021).

[130] Q. Wang, C. Zhao, S. Wang, J. Wang, M. Liu, S. Ganapathy, X. Bai, B. Li, M. Wagemaker, Clarifying the Relationship between the Lithium Deposition Coverage and Microstructure in Lithium Metal Batteries, J Am Chem Soc 144 (2022) 21961-21971.

[131] S. Kim, G. Park, S.J. Lee, S. Seo, K. Ryu, C.H. Kim, J.W. Choi, Lithium Metal Batteries: From Fundamental Research to Industrialization, Adv Mater (2022) e2206625.

[132] H. Zhang, G.G. Eshetu, X. Judez, C. Li, L.M. Rodriguez-Martinez, M. Armand, Electrolyte Additives for Lithium Metal Anodes and Rechargeable Lithium Metal Batteries: Progress and Perspectives, Angew Chem Int Ed 57 (2018) 15002-15027.

[133] Z. Yu, H. Wang, X. Kong, W. Huang, Y. Tsao, D.G. Mackanic, K. Wang, X. Wang, W. Huang, S. Choudhury, Y. Zheng, C.V. Amanchukwu, S.T. Hung, Y. Ma, E.G. Lomeli, J. Qin, Y. Cui, Z. Bao, Molecular design for electrolyte solvents enabling energy-dense and long-cycling lithium metal batteries, Nat Energy 5 (2020) 526-533.

[134] R. Weber, M. Genovese, A.J. Louli, S. Hames, C. Martin, I.G. Hill, J.R. Dahn, Long cycle life and dendrite-free lithium morphology in anode-free lithium pouch cells enabled by a dual-salt liquid electrolyte, Nat Energy 4 (2019) 683-689.

[135] J. Chen, Q. Li, T.P. Pollard, X. Fan, O. Borodin, C. Wang, Electrolyte design for Li metal-free Li batteries, Mater Today 39 (2020) 118-126.

[136] Y. Yamada, J. Wang, S. Ko, E. Watanabe, A. Yamada, Advances and issues in developing salt-concentrated battery electrolytes, Nat Energy 4 (2019) 269-280.

[137] X. Ren, L. Zou, X. Cao, M.H. Engelhard, W. Liu, S.D. Burton, H. Lee, C. Niu, B.E. Matthews, Z. Zhu, C. Wang, B.W. Arey, J. Xiao, J. Liu, J.-G. Zhang, W. Xu, Enabling High-Voltage Lithium-Metal Batteries under Practical Conditions, Joule 3 (2019) 1662-1676.

[138] Z. Yu, P.E. Rudnicki, Z. Zhang, Z. Huang, H. Celik, S.T. Oyakhire, Y. Chen, X. Kong, S.C. Kim, X. Xiao, H. Wang, Y. Zheng, G.A. Kamat, M.S. Kim, S.F. Bent, J. Qin, Y. Cui, Z. Bao, Rational solvent molecule tuning for high-performance lithium metal battery electrolytes, Nat Energy 7 (2022) 94-106.

[139] Y. Zheng, N. Yang, R. Gao, Z. Li, H. Dou, G. Li, L. Qian, Y. Deng, J. Liang, L. Yang, Y. Liu, Q. Ma, D. Luo, N. Zhu, K. Li, X. Wang, Z. Chen, "Tree-Trunk" Design for Flexible Quasi-Solid-State Electrolytes with Hierarchical Ion-Channels Enabling Ultralong-Life Lithium-Metal Batteries, Adv Mater 34 (2022) e2203417.

[140] W. Zhang, Z. Tu, J. Qian, S. Choudhury, L.A. Archer, Y. Lu, Design Principles of Functional Polymer Separators for High-Energy, Metal-Based Batteries, Small 14 (2018) e1703001.

[141] Y. Yang, B. Li, L. Li, S. Seeger, J. Zhang, A Superlephilic/Superhydrophobic and Thermostable Separator Based on Silicone Nanofilaments for Li Metal Batteries, iScience 16 (2019) 420-432.

[142] C. Zhou, Q. He, Z. Li, J. Meng, X. Hong, Y. Li, Y. Zhao, X. Xu, L. Mai, A robust electrospun separator modified with in situ grown metal-organic frameworks for lithium-sulfur batteries, Chem Eng J 395 (2020).

[143] L. Kong, X. Fu, X. Fan, Y. Wang, S. Qi, D. Wu, G. Tian, W.H. Zhong, A Janus nanofiber-based separator for trapping polysulfides and facilitating ion-transport in lithium-sulfur batteries, Nanoscale 11 (2019) 18090-18098.

[144] M. Eftekharnia, M. Hasanpoor, M. Forsyth, R. Kerr, P.C. Howlett, Toward Practical Li Metal Batteries: Importance of Separator Compatibility Using Ionic Liquid Electrolytes, ACS Appl Energy Mater 2 (2019) 6655-6663.

[145] M. Hu, Q. Ma, Y. Yuan, Y. Pan, M. Chen, Y. Zhang, D. Long, Grafting polyethyleneimine on electrospun nanofiber separator to stabilize lithium metal anode for lithium sulfur batteries, Chem Eng J 388 (2020).

[146] S. Xu, T. Zhao, Y. Ye, T. Yang, R. Luo, L. Li, F. Wu, R. Chen, A Designed Lithiophilic Carbon Channel on Separator to Regulate Lithium Deposition Behavior, Small 18 (2022) e2104390.

[147] J. Li, L. Chen, F. Wang, Z. Qin, Y. Zhang, N. Zhang, X. Liu, G. Chen, Anionic metal-organic framework modified separator boosting efficient Li-ion transport, Chem Eng J 451 (2023).

[148] S. Sun, J. Wang, X. Chen, Q. Ma, Y. Wang, K. Yang, X. Yao, Z. Yang, J. Liu, H. Xu, Q. Cai, Y. Zhao, W. Yan, Thermally Stable and Dendrite - Resistant Separators toward Highly Robust Lithium Metal Batteries, Adv Energy Mater 12 (2022).

[149] C. Li, S. Liu, C. Shi, G. Liang, Z. Lu, R. Fu, D. Wu, Two-dimensional molecular brush-functionalized porous bilayer composite separators toward ultrastable high-current density lithium metal anodes, Nat Commun 10 (2019) 1363.

[150] T.S. Wang, X. Liu, Y. Wang, L.Z. Fan, High Areal Capacity Dendrite - Free Li Anode Enabled by Metal – Organic Framework - Derived Nanorod Array Modified Carbon Cloth for Solid State Li Metal Batteries, Adv Funct Mater 31 (2020).

[151] J. Cao, Y. Xie, W. Li, X. Wang, Y. Yang, Q. Zhang, J. Guo, C. Yang, S. Cheng, C.

Zhang, K. Wang, Rationally optimized carbon fiber cloth as lithiophilic host for highly stable Li metal anodes, Mater Today Energy 20 (2021).
[152] P. Shi, X.Q. Zhang, X. Shen, R. Zhang, H. Liu, Q. Zhang, A Review of Composite Lithium Metal Anode for Practical Applications, Adv Mater Technol 5 (2019).
[153] C. Yang, Y. Yao, S. He, H. Xie, E. Hitz, L. Hu, Ultrafine Silver Nanoparticles for Seeded Lithium Deposition toward Stable Lithium Metal Anode, Adv Mater 29 (2017).
[154] D. Lin, Y. Liu, Z. Liang, H.W. Lee, J. Sun, H. Wang, K. Yan, J. Xie, Y. Cui, Layered reduced graphene oxide with nanoscale interlayer gaps as a stable host for lithium metal anodes, Nat Nanotechnol 11 (2016) 626-632.
[155] J.-K. Meng, W.-W. Wang, X.-Y. Yue, H.-Y. Xia, Q.-C. Wang, X.-X. Wang, Z.-W. Fu, X.-J. Wu, Y.-N. Zhou, Cotton-derived carbon cloth enabling dendrite-free Li deposition for lithium metal batteries, J Power Sources 465 (2020).
[156] D. Li, Y. Gao, C. Xie, Z. Zheng, Au-coated carbon fabric as Janus current collector for dendrite-free flexible lithium metal anode and battery, Appl Phys Rev 9 (2022).
[157] K. Baek, W.G. Lee, E. Im, J.H. Ha, S. Ahn, Y. Kim, Y. Choi, S.J. Kang, Gradient Lithium Metal Infusion in Ag-Decorated Carbon Fibers for High-Capacity Lithium Metal Battery Anodes, Nano Lett 23 (2023) 8515-8523.
[158] F. Zhao, X. Zhou, W. Deng, Z. Liu, Entrapping lithium deposition in lithiophilic reservoir constructed by vertically aligned ZnO nanosheets for dendrite-free Li metal anodes, Nano Energy 62 (2019) 55-63.
[159] B.G. Son, C. Kwon, Y. Cho, T. Jang, H.R. Byon, S. Kim, E.S. Cho, Constructing Reversible Li Deposition Interfaces by Tailoring Lithiophilic Functionalities of a Heteroatom-Doped Graphene Interlayer for Highly Stable Li Metal Anodes, ACS Appl Mater Interfaces 16 (2024) 32259-32270.
[160] X. Chen, X.-R. Chen, T.-Z. Hou, B.-Q. Li, X.-B. Cheng, R. Zhang, Q. Zhang, Lithiophilicity chemistry of heteroatom-doped carbon to guide uniform lithium nucleation in lithium metal anodes, (2019).
[161] X. Fu, C. Shang, G. Zhou, X. Wang, Lithiophilic Sb surface modified Cu

nanowires grown on Cu foam: a synergistic 1D@3D hierarchical structure for stable lithium metal anodes, J Mater Chem A 9 (2021) 24963-24970.

[162] Y. Liu, D. Lin, Z. Liang, J. Zhao, K. Yan, Y. Cui, Lithium-coated polymeric matrix as a minimum volume-change and dendrite-free lithium metal anode, Nat Commun 7 (2016) 10992.

[163] F. Liu, R. Xu, Z. Hu, S. Ye, S. Zeng, Y. Yao, S. Li, Y. Yu, Regulating Lithium Nucleation via CNTs Modifying Carbon Cloth Film for Stable Li Metal Anode, Small 15 (2019) e1803734.

[164] R. Zhang, X. Chen, X. Shen, X.-Q. Zhang, X.-R. Chen, X.-B. Cheng, C. Yan, C.-Z. Zhao, Q. Zhang, Coralloid Carbon Fiber-Based Composite Lithium Anode for Robust Lithium Metal Batteries, Joule 2 (2018) 764-777.

[165] Y. Zhang, C. Wang, G. Pastel, Y. Kuang, H. Xie, Y. Li, B. Liu, W. Luo, C. Chen, L. Hu, 3D Wettable Framework for Dendrite‐Free Alkali Metal Anodes, Adv Energy Mater 8 (2018).

[166] H. Cheng, S. Zhang, J. Mei, L. Qiu, P. Zhang, X. Xu, J. Tu, J. Xie, X. Zhao, Lithiated carbon cloth as a dendrite-free anode for high-performance lithium batteries, Sustainable Energy Fuels 4 (2020) 5773-5782.

[167] A.J. Louli, A. Eldesoky, R. Weber, M. Genovese, M. Coon, J. deGooyer, Z. Deng, R.T. White, J. Lee, T. Rodgers, R. Petibon, S. Hy, S.J.H. Cheng, J.R. Dahn, Diagnosing and correcting anode-free cell failure via electrolyte and morphological analysis, Nat Energy 5 (2020) 693-702.

[168] S. Lobe, A. Bauer, S. Uhlenbruck, D. Fattakhova-Rohlfing, Physical Vapor Deposition in Solid-State Battery Development: From Materials to Devices, Adv Sci 8 (2021) e2002044.

[169] Z. Shi, Z. Sun, X. Yang, C. Lu, S. Li, X. Yu, Y. Ding, T. Huang, J. Sun, Synergizing Conformal Lithiophilic Granule and Dealloyed Porous Skeleton toward Pragmatic Li Metal Anodes, Small Sci 2 (2022).

[170] G. Zhang, K. Wang, Y. Xu, X. Zhang, Q. Peng, Y. Ma, S. Li, X. Zhang, X. Sun, Y. Ma, A 10‐μm Ultrathin Lithium Metal Composite Anodes with Superior

Electrochemical Kinetics and Cycling Stability, Energy Environ Mater (2023).
[171] J. Gao, C. Chen, Q. Dong, J. Dai, Y. Yao, T. Li, A. Rundlett, R. Wang, C. Wang, L. Hu, Stamping Flexible Li Alloy Anodes, Adv Mater 33 (2021) e2005305.
[172] J. Xing, T. Chen, L. Yi, Z. Wang, Z. Song, X. Chen, C. Wei, A. Zhou, H. Li, J. Li, Endowing Cu foil self-wettable in molten lithium: A roll-to-roll wet coating strategy to fabricate high-performance ultrathin lithium metal anodes, Energy Storage Mater 63 (2023).
[173] Z. Liang, K. Yan, G. Zhou, A. Pei, Y. Sun, J. Xie, Y. Li, F. Shi, Y. Liu, D. Lin, K. Liu, H. Wang, H. Wang, L. Lu, Y. Cui, Composite lithium electrode with mesoscale skeleton via simple mechanical deformation, Sci Adv 5 (2019) eaau5655.
[174] M. Wan, S. Kang, L. Wang, H.W. Lee, G.W. Zheng, Y. Cui, Y. Sun, Mechanical rolling formation of interpenetrated lithium metal/lithium tin alloy foil for ultrahigh-rate battery anode, Nat Commun 11 (2020) 829.
[175] Z. Cao, B. Li, S. Yang, Dendrite-Free Lithium Anodes with Ultra-Deep Stripping and Plating Properties Based on Vertically Oriented Lithium-Copper-Lithium Arrays, Adv Mater 31 (2019) e1901310.
[176] X. Chen, M. Shang, J. Niu, Inter-layer-calated Thin Li Metal Electrode with Improved Battery Capacity Retention and Dendrite Suppression, Nano Lett 20 (2020) 2639-2646.
[177] S. Huang, Z. Wu, B. Johannessen, K. Long, P. Qing, P. He, X. Ji, W. Wei, Y. Chen, L. Chen, Interfacial friction enabling ≤ 20 mum thin free-standing lithium strips for lithium metal batteries, Nat Commun 14 (2023) 5678.
[178] J. Shang, W. Yu, L. Wang, C. Xie, H. Xu, W. Wang, Q. Huang, Z. Zheng, Metallic Glass-Fiber Fabrics: A New Type of Flexible, Super-Lightweight, and 3D Current Collector for Lithium Batteries, Adv Mater 35 (2023) e2211748.
[179] R. Choudhury, J. Wild, Y. Yang, Engineering current collectors for batteries with high specific energy, Joule 5 (2021) 1301-1305.
[180] Y. Ye, L.-Y. Chou, Y. Liu, H. Wang, H.K. Lee, W. Huang, J. Wan, K. Liu, G. Zhou, Y. Yang, A. Yang, X. Xiao, X. Gao, D.T. Boyle, H. Chen, W. Zhang, S.C. Kim, Y. Cui,

Ultralight and fire-extinguishing current collectors for high-energy and high-safety lithium-ion batteries, Nat Energy 5 (2020) 786-793.

[181] B. Rieger, S. Schlueter, S.V. Erhard, J. Schmalz, G. Reinhart, A. Jossen, Multi-scale investigation of thickness changes in a commercial pouch type lithium-ion battery, J Energy Storage 6 (2016) 213-221.

[182] H.-C. Chu, H.-Y. Tuan, High-performance lithium-ion batteries with 1.5 μm thin copper nanowire foil as a current collector, J Power Sources 346 (2017) 40-48.

[183] S. Zhang, M. Sakane, T. Nagasawa, K. Kobayashi, Mechanical Properties of Copper Thin Films Used in Electronic Devices, Procedia Eng 10 (2011) 1497-1502.

[184] R. A. M. Hikmet, H. Feil, Lithium Secondary Battery Comprising IndividualCells with One Another, as well as Watches, Computers and Communication Equipment Provided with A Battery, 2003.

[185] S. Xu, Y. Zhang, J. Cho, J. Lee, X. Huang, L. Jia, J.A. Fan, Y. Su, J. Su, H. Zhang, H. Cheng, B. Lu, C. Yu, C. Chuang, T.I. Kim, T. Song, K. Shigeta, S. Kang, C. Dagdeviren, I. Petrov, P.V. Braun, Y. Huang, U. Paik, J.A. Rogers, Stretchable batteries with self-similar serpentine interconnects and integrated wireless recharging systems, Nat Commun 4 (2013) 1543.

[186] G. Qian, B. Zhu, X. Liao, H. Zhai, A. Srinivasan, N.J. Fritz, Q. Cheng, M. Ning, B. Qie, Y. Li, S. Yuan, J. Zhu, X. Chen, Y. Yang, Bioinspired, Spine-Like, Flexible, Rechargeable Lithium-Ion Batteries with High Energy Density, Adv Mater 30 (2018) e1704947.

[187] Z. Suo, E.Y. Ma, H. Gleskova, S. Wagner, Mechanics of rollable and foldable film-on-foil electronics, Appl Phys Lett 74 (1999) 1177-1179.

[188] K.K. Fu, J. Cheng, T. Li, L. Hu, Flexible Batteries: From Mechanics to Devices, ACS Energy Lett 1 (2016) 1065-1079.

[189] L. Hu, H. Wu, F.L. Mantia, Y. Yang, Y. Cui, Thin, Flexible Secondary Li-Ion Paper Batteries, ACS Nano 4 (2010) 5843–5848.

[190] J. Cai, L. Wang, Q. Huang, W. Yu, C. Xie, Z. Zheng, A Thin, Stable, and Flexible

Janus Lithium-Textile Anode for Long-Life and High-Energy Lithium Metal Battery, Adv Energy Mater 14 (2023).

[191] J. Deng, C. Bae, A. Denlinger, T. Miller, Electric Vehicles Batteries: Requirements and Challenges, Joule 4 (2020) 511-515.

[192] J.P. Wang, F. Lang, Q. Li, In situ tailoring solid electrolyte interphase of three-dimensional Li metal electrode for enhanced Coulombic efficiency, EcoMat 5 (2023).

[193] G. Yang, W. Hou, Y. Zhai, Z. Chen, C. Liu, C. Ouyang, X. Liang, P. Paoprasert, N. Hu, S. Song, Polymeric concentrated electrolyte enables simultaneous stabilization of electrode/electrolyte interphases for quasi-solid-state lithium metal batteries, EcoMat 5 (2023).

[194] G. Li, Z. Liu, Q. Huang, Y. Gao, M. Regula, D. Wang, L.-Q. Chen, D. Wang, Stable metal battery anodes enabled by polyethylenimine sponge hosts by way of electrokinetic effects, Nat Energy 3 (2018) 1076-1083.

[195] B. Han, D. Xu, S.S. Chi, D. He, Z. Zhang, L. Du, M. Gu, C. Wang, H. Meng, K. Xu, Z. Zheng, Y. Deng, 500 Wh kg^{-1} Class Li Metal Battery Enabled by a Self-Organized Core-Shell Composite Anode, Adv Mater 32 (2020) e2004793.

[196] Z. Gong, C. Lian, P. Wang, K. Huang, K. Zhu, K. Ye, J. Yan, G. Wang, D. Cao, Lithiophilic Cu-Li_2O matrix on a Cu Collector to Stabilize Lithium Deposition for Lithium Metal Batteries, Energy Environ Mater 5 (2021) 1270-1277.

[197] X.Q. Zhang, X. Chen, R. Xu, X.B. Cheng, H.J. Peng, R. Zhang, J.Q. Huang, Q. Zhang, Columnar Lithium Metal Anodes, Angew Chem 56 (2017) 14207-14211.

[198] D. Jin, Y. Roh, T. Jo, M.H. Ryou, H. Lee, Y.M. Lee, Robust Cycling of Ultrathin Li Metal Enabled by Nitrate-Preplanted Li Powder Composite, Adv Energy Mater 11 (2021).

[199] K. Schönherr, B. Schumm, F. Hippauf, R. Lissy, H. Althues, C. Leyens, S. Kaskel, Liquid lithium metal processing into ultrathin metal anodes for solid state batteries, Chem Eng J Adv 9 (2022).

[200] W. Wu, Z. Song, Y. Dai, X. Zheng, G. Chai, J. Yang, W. Luo, Magnetic Actuation

Enables Programmable Lithium Metal Engineering, Adv Energy Mater 12 (2022).
[201] Q. Xu, X. Yang, M. Rao, D. Lin, K. Yan, R. Du, J. Xu, Y. Zhang, D. Ye, S. Yang, G. Zhou, Y. Lu, Y. Qiu, High energy density lithium metal batteries enabled by a porous graphene/MgF2 framework, Energy Storage Mater 26 (2020) 73-82.
[202] L. Chen, G. Chen, W. Tang, H. Wang, F. Chen, X. Liu, R. Ma, A robust and lithiophilic three-dimension framework of CoO nanorod arrays on carbon cloth for cycling-stable lithium metal anodes, Mater Today Energy 18 (2020).
[203] S.-S. Chi, Y. Liu, W.-L. Song, L.-Z. Fan, Q. Zhang, Prestoring Lithium into Stable 3D Nickel Foam Host as Dendrite-Free Lithium Metal Anode, Adv Funct Mater 27 (2017).
[204] G. Jiang, N. Jiang, N. Zheng, X. Chen, J. Mao, G. Ding, Y. Li, F. Sun, Y. Li, MOF-derived porous Co3O4-NC nanoflake arrays on carbon fiber cloth as stable hosts for dendrite-free Li metal anodes, Energy Storage Mater 23 (2019) 181-189.
[205] H. Shi, C.J. Zhang, P. Lu, Y. Dong, P. Wen, Z.S. Wu, Conducting and Lithiophilic MXene/Graphene Framework for High-Capacity, Dendrite-Free Lithium-Metal Anodes, ACS Nano 13 (2019) 14308-14318.
[206] S. Li, Q. Liu, J. Zhou, T. Pan, L. Gao, W. Zhang, L. Fan, Y. Lu, Hierarchical Co3O4 Nanofiber – Carbon Sheet Skeleton with Superior Na/Li - Philic Property Enabling Highly Stable Alkali Metal Batteries, Adv Funct Mater 29 (2019).
[207] K. Qin, J. Baucom, D. Liu, W. Shi, N. Zhao, Y. Lu, A Powder Metallurgic Approach toward High-Performance Lithium Metal Anodes, Small 16 (2020) e2000794.
[208] L. Tao, B. Ma, F. Luo, Z. Xu, Z. Zheng, H. Huang, P. Bai, F. Lin, Gradient lithiation to load controllable, high utilization lithium in graphitic carbon host for high-energy batteries, Nano Energy 93 (2022).
[209] B. Yu, T. Tao, S. Mateti, S. Lu, Y. Chen, Nanoflake Arrays of Lithiophilic Metal Oxides for the Ultra-Stable Anodes of Lithium-Metal Batteries, Adv Funct Mater 28 (2018).
[210] T. Le, C. Yang, W. Lv, Q. Liang, X. Huang, F. Kang, Y. Yang, Deeply Cyclable

and Ultrahigh-Rate Lithium Metal Anodes Enabled by Coaxial Nanochamber Heterojunction on Carbon Nanofibers, Adv Sci 8 (2021) e2101940.

[211] S. Huang, L. Chen, T. Wang, J. Hu, Q. Zhang, H. Zhang, C. Nan, L.Z. Fan, Self-Propagating Enabling High Lithium Metal Utilization Ratio Composite Anodes for Lithium Metal Batteries, Nano Lett 21 (2021) 791-797.

[212] Y. Fang, S.L. Zhang, Z.-P. Wu, D. Luan, X.W. (David) Lou, A highly stable lithium metal anode enabled by Ag nanoparticle–embedded nitrogen-doped carbon macroporous fibers, Sci Adv 7 (2021) eabg3626.

[213] L. Lin, W. Lu, F. Zhao, S. Chen, J. Liu, H. Xie, Y. Liu, 20 μm Li metal modified with phosphate rich polymer-inorganic interphase applied in commercial carbonate electrolyte, J Energy Chem 76 (2023) 233-238.

[214] C. Gao, J. Li, K. Sun, H. Li, B. Hong, M. Bai, K. Zhang, Z. Zhang, Y. Lai, Controllable lithium deposition behavior hollow of N, O co-doped carbon nanospheres for practical lithium metal batteries, Chem Eng J 412 (2021).

[215] Y. Chen, A. Elangovan, D. Zeng, Y. Zhang, H. Ke, J. Li, Y. Sun, H. Cheng, Vertically Aligned Carbon Nanofibers on Cu Foil as a 3D Current Collector for Reversible Li Plating/Stripping toward High-Performance Li–S Batteries, Adv Funct Mater 30 (2020) 1906444.

[216] C.-Y. Wang, Z.-J. Zheng, Y.-Q. Feng, H. Ye, F.-F. Cao, Z.-P. Guo, Topological design of ultrastrong MXene paper hosted Li enables ultrathin and fully flexible lithium metal batteries, Nano Energy 74 (2020).

[217] S.H. Kim, N.Y. Kim, U.J. Choe, J.M. Kim, Y.G. Lee, S.Y. Lee, Ultrahigh-Energy-Density Flexible Lithium-Metal Full Cells based on Conductive Fibrous Skeletons, Adv Energy Mater 11 (2021).

[218] Y. Li, S. Ye, J. Lin, Y. Song, X. Wu, J. Zhang, C. Shao, Z. Su, H. Sun, D.S. Seferos, A Pore-Forming Strategy Toward Porous Carbon-Based Substrates for High Performance Flexible Lithium Metal Full Batteries, Energy Environ Mater 6 (2022).

[219] L. Chen, Y. Yuan, R. Orenstein, M. Yanilmaz, J. He, J. Liu, Y. Liu, X. Zhang,

Carbon materials dedicate to bendable supports for flexible lithium-sulfur batteries, Energy Storage Mater 60 (2023).

[220] Y. Sun, K. Zhang, R. Chai, Y. Wang, X. Rui, K. Wang, H. Deng, H. Xiang, In Situ Artificial Hybrid SEI Layer Enabled High-Performance Prelithiated SiOx Anode for Lithium-Ion Batteries, Adv Funct Mater 33 (2023).

[221] K.H. Han, J.Y. Seok, I.H. Kim, K. Woo, J.H. Kim, G.G. Yang, H.J. Choi, S. Kwon, E.I. Jung, S.O. Kim, A 2D Ultrathin Nanopatterned Interlayer to Suppress Lithium Dendrite Growth in High-Energy Lithium-Metal Anodes, Adv Mater 34 (2022) e2203992.

[222] L. Liu, Y.X. Yin, J.Y. Li, S.H. Wang, Y.G. Guo, L.J. Wan, Uniform Lithium Nucleation/Growth Induced by Lightweight Nitrogen-Doped Graphitic Carbon Foams for High-Performance Lithium Metal Anodes, Adv Mater 30 (2018).

[223] K. Lin, X. Qin, M. Liu, X. Xu, G. Liang, J. Wu, F. Kang, G. Chen, B. Li, Ultrafine Titanium Nitride Sheath Decorated Carbon Nanofiber Network Enabling Stable Lithium Metal Anodes, Adv Funct Mater 29 (2019).

[224] Z. Xu, L. Xu, Z. Xu, Z. Deng, X. Wang, N, O-Codoped Carbon Nanosheet Array Enabling Stable Lithium Metal Anode, Adv Funct Mater 31 (2021).

[225] B. Moorthy, J.-H. Kim, H.-W. Lee, D.K. Kim, Vertically aligned carbon nanotubular structure for guiding uniform lithium deposition via capillary pressure as stable metallic lithium anodes, Energy Storage Mater 24 (2020) 602-609.

[226] Z. Li, W. Liang, J. Chen, L. Song, T. Xiong, W. Xie, S. Wu, D. Hu, X. Yao, Z. Peng, In-depth Li+ transportation in three-dimensionalized nanodiamond network for improved liquid and solid lithium metal batteries, Nano Energy 110 (2023).

[227] M. Koo, K.I. Park, S.H. Lee, M. Suh, D.Y. Jeon, J.W. Choi, K. Kang, K.J. Lee, Bendable inorganic thin-film battery for fully flexible electronic systems, Nano Lett 12 (2012) 4810-4816.

[228] M.H. Park, M. Noh, S. Lee, M. Ko, S. Chae, S. Sim, S. Choi, H. Kim, H. Nam, S. Park, J. Cho, Flexible high-energy Li-ion batteries with fast-charging capability,

Nano Lett 14 (2014) 4083-4089.

[229] H. Porthault, C. Calberg, J. Amiran, S. Martin, C. Páez, N. Job, B. Heinrichs, D. Liquet, R. Salot, Development of a thin flexible Li battery design with a new gel polymer electrolyte operating at room temperature, J Power Sources 482 (2021).

[230] Flexible Lithium Polymer Battery, Jenaxinc, https://jenaxinc.com/ko/flexible-battery/, Nov 2021.

[231] Panasonic Develops Bendable, Twistable, Flexible Lithium-ion Battery, https://news.panasonic.com/global/press/data/2016/09/en160929-8/en160929-8.pdf Nov 2021.

[232] Q. Meng, H. Wu, L. Mao, H. Yuan, A. Ahmad, Z. Wei, Combining Electrode Flexibility and Wave-Like Device Architecture for Highly Flexible Li-Ion Batteries, Adv Mater Technol 2 (2017).

[233] L. Xue, S.V. Savilov, V.V. Lunin, H. Xia, Self-Standing Porous LiCoO2 Nanosheet Arrays as 3D Cathodes for Flexible Li-Ion Batteries, Adv Funct Mater 28 (2017).

[234] M. Yao, R. Wang, Z. Zhao, Y. Liu, Z. Niu, J. Chen, A Flexible All-in-One Lithium-Sulfur Battery, ACS Nano 12 (2018) 12503-12511.

[235] W. Shen, K. Li, Y. Lv, T. Xu, D. Wei, Z. Liu, Highly-Safe and Ultra-Stable All-Flexible Gel Polymer Lithium Ion Batteries Aiming for Scalable Applications, Adv Energy Mater 10 (2020).

[236] J.H. Han, K.H. Shin, Y.J. Lee, Scalable Binder-Free Freestanding Electrodes Based on a Cellulose Acetate-Assisted Carbon Nanotube Fibrous Network for Practical Flexible Li-Ion Batteries, ACS Appl Mater Interfaces 13 (2021) 6375-6384.

[237] C. Xie, J. Chang, J. Shang, L. Wang, Y. Gao, Q. Huang, Z. Zheng, Hybrid Lithium-Ion/Metal Electrodes Enable Long Cycle Stability and High Energy Density of Flexible Batteries, Adv Funct Mater 32 (2022).

[238] R. Lu, M. Cheng, L. Mao, M. Zhang, H. Yuan, K. Amin, C. Yang, Y. Cheng, Y.

Meng, Z. Wei, Nitrogen-doped nanoarray-modified 3D hierarchical graphene as a cofunction host for high-performance flexible Li-S battery, EcoMat 2 (2020).

[239] X. Ding, Z. Pan, N. Liu, L. Li, X. Wang, G. Xu, J. Yang, J. Yang, N. Yu, M. Liu, W. Li, Y. Zhang, Freestanding Carbon Nanotube Film for Flexible Straplike Lithium/Sulfur Batteries, Chem. Eur. J. 25 (2019) 3775-3780.

[240] Y. Qiao, H. Yang, Z. Chang, H. Deng, X. Li, H. Zhou, A high-energy-density and long-life initial-anode-free lithium battery enabled by a Li2O sacrificial agent, Nat Energy 6 (2021) 653-662.

[241] L. Lin, K. Qin, Q. Zhang, L. Gu, L. Suo, Y.S. Hu, H. Li, X. Huang, L. Chen, Li-Rich Li(2) [Ni(0.8) Co(0.1) Mn(0.1)]O(2) for Anode-Free Lithium Metal Batteries, Angew Chem Int Ed 60 (2021) 8289-8296.

[242] C.J. Huang, B. Thirumalraj, H.C. Tao, K.N. Shitaw, H. Sutiono, T.T. Hagos, T.T. Beyene, L.M. Kuo, C.C. Wang, S.H. Wu, W.N. Su, B.J. Hwang, Decoupling the origins of irreversible coulombic efficiency in anode-free lithium metal batteries, Nat Commun 12 (2021) 1452.

[243] T.T. Beyene, B.A. Jote, Z.T. Wondimkun, B.W. Olbassa, C.J. Huang, B. Thirumalraj, C.H. Wang, W.N. Su, H. Dai, B.J. Hwang, Effects of Concentrated Salt and Resting Protocol on Solid Electrolyte Interface Formation for Improved Cycle Stability of Anode-Free Lithium Metal Batteries, ACS Appl Mater Interfaces 11 (2019) 31962-31971.

[244] L. Lin, L. Suo, Y.s. Hu, H. Li, X. Huang, L. Chen, Epitaxial Induced Plating Current-Collector Lasting Lifespan of Anode-Free Lithium Metal Battery, Adv Energy Mater 11 (2021).

[245] S. Kim, M. Lee, S. Oh, W.-H. Ryu, Li-Dendrite cage electrode with 3-D interconnected pores for Anode-Free Lithium-Metal batteries, Chem Eng J 474 (2023).

[246] A.A. Assegie, J.H. Cheng, L.M. Kuo, W.N. Su, B.J. Hwang, Polyethylene oxide film coating enhances lithium cycling efficiency of an anode-free lithium-metal battery, Nanoscale 10 (2018) 6125-6138.

[247] R. Rodriguez, K.E. Loeffler, R.A. Edison, R.M. Stephens, A. Dolocan, A. Heller, C.B. Mullins, Effect of the Electrolyte on the Cycling Efficiency of Lithium-Limited Cells and their Morphology Studied Through in Situ Optical Imaging, ACS Appl Energy Mater 1 (2018) 5830-5835.

[248] Z.L. Brown, S. Heiskanen, B.L. Lucht, Using Triethyl Phosphate to Increase the Solubility of LiNO3 in Carbonate Electrolytes for Improving the Performance of the Lithium Metal Anode, J Electrochem Soc 166 (2019) A2523-A2527.

[249] J. Zhang, H. Zhang, L. Deng, Y. Yang, L. Tan, X. Niu, Y. Chen, L. Zeng, X. Fan, Y. Zhu, An additive-enabled ether-based electrolyte to realize stable cycling of high-voltage anode-free lithium metal batteries, Energy Storage Mater 54 (2023) 450-460.

[250] B. Wu, C. Chen, D.L. Danilov, Z. Chen, M. Jiang, R.A. Eichel, P.H.L. Notten, Dual Additives for Stabilizing Li Deposition and SEI Formation in Anode‐Free Li‐Metal Batteries, Energy Environ Mater 7 (2023).

[251] S. Zhang, J. Zeng, Y. Ma, Y. Zhao, Y. Qian, L. Suo, J. Huang, X. Wang, W. Li, B. Zhang, Ultrathin hierarchical porous Cu current collector fabricated by anodic oxidation in complexing agent system for stable anode-free Lithium metal batteries, Electrochimica Acta 442 (2023).

[252] E. Kim, W. Choi, S. Ryu, Y. Yun, S. Jo, J. Yoo, Effect of 3D lithiophilic current collector for anode-free Li ion batteries, J Alloys Compd 966 (2023).

[253] N. Li, T. Jia, Y. Liu, Y. Ouyang, Y. Lv, G. Zhong, Y. Wang, B. Sun, S. Lu, S. Huang, F. Kang, Y. Cao, Super-three-dimensional lithiophilic Cu-based current collector for anode-free lithium metal battery, Mater Today Energy 36 (2023).

[254] O. Tamwattana, H. Park, J. Kim, I. Hwang, G. Yoon, T.-h. Hwang, Y.-S. Kang, J. Park, N. Meethong, K. Kang, High-Dielectric Polymer Coating for Uniform Lithium Deposition in Anode-Free Lithium Batteries, ACS Energy Lett 6 (2021) 4416-4425.

[255] W. Chen, R.V. Salvatierra, M. Ren, J. Chen, M.G. Stanford, J.M. Tour, Laser-Induced Silicon Oxide for Anode-Free Lithium Metal Batteries, Adv Mater 32 (2020) e2002850.

[256] S. Liu, X. Ji, J. Yue, S. Hou, P. Wang, C. Cui, J. Chen, B. Shao, J. Li, F. Han, J.

Tu, C. Wang, High Interfacial-Energy Interphase Promoting Safe Lithium Metal Batteries, J Am Chem Soc 142 (2020) 2438-2447.
[257] Z. Tu, S. Choudhury, M.J. Zachman, S. Wei, K. Zhang, L.F. Kourkoutis, L.A. Archer, Designing Artificial Solid-Electrolyte Interphases for Single-Ion and High-Efficiency Transport in Batteries, Joule 1 (2017) 394-406.
[258] S. Li, F. Lorandi, H. Wang, T. Liu, J.F. Whitacre, K. Matyjaszewski, Functional polymers for lithium metal batteries, Prog Polym Sci 122 (2021).